Entanglement detection schemes and coherent manipulation of spin in quantum dots

Malkoc, Ognjen

2016

Entanglement detection schemes and coherent manipulation of spin in quantum dots

OGNJEN MALKOC
FACULTY OF SCIENCE, DEPARTMENT OF PHYSICS | LUND UNIVERSITY 2017

Entanglement detection schemes and coherent manipulation of spin in quantum dots

Entanglement detection schemes and coherent manipulation of spin in quantum dots

by Ognjen Malkoc

LUND
UNIVERSITY

Thesis for the degree of Doctor of Philosophy in Engineering
Thesis advisors: Assoc. Prof. Peter Samuelsson, Assoc. Prof. Gillis Carlsson
Faculty opponent: Prof. Wolfgang Belzig

To be presented, with the permission of the Faculty of Science of Lund University, for public criticism in the Rydberg lecture hall (Rydbergsalen) at the Department of Physics on Friday, the 3rd of February 2017 at 13:15.

Organization
LUND UNIVERSITY

Department of Physics
Box 118
SE–221 00 LUND
Sweden

Author(s)
Ognjen Malkoc

Document name
DOCTORAL DISSERTATION

Date of disputation
2017-02-03

Sponsoring organization

Title and subtitle
Entanglement detection schemes and coherent manipulation of spin in quantum dots

Abstract
The work contained in this thesis deals with two closely related topics. Papers I-III deal with charge transport statistics in nanoscale devices to investigate the presence of entanglement in the constituent electrons. We identify the contributions of entangled electron pairs to the current cross-correlations as a signature of entanglement. Paper IV treats the electric control of a quantum dot based spin qubit via Electric Dipole Spin Resonance.

In Paper I, we present a spin entanglement detection model in a hybrid nanoscale device, with a general entangler connected to a set of quantum dots and anti-collinear ferromagnetic contacts. Our model allows us to study the implications of a non-ideal detector in an entanglement detection scheme.

In Paper II, we investigate a scheme for generating and detecting orbitally entangled states in a device consisting of six quantum dots. The underlying process which enables our proposed scheme is sufficiently fast, even for the rapidly decaying quantum coherence of orbital states defined in a solid.

In Paper III, we investigate a minimal entanglement detection scheme based on measurements of current cross correlations. We find a significant reduction in the number of measurements required for an entanglement test.

In Paper IV, we investigate the optimisation of electrically controlling an electron spin in a gate defined semiconductor quantum dot. Specifically, we study how the shape of the quantum dot together with the direction of an in-plane magnetic field affect the spin relaxation rate and frequency of the induced Rabi oscillations.

Key words
Quantum dots, Spin relaxation, Quantum transport, Current noise, Entanglement

Classification system and/or index terms (if any)

Supplementary bibliographical information

Language
English

ISSN and key title

ISBN
978-91-7753-132-6 (print)
978-91-7753-133-3 (pdf)

Recipient's notes

Number of pages
162

Price

Security classification

Distributor
Ognjen Malkoc, Division of Mathematical Physics, Department of Physics, Sölvegatan 14, S-223 62 Lund, Sweden

Entanglement detection schemes and coherent manipulation of spin in quantum dots

by Ognjen Malkoc

LUND
UNIVERSITY

A doctoral thesis at a university in Sweden takes either the form of a single, cohesive research study (monograph) or a summary of research papers (compilation thesis), which the doctoral student has written alone or together with one or several other author(s).

In the latter case the thesis consists of two parts. An introductory text puts the research work into context and summarizes the main points of the papers. Then, the research publications themselves are reproduced, together with a description of the individual contributions of the authors. The research papers may either have been already published or are manuscripts at various stages (in press, submitted, or in draft).

Funding information: The thesis work was financially supported by the Swedish Research Council (VR) and the Japanese Society for the Promotion of Science (JSPS).

Faculty of Science, Department of Physics

ISBN: 978-91-7753-132-6 (print)
ISBN: 978-91-7753-133-3 (pdf)

Printed in Sweden by Media-Tryck, Lund University, Lund 2017

Contents

List of publications and Author's contributions

This thesis is based on the following publications, referred to by their Roman numerals:

I **Full counting statistics of generic spin entangler with quantum dot-ferromagnet detectors**
Ognjen Malkoc, Christian Bergenfeldt and Peter Samuelsson
Europhys. Lett. 105, 47013 (2014)

We investigate the transport statistics of an entangler device coupled to a quantum dot-ferromagnetic contact detector. An effective model is proposed which permits a generic entangler subsystem. We study how spin properties of entangled particles emitted from the entangler are manifested in the detector, in the presence of nonidealities and discuss its impact on entanglement detection strategies.

Contribution: O. Malkoc participated in formulating the project, carried out all calculations and wrote the first draft of the manuscript.

II **Subdecoherence Time Generation and Detection of Orbital Entanglement in Quantum Dots**
Fredrik Brange, Ognjen Malkoc, and Peter Samuelsson
Phys. Rev. Lett. 114, 176803 (2015)

We propose a scheme for generating and detecting pairs of orbitally entangled electrons in a quantum dot device. Studying the transport statistics, we describe how cotunneling events can be used to produce and detect entangled electron pairs. Also, we discuss the prospects of a real-time Bell test in the proposed device.

Contribution: O. Malkoc together with P. Samuelsson conceived the idea of a six-dot entangler-detector system. In the capacity as co-supervisor of the project, O. Malkoc participated in most of the calculations and joint discussions.

III **Minimal Entanglement Witness From Electrical Current Correlations**
Fredrik Brange, Ognjen Malkoc, and Peter Samuelsson
Submitted (2016)

In Paper III we propose a minimal entanglement detection scheme based on current cross-correlation measurements. We show that two cross-correlation measurements are sufficient to detect all pure entangled states, except the maximally entangled Bell states. The Bell states are resolved with a minimum of three measurements.

Contribution: O. Malkoc participated in formulating the project. Carried a large fraction of the calculations and participated in writing the first draft of the manuscript.

IV **Optimal geometry of lateral GaAs and Si/SiGe quantum dots for electrical control of spin qubits**
Ognjen Malkoc, Peter Stano, and Daniel Loss
Phys. Rev. B 93, 235413 (2016)

We investigate the efficiency of a typical EDSR setup of a single spin qubit in lateral GaAs and Si/SiGe quantum dots. We describe the effects of the orientation of the applied magnetic field and the main axis of a dot on the efficiency. We identify when re-orienting the applied magnetic field is sufficient to obtain an optimal setup, and when the orientation of the dot plays a role. Our findings reveal a robust optimal quantum dot geometry, with the main dot axis along $[110]$ or $[1\bar{1}0]$ depending on the sign of intrinsic spin-orbit interactions.

Contributions: O. Malkoc carried out all the calculations and wrote the first draft of the manuscript.

All papers are reproduced with permission of their respective publishers.

Acknowledgements

I am finishing this thesis in a mixed state of excitement and melancholy. Looking back on the past five years, I realise that I have been very fortunate. I have had the pleasure of spending time doing what I enjoy (for the most part), and doing so in an environment of exceptional people. It is unfortunate good things also come to an end. Here I wish to express my gratitude to the many individuals who have impacted my time as a PhD student.

I would like first thank my supervisor, Peter Samuelsson. I have learned a lot over the years. While I am still utterly confused, I am so on a much higher plane. I am also thankful for your support of my spending a sizeable fraction of the PhD studies abroad. It was a rewarding experience, both academically and personally.

During my years at the Division of Mathematical Physics, I have had the pleasure of working with many impressive colleagues. I have enjoyed many interesting physics discussions with Christian Bergenfeldt, Daniel Karlsson, Gediminas Kirsanskas and Fredrik Brange. Thank you Gediminas and Fredrik, for the helpful comments during my writing of the thesis. My office mates over the years, Olov Karlström, Francesca Battista, Alexey Kartsev, Miroslav Hopjan, Jakob Bengtsson, Sara Kheradsoud and Nastaran Dashty. Because of you, there have been very few dull days in the office.

A special thank you to Fikeraddis Damtie and Gunnar Eriksson, whom I have turned to for advice on far too many occasions. I have enjoyed our many conversations, even those about physics.

I would like to thank Andreas Wacker and Claudio Verdozzi, for the discussions. It has helped me get a more firm grasp on concepts in solid state physics. I am indebted to Katarina Lindqvist, whom I have frequently approached with too many questions. Your excellent support has made administrative matters much easier.

Thank you Cecilia Jarlskog for all the discussions, ranging from supersymmetric quantum mechanics to the nature of mankind. Our discussions have been very enlightening, and many times it has helped me tremendously.

I am very thankful to Daniel Loss for the opportunity to spend more than a year as a visiting researcher in his group in RIKEN. It has contributed substantially to my growth as a researcher and allowed me to obtain a much greater insight into

my research.

I also owe a big thank you to Peter Stano, who has been incredibly helpful and always available to provide sound advice. Thank you, Jin-Hong Park, Guang Yang, Chen-Hsuan Hsu and Jorge Cayao, I had a great time working with you.

During my stay in RIKEN, I have spent a lot of time with people outside the group I was visiting. In particular, Matthieu Delbecq, Giles Allison, Marian Marx and Tomohiro Otsuka. The coffee break gatherings quickly became a daily highlight. The discussions about your experiments and guided lab tours were highly appreciated.

Thank you Ferdi Aryasetiawan and Rika Hayashi for your support while my family was staying with me in Lund. It made a world of difference.

I wish to also acknowledge the incredible support from my parents and brother, I would have accomplished much less had it not been for them. You continue to amaze and inspire me.

Finally, and most importantly, I want to thank Mai. Your unconditional love and support throughout the years are what made this thesis possible. You and Haruki have made my life richer than I ever could have imagined. Thank you.

Haruki, I look forward to our discussions.

Popular summary in English

Modern computers have been steadily shrinking in size owing to the ever increasing capability of fabricating transistors with a remarkable accuracy. Presently, the state-of-the-art transistors are approaching the size of a handful of atoms. On this scale, quantum physics dominates and presents a fundamental obstacle to traditional computer chips. However, this scale does not only imply a limitation - but it also opens up new possibilities.

The idea of a computer which can harness the rich physics that emerges on the microscopic scale has for a long time been a tantalising thought. The enthusiasm has been spurred by several theoretical predictions which indicate that a quantum computer for specific tasks would be exponentially faster than the traditional one. A prime example is Shor's algorithm, which can factorise large numbers in their prime factors efficiently. This is a notoriously difficult task for classical computers, so much so that modern cryptography relies on it being a practically impossible task for very large numbers.

Much research has been devoted to realising a device which can process quantum information on a chip, as an extension of the conventional computer. One compelling proposal is to use single electrons, artificially confined in a cage of only hundreds of atoms. Fabrication methods have grown sophisticated enough that these structures, referred to as quantum dots, can be constructed routinely. Complete control over how many electrons are in confinement has also been demonstrated, together with the ability to encode information onto individual electrons.

With this success, it may then be perplexing why quantum computers as a technology, despite being theoretically investigated since the 1960s, remains in its infancy. To understand this, it is necessary to understand the properties of quantum physics which enable the remarkable improvement promised by quantum computation.

In contrast to the classical bit taking values 1 or 0, a qubit, the basic unit of quantum information, is allowed to take the values 1, 0 or an arbitrary combination of them. This is referred to as the superposition principle. Moreover, quantum algorithms require entanglement: a phenomenon exclusive to quantum physics where two particles, which in the past have interacted, can no longer be described as two separate entities. These properties serve as the backbone of a quantum computer, and they share one detrimental feature - any measurement will cause

the quantum properties to vanish.

Quantum information is therefore extremely sensitive. For electrons confined in a quantum dot, the effects will typically vanish faster than a millionth of a second. To make matters worse, the entanglement of an electron pair is an elusive property that can only be revealed using a very complicated detector, which is hard to achieve in a microscopic device. This presents an intriguing theoretical challenge: to propose creative schemes which generate and detect entangled pairs of electrons, and control them sufficiently fast without resorting to direct measurements.

The aim of our work has been to face this challenge.

With the works in Papers I, II, and III we have aimed to facilitate detection of entanglement in devices comprising quantum dots. Our approach has been to study how the electric current traversing the device fluctuates when a voltage is applied. In contrast to the prevailing mindset that a noisy signal is bad, for us these fluctuations are a source of information. These fluctuations are namely related to how the constituent electrons of the current behave, by, e.g., showing if they arrive one by one or in pairs. We have used this phenomenon, to devise schemes which relate the measured fluctuations of spatially separated currents, to the existence of entangled electron pairs. In Paper IV we have investigated the control of the state of an electron in a quantum dot. In particular, we have investigated whether the control of an electron can be improved by design, by changing the shape of the quantum dot and placing a small magnet nearby.

Populärvetenskaplig sammanfattning på svenska

Dagens datorer har krympt i storlek i takt med den ständigt ökande kompetensen att tillverka transistorer med en anmärkningsvärd noggrannhet. Storleksskalan av nya transistorer börjar motsvara den av en handfull atomer. På denna skala dominerar kvantfysik, vilket är ett väsentligt hinder för de traditionella datorkomponenterna. Men detta innebär inte bara en begränsning - det öppnar även upp för nya möjligheter.

Datorer som kan utnyttja den kvantfysik som framträder på mikroskopisk skala har under lång tid varit en åtrovärd tanke. Entusiasmen har drivits av flera teoretiska undersökningar som tyder på att en 'kvantdator', för specifika uppgifter, skulle vara exponentiellt snabbare än en vanlig (så kallad klassisk) dator. Ett bra exempel på detta är Shors algoritm, som kan snabbt faktorisera mycket stora tal i deras primtalsfaktorer. Detta är en notoriskt svår uppgift för klassiska datorer. Säkerheten av dagens krypteringsalgoritmer bygger på antagandet att detta är en omöjlig uppgift för ett tillräckligt stort tal.

Mycket forskning har bedrivits med målet att förverkliga en anordning, som kan bearbeta kvantinformation och utföra kvantalgoritmer på ett chip, likt den klassiska datorn. Ett tilltalande förslag är att använda enstaka elektroner, artificiellt instängda i en bur av endast hundratals atomer. Metoderna att tillverka dessa mikroskopiska burar har blivit så pass sofistikerade, att dessa strukturer, som kallas kvantprickar, kan idag tillverkas rutinmässigt. Precis kontroll över hur många elektroner är i fångenskap har även demonstrerats, tillsammans med förmågan att koda information på enskilda elektroner.

Med dessa framsteg, kan det då verka förbryllande att kvantdatorer, trots teoretiska undersökningar sedan 1960-talet, fortfarande inte har förverkligats. För att förstå detta, är det nödvändigt att förstå de egenskaper av kvantfysik som möjliggör den anmärkningsvärda förbättring som utlovats av kvantdatorernas förespråkare.

Till skillnad från den klassiska enheten för information, en *bit*, som kan anta värdet 1 eller 0, så kan motsvarande enhet för kvantinformation, en *kvantbit*, bära på 1, 0 eller en kombination av dessa - ett så kallat superpositionstillstånd. Dessutom kräver kvantalgoritmer *sammanflätning* (entanglement på engelska): ett exklusivt kvantfysikikaliskt fenomen där två partiklar, som tidigare har samverkat, inte längre kan beskrivas som två separata enheter, utan de delar varandras egenskaper.

Dessa effekter utgör fundamentet för en kvantdator, och de delar en gemensam svaghet - en mätning får båda effekterna att försvinna.

Av den anledningen är kvantinformation extremt känslig. Kvanteffekterna för elektroner i en kvantprick försvinner vanligtvis snabbare än en miljarddels sekund. Detta försvåras ytterligare av att sammanflätning hos ett par av elektroner är en svårfångad egenskap, som endast avslöjas med hjälp av en mycket komplicerad detektor. Dessa detektorer är svåra att implementera på ett mikroskopisk chip. Detta är en spännande teoretisk utmaning: att föreslå kreativa tillvägagångssätt att generera och upptäcka sammanflätade elektronpar, samt kontrollera dem tillräckligt snabbt utan att tillgripa direkta mätningar.

Målet med vårt arbete har varit att bemöta denna utmaning.

Med arbetet i artikel I, II och III har vi haft som mål att underlätta detektion av sammanflätning i chip med kvantprickar. Vår strategi har varit att studera hur den elektriska strömmen som flödar genom chippet fluktuerar då en spänning är pålagd. I motsats till det vanliga tankesättet att brus i mätningen är dålig, så är dessa fluktuationer för oss en källa till information. Dessa variationer i strömmen är nämligen relaterade till hur de individuella elektronerna som utgör strömmen beter sig, om de exempelvis kommer en efter en, eller om de transporteras parvis. Vi har använt detta fenomen, för att utforma ett test som kan detektera förekomsten av elektronpar som är sammanflätade. I artikel IV har vi studerat styrningen av en elektrons tillstånd som befinner sig i en kvantprick. Specifikt har vi fokuserat på om det är möjligt att förbättra styrningen genom att ändra formen på den kvantprick som fångar elektronen, samt placera små magneter i närheten.

Chapter 1

Introduction

The topic to which this thesis aims to contribute is quantum information processing in nanoscale devices. The original ideas date back to the early 1980s, with the novel suggestion of R. P. Feynman [1], of realising a type of quantum analogue to the classical computer. Aside from the gains that come with using a quantum unit of information (later termed qubit), which also allows for superposition of logical states, he recognised that quantum physics is essential when attempting to, with a computer, simulate physics where quantum phenomena are prevalent. These ideas motivated future investigations into realising a type of 'quantum computer', which is believed to efficiently, not only simulate quantum physics but also solve computational problems that classical computers can not. Here the notions of efficient and inefficient solutions refer to the time complexity. An efficient solution will have an increasing computation time which is at most polynomial in the problem size [2].

Spurred by the idea of harnessing the computational power of quantum physics, the subject of quantum computation has developed into an active research field, with prolific studies in the 1980s and 1990s, resulting in the development of quantum algorithms. For some tasks, it was found, that the quantum algorithms would excel in comparison to their classical counterpart. A notable example is Shor's algorithm, which can find the prime factors of an integer N on a time scale which is polynomial in $\log N$ [3], a task the fastest classical algorithm solves on a time which scales almost exponentially in $\log N$ [4].

Despite a notable enthusiasm, these ideas, however, remain to a large extent theoretical, owing to the difficulty of preparing enough robust, connected qubits which can at the same time be coherently controlled. Various architectures are actively being pursued in the hopes of realising quantum computers [5]. Qubits have been realised in different physical systems, ranging from superconducting circuits [6] and vibrational states of trapped ions [7, 8] to the spin states of electrons in a solid state device [9, 10].

In this thesis, we focus on using the state of electrons trapped in quantum dots as logical qubit states (to be discussed in Chapter 3) [11, 12]. This is a compelling platform, owing to its potential for scalability where, e.g., an array of electrostatically defined quantum dots can be controlled by applying a varying voltage to nearby electrodes. Another advantage is the compatibility of these, in particular, silicon based, qubits with modern semiconductor electronics. However, there is a critical downside.

The major culprits for quantum dot based qubits are the Coulomb-, and hyperfine interactions. Inside a solid, electrons are surrounded by a perturbing environment of, e.g., vibrating ions of the crystal lattice and fluctuating nuclear spins. As a consequence, the qubit is highly susceptible to decoherence, the process by which the qubit retreats to a classical state. As an example, if the charge state of quantum dots is used to encode information, the fluctuating background charge will result in loosing the quantum information on the order of nanoseconds [13, 14].

While the above discussion paints a dire picture, recent advances in the fabrication of semiconductor devices have made the prospects of solid state qubit devices promising. Several groups have demonstrated a remarkable precision, allowing the limit of few trapped electrons to be explored [15] together with targeted coherent spin manipulation [16, 17]. The fabrication has become precise enough to routinely define qubits in quantum dots and to explore the idea of multiple quantum dots on the same chip [18]. However, for these systems to be viable, the errors induced by the background noise have to be accounted for and corrected. To this end, special protocols for error correction have been devised [2], which introduces a threshold that the coherence time has to surpass. With this, prolonging the coherence time of qubits, or, increasing the speed of coherent control, has become an active area of research [19, 20]. In Paper IV we explore ways of addressing this issue. In particular, we study a qubit defined by the spin of an electron residing on a quantum dot, which is controlled by an on-chip electric field. We investigate

if dot geometry and orientation of an applied magnetic field could improve the ratio of time required for coherent manipulation to the decoherence rate due to background charge noise.

Physically realising robust qubits is, however, not enough for quantum computation. Another essential component is entanglement, a type of correlations between particles which is only permitted in quantum physics. These quantum correlations are an indispensable resource for quantum algorithms. Experiments on detecting and generating the entanglement of electron pairs in solid state devices have, however, met limited success up to now. In particular, owing to the inherent problems described above, it remains a theoretical challenge to propose a feasible scheme that can unambiguously detect entanglement in pairs of transport electrons. Conventional entanglement detection schemes also present a significant engineering obstacle, as they typically require a versatile detector and many measurements.

With our work in the appended Papers I, II and III we have aimed to facilitate detection of entanglement in electron pairs in a transport setup. We present an entanglement detection model which relates the measured current noise to the presence of spin-entangled (Paper I) and orbitally entangled (Paper II) electron pairs. Additionally, we propose in Paper II a quantum dot based solid state device which both generates and detects entangled electron pairs, on a time scale much smaller than the reported decoherence time. With the work in Paper III, we further address the issue of a demanding detector. Here we propose a minimal detection scheme, which unambiguously detects entanglement in electrical conductors with only two current correlation measurements.

We return to the results of these works in Chapters 6 through 9, followed by an outlook in Chapter 10, with the preceding chapters dedicated to describing the theoretical methods we have employed.

Structure of the thesis

This thesis is naturally divided into two parts. The first part, chapters 2 through 5, introduces the basic theory which has been employed to obtain the results of the appended papers.

In Chapter 2, we present the preliminaries for the work on entanglement detection

in quantum dot devices. This chapter introduces the notion of entanglement, before describing methods for discerning whether two particles are entangled or not.

A lateral quantum dot structure in semiconductor heterostructures is introduced in Chapter 3, which will serve as common ground for the work we have conducted on quantum dot devices. We further present the technical preliminaries of Paper IV. In particular, we discuss the intrinsic spin-orbit interaction present in GaAs and silicon and how it enables electrical control of the electron spin. In addition, we describe the Hamiltonian for the piezoelectric interaction and deformation potential, the two types of electron-phonon interaction which play a prominent role in Paper IV.

For our work on the transport of electrons through nano-scale devices, the principal tool has been the Markovian Quantum Master Equation, which is introduced in Chapter 4.

In Chapter 5 the theory underlying electron counting statistics is described. In particular, we show how to extend the Quantum Master Equation of preceding chapter by including 'counting fields'. This technique allows us to study the transport statistics in the quantum dot devices described in Papers I and II. Furthermore, we introduce the concept of current noise, in particular shot noise, and how it is theoretically quantified. Shot noise plays a crucial role in our entanglement detection schemes of transport electrons.

The second part of the thesis provides an overview of the main results of the appended papers. Here the papers are summarised separately in chapters 6 through 9, before concluding with an outlook in Chapter 10.

Chapter 2

Entanglement

Entanglement is a central notion which permeates the major part of this thesis. As such this chapter is devoted to briefly introduce the concept and the formalism which we have used in Papers I, II and III. While a rich topic, here the scope will be limited to presenting the basics of the methods we have employed in our work, pertaining to Papers I-III.
The term entanglement was introduced by Schrödinger in 1935 [21], to refer to the peculiar property of states allowed by quantum mechanics, where the total state of a composite system cannot be described as the product of states of its constituent parts. While at first glance appearing to be an innocuous technicality, the consequence of such states has led to some questioning the validity of quantum mechanics as a complete description of physics.

Schrödinger's investigation into these states was prompted by another famous paper from the same year, authored by Einstein, Podolsky and Rosen (EPR) [22]. In their paper, they explore the implications of correlations made accessible by quantum mechanics. They note that if two spatially separated systems A and B had been interacting in the past, resulting in an entangled state, a measurement of system A would unavoidably affect the uncertainty of system B, despite the arbitrary distance between them. They voiced concern that quantum theory can therefore not be considered a complete description of physical reality. To ensure a consistent theory, a proposed general framework would have to abandon the idea of wavefunctions as containing all physical information.

While the proposal of a more general theory at first appears to border on metaphysics, it was found by J.S. Bell that in fact quantum mechanics enables a quantitative test, which clearly differentiates quantum mechanics from the proposed theory. Using the hypothesis of EPR he identified that a theory with a set of local hidden variables (LHV) satisfies the criteria of the proposed complete theory, which he compared with predictions of quantum mechanics. Using a reformulation of the EPR thought experiment in terms of two atoms with known total spin zero, due to D. Bohm [23], in his seminal work he proposes an experiment which uses the correlation measurements of separate particles [24]. Bell showed that an upper bound is obtained for correlations within a LHV theory, here referred to as classical correlations, which is violated by the predictions of quantum physics. The violation of the so-called Bell inequality has since been studied in many experiments to verify that in fact the correlations predicted by quantum mechanics, and not by a LHV theory, agree well with experiments.

It should, however, be stressed, that the validity of applying the measurement results straightforwardly to the Bell inequality, can be questioned. To fully prove the absence of a LHV theory, many experimental imperfections have to be taken into account to ensure that no possible loopholes exist which could again allow for a LHV theory to be reformulated. Closing these loopholes is a current area of research, with an increasing number of experiments reporting loophole-free Bell inequality violations [25, 26, 27].

Aside from disproving LHV theories, there is a growing interest in studying correlations with the primary intention to detect entangled states, disregarding loopholes which enable a LHV theory. For this purpose, new methods for entanglement detection have emerged. A prime example is the approach of entanglement witnesses, to be discussed later in this chapter. It is important to note that, since not all entangled states imply a violation of the Bell inequality [28], the approach of entanglement witnesses is more suited for the task of detecting entanglement.

So far, detecting the existence of entanglement has been presented here as a fundamental curiosity. In reality, an essential motivation for generating and detecting entanglement is the possible technological applications. With the discoveries of e.g. superdense coding, quantum teleportation and entanglement-assisted error-correction [2], the role of entanglement was recognised to be the essential resource for quantum information protocols. This aspect of entanglement, as a precious resource for future quantum information processing devices, has served as the prin-

cipal motivation for our work on entanglement detection in Papers I, II and III.

While there is active research into generation and detection of entanglement with three or more particles [29], in this thesis we restrict ourselves to the phenomenon of two-particle-, or bipartite entanglement.

2.1 Entanglement definitions

In accordance with Schrödinger's observation, the definition of a pure entangled state is a state which cannot be descibed as a product of its subsystems, that is

$$|\Psi_E\rangle \neq |\Psi_A\rangle \otimes |\Psi_B\rangle, \tag{2.1}$$

where the non-entangled state is often referred to as separable. Here $\otimes$ is the direct product, which is implied when writing $|A\rangle|B\rangle$, and $|\psi_k\rangle$ is the state of subsystem k.

Typically it is necessary to consider a statistical mixture of states, rather than a single pure state. This is in particular the case for our work related to entanglement. In Papers I, II and III we consider a small quantum system which is in contact with a large reservoir of electrons. By tracing out the degrees of freedom of the large reservoir, we obtain an effective description of the small subsystem in terms of a, reduced, density matrix, which in general is not a pure state. The reduced density matrix correctly describes the outcome of any measurement on the smaller system [2]. A general density matrix ρ, can be decomposed into a sum of states $|\psi_i\rangle$, weighted by their statistical probability p_i,

$$\rho = \sum_i p_i |\psi_i\rangle\langle\psi_i|, \quad \sum_i p_i = 1, \quad p_i \geq 0. \tag{2.2}$$

The density matrix operator is a convenient state representation, and corresponds to a pure state when $\mathrm{tr}\left[\rho^2\right] = 1$ is satisfied. The expectation value of an operator V in a system described by a, possibly mixed, state ρ is $\langle V\rangle = \mathrm{tr}[V\rho]$.

In the density matrix picture the definition of entanglement for pure states, i.e. product of states in the subsystems, is not straightforwardly applicable. Instead, as introduced by Werner [28, 29], the definition is extended to density matrices, as the state which cannot be decomposed as a mixture of separable pure states $|\Psi^i_\alpha\rangle$,

$$\rho_{sep} = \sum_i p_i \varrho^i_A \otimes \varrho^i_B, \quad \varrho^i_\alpha = |\Psi^i_\alpha\rangle\langle\Psi^i_\alpha|. \tag{2.3}$$

Before describing how entangled mixed states, i.e. states for which $\mathrm{tr}[\rho^2] < 1$, can be detected, we introduce a convenient tool for studying entanglement of pure states.

2.2 Schmidt decomposition

Using the Schmidt decomposition theorem [2] theorem we are able to decompose the pure states of a composite system as

$$|\Psi\rangle = \sum_i s_i |\psi_A^i\rangle |\psi_B^i\rangle, \tag{2.4}$$

which is called the Schmidt form. Here the number of s_i's corresponds to the Schmidt number, or rank, from which we can infer if a state is entangled. Specifically, a state is a product state if and only if its schmidt number is unity. As an example, for the maximally entangled triplet state,

$$|\psi_{\mathrm{triplet}}\rangle = (|11\rangle + |00\rangle)/\sqrt{2}, \tag{2.5}$$

the Schmidt rank is naturally greater than unity. This Schmidt form decomposition is unique if and only if all s_i's are different.

2.3 Bell inequality

Here we briefly describe the basic idea behind the Bell inequality, the first feasible test of entanglement in terms of correlation measurements. The description here follows [30, 31], and takes a pair of spin-$1/2$ particles A and B with a known total spin zero, as our composite system.

The two correlated particles are sent in opposite directions where the spins of the individual particles are detected at two spatially separated detectors A and B, along variable spin quantisation axes $\mathbf{a}$ and $\mathbf{b}$ respectively. The expectation values of A and B are ± 1, that is, the measured spin is either parallel or antiparallel to $\mathbf{a}$ and $\mathbf{b}$ respectively.

The principal idea is, by presuming the existence of a hidden variable which is responsible for the measured statistical correlations, we may write the resulting

correlation function as $E(\mathbf{a},\mathbf{b}) = \int A(\mathbf{a},\lambda)B(\mathbf{b},\lambda)p(\lambda)d\lambda$. Here it is implied that the measurement outcomes at detector A (B) should only depend on the settings of detector A (B) and the hidden variable λ, as the detectors can be separated arbitrarily far from each other. In addition, the probability distribution for the ensemble of particle pairs being emitted towards the detectors should not depend on the detector settings. From these assumptions it is possible to choose two additional axes $\mathbf{a}'$ and $\mathbf{b}'$ to formulate a Bell inequality,

$$S = |E(\mathbf{a},\mathbf{b}) - E(\mathbf{a},\mathbf{b}') + E(\mathbf{a}',\mathbf{b}) + E(\mathbf{a}',\mathbf{b}')| < 2, \tag{2.6}$$

which specifies an upper bound for the statistical correlations in a LHV theory. To measure this quantity in practice, in the proposed experiment, the correlation functions $E(\mathbf{a},\mathbf{b})$ correspond to

$$E(\mathbf{a},\mathbf{b}) = \frac{n_{++} - n_{+-} - n_{-+} + n_{--}}{n_{++} + n_{+-} + n_{-+} + n_{--}}. \tag{2.7}$$

Here n_{+-} denotes the coincidence detection, where spin along (spin opposite to) the quantisation axis $\mathbf{a}$ ($\mathbf{b}$) is measured at detector A (B), and other terms defined analogously. If the resulting quantity S is greater than 2, the Bell inequality is said to be violated, and LHV theories are ruled out. It can be shown that by permitting a quantum mechanical treatment, the proper bound is the Tsirelson's bound[1] $|S| < 2\sqrt{2}$ [32]. This upper limit is achieved for a certain set of states,

$$\frac{1}{\sqrt{2}}\left(|\downarrow\uparrow\rangle \pm |\uparrow\downarrow\rangle\right), \quad \frac{1}{\sqrt{2}}\left(|\uparrow\uparrow\rangle \pm |\downarrow\downarrow\rangle\right), \tag{2.8}$$

which are referred to as the Bell states, or maximally entangled states. Since a violation of the Bell inequality will imply entanglement (in general the reverse does not hold [28]), this constitutes a solid scheme for detecting entangled states.

2.4 Quantum state tomography

An alternative to the Bell inequality is to use information about the detected state, in combination with the definition of an entangled state. For this it is possible to employ quantum state tomography (QST). The fundamental idea is to relate the matrix elements of the density matrix to an observable.

[1]Named after B.S. Tsirelson, or B.S. Cirel'son depending on transliteration.

Continuing with the picture of two spin 1/2-particles, in an ideal experiment an identical state is prepared and repeatedly sent to two adjustable, spin sensitive, detectors. After a series of measurements where an identical state is prepared repeatedly, the relative frequency of the outcome can be used to infer a density matrix which would fully reproduce the measurement results [33]. That is, the state can be represented as

$$\rho = \frac{(1 + \mathbf{a} \cdot \boldsymbol{\sigma}) \otimes (1 + \mathbf{b} \cdot \boldsymbol{\sigma})}{4}, \quad \boldsymbol{\sigma} = (\sigma_x, \sigma_y, \sigma_z) \tag{2.9}$$

where the vector components a_i (b_i) denote spin measurements at detector A (B) along direction $i = x, y, z$.

The clear benefit of QST is that complete information about the two-particle state is made accessible. This in turn enables also entanglement tests which require non-unitary operations [29]. An example is Peres' criterion of separability, which has a greater detection range than Bell's inequality [34], where partial transposition is used[2]. In addition, equipped with the two-particle state, entanglement measures, discussed below, can be used to quantify the amount of entanglement present in the system [35].

However, the amount of measurements necessary for a complete tomographic state reconstruction, in conjunction with a possibility for inaccurate measurements, forces a very stringent tolerance for measurement errors. In Paper I we further discuss the viability of QST in cases of non-ideal detector efficiencies, where we show how non-ideal detector efficiencies can lead to false signatures of entanglement.

2.5 Concurrence

In addition to detecting the presence of an entangled state, it is possible to quantify the amount of entanglement of a state ρ via an entanglement measure $\mathcal{E}(\rho)$. While there are different measures for entanglement, they share a set of required properties. The most relevant properties for our work are

[2]Partial transposition is a non-unitary operation which transforms $\rho = \sum_i p_i \rho_A^i \otimes \rho_B^i$ into the Hermitian matrix $\sigma = \sum_i p_i [\rho_A^i]^T \otimes \rho_B^i$. If ρ is separable, it holds that σ is a density matrix. Hence a negative eigenvalue of σ is a signature of an entangled state.

- Vanish for product states. $\mathcal{E}(\rho_1 \otimes \rho_2) = 0$
- Entanglement of a state is invariant under a local basis change. $\mathcal{E}(U_1 \otimes U_2 \rho U_1^\dagger \otimes U_2^\dagger) = \mathcal{E}(\rho)$
- Entanglement does not increase under local operations and classical communication (LOCC) operations.

In the Papers II and III we have used a convenient entanglement measure for bipartite states, introduced by W. K. Wooters in Ref. [36]. The strength of the so-called concurrence is its tractable expression for the entanglement of a state. Explicitly for a pure state ψ, the concurrence reads,

$$C(\psi) = 2|c_{00}c_{11} - c_{10}c_{01}|, \quad \psi = c_{00}|00\rangle + c_{10}|10\rangle + c_{01}|01\rangle + c_{11}|11\rangle. \tag{2.10}$$

What makes concurrence particularly suitable for our work is that it can be straightforwardly extended to a statistical mixture of states. In this scenario concurrence of a state takes the form,

$$C(\rho) = \max(0, \Lambda_1 - (\Lambda_2 + \Lambda_3 + \Lambda_4)), \quad \Lambda_1 > \Lambda_2, \Lambda_3, \Lambda_4, \tag{2.11}$$

where the Λ_i's are the eigenvalues of the operator,

$$R = \sqrt{\sqrt{\rho}(\sigma_y \otimes \sigma_y)\rho^*(\sigma_y \otimes \sigma_y)\sqrt{\rho}}. \tag{2.12}$$

As an illustrative example, we consider the Werner state,

$$\rho_w = \frac{p}{2}(|10\rangle - |01\rangle)(\langle 10| - \langle 01|) + (1-p)\hat{1}/4, \tag{2.13}$$

describing a statistical mixture of a singlet state with probability p and a completely mixed state with probability $(1-p)$. The state ρ_w describes the typical scenario where a singlet state is studied in a noisy environment. The interesting question is; how much noise is permitted before the statistical mixture can be decomposed as a mixture of separable states? Concurrence allows us to quantify this condition. For example, the concurrence of ρ_w reads,

$$C(\rho) = \max(0, \frac{3p-1}{2}). \tag{2.14}$$

From this result we note that Werner states ρ_w are entangled if $p > 1/3$, and equivalent to a combination of separable states otherwise.

2.6 Entanglement witness

By formulating Bell's inequality in the form of Eq. (2.6), we can infer that an operator exists which clearly differentiates classical correlations from quantum correlations, on the basis of violating LHV theories. A natural question is then - if we are only interested in detecting non-separable states, as opposed to also ruling out a LHV theory, is it possible to construct an operator which directly targets the non-separability of a state?

This describes the underlying principle for the alternative approach of entanglement witnesses [35]. An entanglement witness W, or witness operator for short, is a self-adjoint operator which is mathematically designed to fulfill the criterion,

$$\min_{\varrho} \mathrm{tr}\left[W\varrho\right] > \min_{\rho} \mathrm{tr}\left[W\rho\right] \quad \text{or} \quad \max_{\varrho} \mathrm{tr}\left[W\varrho\right] < \max_{\rho} \mathrm{tr}\left[W\rho\right] \tag{2.15}$$

That is, W is an operator for which the expectation value of a given entangled state ρ_e lies outside the range of separable states ϱ. We stress here that it is enough to consider pure separable states,

$$\min_{\phi_a,\phi_b} \langle\phi_a|\langle\phi_b|W|\phi_a\rangle|\phi_b\rangle > \lambda_{\min} \quad \text{or} \quad \max_{\phi_a,\phi_b} \langle\phi_a|\langle\phi_b|W|\phi_a\rangle|\phi_b\rangle < \lambda_{\max}, \tag{2.16}$$

where $\lambda_{\min}$ ($\lambda_{\max}$) is the smallest (largest) eigenvalue of the witness operator W. Furthermore, it can be shown that a Bell inequality can be considered a non-optimal witness [35], since there exist entangled states which permit a LHV theory and thereby cannot be detected. Meanwhile, in Ref. [37] the completeness of witnesses was proved. This theorem implies that for each entangled state, there exists an entanglement witness can detect it.

In addition to these properties, a witness operator allows in principle for an entanglement detection scheme with fewer correlation measurements. The power of witnesses in facilitating detection is what motivated our work resulting in Paper III. There we employ the witness operator approach to investigate the minimum amount of current cross correlation measurements required to detect entangled states in electrical conductors.

Chapter 3

Lateral quantum dots

With the precision of current nanoscale fabrication methods, it is possible in semiconductors to design a confinement potential on a length scale comparable to the wavelength of confined electrons. These artificial structures, referred to as quantum dots, are a central component of this thesis. Specifically, we consider lateral quantum dots. These dots can be electrostatically defined by applying a negative voltage to metal gate electrodes, which deplete a local region of electrons in a Two-Dimensional Electron Gas (2DEG) that is localised at the interface of two semiconductors. One such heterostructure, which is frequently used, is GaAs/AlGaAs. In current experiments the size of such a dot can be on the order of $10-100$nm in GaAs, which can be compared with the Fermi wavelength $\lambda_{\text{Fermi}} \sim 40$nm [15, 38].

Owing to the close confinement in all directions, quantum dots can display notable quantum effects. The energy spectrum is nearly discrete (broadened by, e.g., a finite lifetime of residing in the dot) and there is a sizable charging energy. Charging energy corresponds to the energy required to introduce an additional electron to the dot, which can result in a complete suppression of currents in transport experiments, known as the Coulomb blockade.

The quantum effects of the dots are most prominent in nearly closed dots, where the conductance G is much smaller than the quantum of conductance, that is $G \ll G_Q = 2e^2/h$. This corresponds to a quantum dot structure with a very narrow opening, resulting in a weak tunnel junction connecting the quantum dot

and free electrons of the 2DEG outside it. Controlling the number of electrons on a dot is experimentally feasible. Lateral quantum dots in the few electron regime have already been demonstrated, where a complete depletion of the dot population one electron at a time was achieved [39]. Theoretically, this is a desirable setup. In this regime, fluctuations in dot occupation are suppressed, and we may employ a picture where the dot state can be entirely described in terms of the number of charges residing on the dots. We can accurately model this transport scenario using a quantum master equation, which we will discuss in Chapter 4.

The above-mentioned effects are also essential ingredients for the entanglement detection schemes proposed in Papers I and II. In particular, by i) Restricting the quantum dot electron population to single occupancy, and ii) Suppressing unwanted single particle transport on energetic grounds, leaving a dominant contribution from a sought-after cotunneling process, where two electrons cooperate and tunnel together.

Moreover, in addition to measuring the conductance, experiments are capable of resolving the statistical profile of the current. For example, in Ref. [40], a quantum point contact, placed in the vicinity of a quantum dot, senses single charge transfers at a frequency of 30kHz. This scheme captures the complete statistical description of an electric current up to $I = 4.8$fA (limited by the sampling rate), using what is known as Full Counting Statistics. We introduce Full Counting Statistics (an important notion in Papers I, II, and III), in Chapter 5.

Another intriguing aspect of quantum dots is the spin degree of freedom of trapped electrons. In their seminal paper [11], D. Loss and D. DiVincenzo proposed the dot spin as a promising candidate to realise controllable qubits. A distinctive advantage of using electron spins in a solid is the relatively long coherence time, a main motivation for our focus on spin entanglement in Paper I. For lateral quantum dots in GaAs, the coherence time for spin qubits is on the order of 1μs [15], in contrast to $\sim$ 1ns for a qubit using the charge states [13, 14]. .

The proposal of Loss and DiVincenzo stimulated extensive efforts to experimentally achieve robust, controllable, spin qubits in semiconductor quantum dots. Current experiments are able to routinely define a spin qubit using a quantum dot [15]. The rotation of a single spin in lateral quantum dots via electron spin resonance has already been demonstrated [9], using an oscillating on-chip magnetic field. An ability to address individual spins in a quadruple quantum dot structure [16] has also been achieved using micromagnets.

In addition, recent experiments have reported successful coherent manipulation of the spin with an electric field in lateral quantum dots [41], using Electric Dipole Spin Resonance (EDSR). In the EDSR scheme, to be discussed below, a local oscillating electric field manipulates the spin via the intrinsic spin-orbit interactions, arising from bulk (Dresselhaus-type) [42] and structural asymmetry (Rashba-type) [43]. Targeted spin rotation via EDSR opens up the possibility of an all-electrical control of a spin qubit, where the local on-chip electric fields can be generated by applying an oscillating voltage to electrodes near the target spin [44].

However, the intrinsic spin-orbit interaction also has a notable downside; namely, the spin qubit becomes vulnerable to the charge fluctuations of its environment. One such source of perturbation is the spin-orbit interaction mediated coupling between the spin and lattice vibrations, or phonons. This, in general anisotropic, coupling results in an additional spin relaxation channel. The competition between coherent EDSR spin manipulation and phonon-induced spin relaxation is the subject of Paper IV. Here we seek to optimise the product of the induced Rabi frequency, discussed below, and the spin lifetime, which we designate as a figure of merit for spin qubit devices.

In the following, we will introduce preliminaries for the model employed in Paper IV. Starting with our model for a singly occupied quantum dot, we follow with an introduction to the quasi-two-dimensional spin-orbit interaction. With the spin-orbit interactions introduced, we describe the EDSR and relevant electron-phonon couplings.

3.1 Quantum dot spin qubit

The quantum dot considered in Paper IV is a lateral quantum dot, where the electrons of a 2DEG at the interface of two heterostructures are strongly confined in the growth direction (which we take to be the z-axis). The dot is depleted of all electrons but one, whose spin degree of freedom is used to define a spin qubit. The two-dimensional biharmonic potential is a suitable model to describe the single particle Hamiltonian of the trapped electron. With applied magnetic field $\mathbf{B}$, for now disregarding spin-orbit interactions, the Hamiltonian reads

$$H = \frac{(-i\hbar\nabla_r + e\mathbf{A})^2}{2m^*} + \frac{\hbar^2}{2m^*}\left(\frac{x'^2}{l_{x'}^4} + \frac{y'^2}{l_{y'}^4}\right) + \frac{g^*\mu_B}{2}\boldsymbol{\sigma}\cdot\mathbf{B}, \tag{3.1}$$

where m^* is the effective mass, $\mathbf{A}$ is the vector potential, $\boldsymbol{\sigma} = (\sigma_x, \sigma_y, \sigma_z)$ is the vector of Pauli matrices and $l_{x'}$ ($l_{y'}$) is the confinement length along the dot major (minor) axis x' (y'). Here we distinguish the dot coordinates x' and y' from the crystallographic axes $x \parallel [100]$ and $y \parallel [010]$. Owing to the strong confinement along the growth direction, we can ignore any orbital effects by considering an in-plane magnetic field, $\mathbf{B} = B(\cos\beta, \sin\beta, 0)$.

To study effects of anisotropy attributed to the confinement potential shape, we introduce the ellipticity parameter $\epsilon = 1 - (l_{y'}/l_{x'})^4$, where $\epsilon = 0$ describes a circular geometry, and elliptical geometry for all $\epsilon > 0$. With these ingredients in place, the effective potential which the trapped electron will experience is,

$$H = \hbar\omega_{x'}\left(n_{x'} + \frac{1}{2}\right) + \hbar\omega_{y'}\left(n_{y'} + \frac{1}{2}\right) + \frac{g^*\mu_B}{2}\boldsymbol{\sigma}\cdot\mathbf{B}. \tag{3.2}$$

Here $n_{x'}$ and $n_{y'}$ correspond to the number operators of the two harmonic oscillators with characteristic frequencies $\omega_{x'} = \hbar/m^* l_{x'}^2$ and $\omega_{y'} = \hbar/m^* l_{y'}^2$ respectively. From expression it is clear that H is diagonal in the eigenbasis of the harmonic oscillators $|\phi_{n_{x'},n_{y'},s}\rangle = |n_{x'}n_{y'}\rangle|s\rangle$, where s is the spin projection along the applied magnetic field $\mathbf{B}$. From the confinement Hamiltonian H, we note that an electric field will not affect the spin. To obtain a coupling of the spin to an applied electric field, the presence of spin-orbit interactions is crucial.

3.2 Spin-orbit interactions

The presence of an intrinsic spin-orbit coupling in semiconductor heterostructures ensures that the spin and motion of an electron can no longer be considered decoupled. For lateral quantum dots defined at the heterostructure interface, due to inversion asymmetry along the growth direction, a coupling term emerges,

$$H_R = \frac{\hbar}{2m^* l_r}(p_x\sigma_y - p_y\sigma_x). \tag{3.3}$$

This term describes the Rashba-type spin-orbit coupling, and is directly applicable to our effective two-dimensional model. Here we have introduced l_r as the Rashba spin-orbit length, to parametrise the spin-orbit strength.

In Ref [45] it was further shown that bulk inversion asymmetry yields an additional term in the Hamiltonian, the spin-orbit coupling

$$H_D^{3D} \propto p_x(p_y^2 - p_z^2)\sigma_x + p_y(p_z^2 - p_x^2)\sigma_y + p_z(p_x^2 - p_y^2)\sigma_z, \tag{3.4}$$

where x, y, and z are here oriented along the crystallographic directions [100], [010], and [001], respectively. To obtain an effective two-dimensional Hamiltonian, H_D^{3D} is averaged along the growth direction. We obtain then a spin-orbit interaction Hamiltonian with the linear,

$$H_D^{2D} \propto \langle p_z^2 \rangle (p_y\sigma_x - p_x\sigma_y) = \frac{\hbar}{2m^* l_d}(p_x\sigma_x - p_y\sigma_y), \tag{3.5}$$

and cubic,

$$H_{cD}^{2D} \propto p_x p_y^2 \sigma_x - p_y p_x^2 \sigma_y, \tag{3.6}$$

Dresselhaus spin-orbit terms. In Paper IV we have disregarded the cubic Dresselhaus term on the basis of strong confinement along the growth direction, such that $\langle p_z^2 \rangle \gg p_x^2, p_y^2$ [15].

Here we remark on the presence of a Dresselhaus spin-orbit term for the quantum dots in Si/SiGe considered in Paper IV. While the crystal structure of silicon does not possess the bulk inversion asymmetry, a generalized Dresselhaus term appears in the quasi-two-dimensional Hamiltonian [46]. The generalised Dresselhaus term is identical in form to H_D^{2D}, and is therefore in this thesis referred to as simply the Dresselhaus term.

3.3 Electric Dipole Spin Resonance

The robustness of spin in a solid is in part due to the lack of direct coupling between electric fields and spin, the background charge noise cannot induce a transition between the bare spin levels. This in turn also implies that to control the spin requires a local magnetic field. Controlling the spin using electric fields is, however, possible with the aid of an indirect transition, mediated by the spin-orbit interactions. For the quantum dots considered in Paper IV, the spin-orbit interactions can be considered a weak perturbation, which leave the spin states almost well defined. Before evaluating the perturbative correction, we first transform the Hamiltonian using a unitary transformation,

$$U = \exp\left(i\mathbf{n}_{so} \cdot \boldsymbol{\sigma}\right), \quad \mathbf{n}_{so} = \left(\frac{x}{l_d} - \frac{y}{l_r}, \frac{x}{l_r} - \frac{y}{l_d}, 0\right). \tag{3.7}$$

The spin-orbit vector $\mathbf{n}_{so}$ can be interpreted as a position dependent spin rotation axis. The transformed Hamiltonian is,

$$H_{\text{eff}}^{\text{so}} = U(H_R + H_D^{2D})U^\dagger = \mu_e(\mathbf{n}_{so} \times \mathbf{B}) \cdot \boldsymbol{\sigma} - \frac{\hbar^2}{4m}\left(\frac{1 + l_z\sigma_z}{l_r^2} + \frac{1 - l_z\sigma_z}{l_d^2}\right), \tag{3.8}$$

where the orbital momentum $l_z = -i(x\partial_y - y\partial_x)$ is in units of $\hbar$ and $\mu_e = g^*\mu_B/2$ is the effective magnetic moment. The first effective term is proportional to the applied magnetic field, with a proportionality which is small for the semiconductor quantum dots we have studied. However, despite the negligible energy contribution, it plays an important role as it couples opposite spins.

In Paper IV we consider a spin qubit defined by the lowest spin pair, $|\Psi_\uparrow\rangle$ and $|\Psi_\downarrow\rangle$. An oscillating electric field $\mathbf{E}(t)$ is applied, which drives Rabi oscillations between these states. We model the electric field with a dipole potential,

$$H_{\text{dipole}} = e\mathbf{E} \cdot \mathbf{r} \cos \omega t. \tag{3.9}$$

Treating $H_{\text{eff}}^{\text{so}}$ as a perturbation, we obtain the on-resonance Rabi frequency $\Omega = \hbar^{-1}\langle\Psi_\uparrow|e\mathbf{E} \cdot \mathbf{r}|\Psi_\downarrow\rangle$ to leading order in the spin-orbit interaction,

$$\Omega = e \sum_{\alpha \neq 00\downarrow} \langle\phi_{00\uparrow}|\mathbf{E}\cdot\mathbf{r}|\phi_\alpha\rangle\langle\phi_\alpha|H_{\text{eff}}^{\text{so}}|\phi_{00\downarrow}\rangle \left(\frac{1}{\varepsilon_{00\downarrow} - \varepsilon_\alpha} - \frac{\tau_{H_{\text{eff}}^{\text{so}}}\tau_{\mathbf{r}}}{\varepsilon_{00\uparrow} - \varepsilon_{\bar{\alpha}}}\right), \tag{3.10}$$

where the notation $\alpha = \{n_{x'}, n_{y'}, s\}$ and $\bar{\alpha} = \{n_{x'}, n_{y'}, -s\}$ is used. We have used the so called Van Vleck cancellation method [47], which allows us to discard some terms of the perturbative correction based on symmetry arguments. Here τ_o denotes how operator o transforms under a time reversal operation. For the quantum dots considered in Paper IV, the orbital excitation energy is far greater than the Zeeman splitting energy. Then, since $\tau_{\mathbf{r}} = 1$, we obtain that only the term $\bar{H}_{\text{so}}^{\text{eff}} = \mu_e(\mathbf{n}_{\text{so}} \times \mathbf{B}) \cdot \boldsymbol{\sigma}$ gives a non-vanishing contribution. The Rabi frequency is

$$\Omega = \sum_{\alpha \neq 00\downarrow} \langle\phi_{00\uparrow}|e\mathbf{E} \cdot \mathbf{r}|\phi_\alpha\rangle\langle\phi_\alpha|\bar{H}_{\text{so}}^{\text{eff}}|\phi_{00\downarrow}\rangle \frac{2}{\varepsilon_{00} - \varepsilon_{n_{x'}n_{y'}}}. \tag{3.11}$$

With this result, we have obtained the expression for the Rabi frequency, Eq. (9) in Paper IV, which we use to quantify the speed of spin qubit control.

3.4 Electron-phonon interactions

When considering a spin qubit defined in a lateral quantum dot, it is necessary also to take into account the perturbing influence of its environment. In Paper IV we investigate in particular the role of phonons on the relaxation of a spin qubit. Here we introduce the two important electron-phonon couplings which we have studied in Paper IV, the coupling of longitudinal and transversal acoustic phonons to electrons via deformation potential and piezoelectric coupling. Specifically, our focus is on quantum dots defined in Si/SiGe and GaAs heterostructures. For both electron-phonon couplings, the strain of the crystal is the core quantity. We describe the strain in terms of a strain tensor $\hat{\varepsilon}$, with components defined as,

$$\varepsilon_{ij} = \frac{1}{2}\left(\frac{\partial u_i}{\partial r_j} + \frac{\partial u_j}{\partial r_i}\right), \tag{3.12}$$

which, due to symmetry of the tensor, can be expressed in the six component notation

$$\begin{array}{lll} \varepsilon_1 = \varepsilon_{xx} & \varepsilon_2 = \varepsilon_{yy} & \varepsilon_3 = \varepsilon_{zz} \\ \varepsilon_4 = \varepsilon_{zy} = \varepsilon_{yz} & \varepsilon_5 = \varepsilon_{zx} = \varepsilon_{xz} & \varepsilon_6 = \varepsilon_{xy} = \varepsilon_{yx}. \end{array} \tag{3.13}$$

The strain tensor can further be expressed in terms of the quantised phonon modes via the lattice displacement vector $\mathbf{u}$,

$$\mathbf{u}(\mathbf{r}) = \sum_{\mathbf{q},\lambda} \sqrt{\frac{\hbar}{2V\rho q c_\lambda}} \mathbf{e}_{\mathbf{q},\lambda} \left[b^\dagger_{\mathbf{q},\lambda} + b_{-\mathbf{q},\lambda} \right] e^{i\mathbf{q}\cdot\mathbf{r}}, \tag{3.14}$$

where $b_{\mathbf{q}\lambda}$ is the phonon annihilation operator, V is the crystal volume, ρ is the mass density, and c_λ is the speed of sound. Here $\mathbf{q}$ denotes the wave vector of the phonon mode and λ is the phonon polarisation, with l for longitudinal acoustic, $t1$ and $t2$ being the two transversal acoustic modes. The unit polarization vectors are

$$\mathbf{e}_l = q^{-1}(q_x, q_y, q_z), \quad \mathbf{e}_{t1} = \mathbf{e}_z \times \mathbf{e}_l / |\mathbf{e}_z \times \mathbf{e}_l|, \quad \mathbf{e}_{t2} = \mathbf{e}_l \times \mathbf{e}_{t1}, \tag{3.15}$$

where we choose $\mathbf{e}_z$ to denote the growth direction of the heterostructures we study.

3.4.1 Deformation potential

The first electron-phonon coupling considered here, is the deformation potential. While it appears in both GaAs and Si/SiGe dots, in the following, we will focus on silicon, where it plays a more notable role. In the limit of long wavelengths, the acoustic phonons will correspond to a deformation of the crystal. Deformation potential theory states that the deformation will result in energy shifts of the conduction and valence bands [48]. To linear order in the deformation, we can account for energy change with the strain tensor and express the energy shift of the conductance band as,

$$\delta E = \sum_{j=1}^{6} \Xi_j \varepsilon_j, \tag{3.16}$$

where Ξ_j are the deformation potential coefficients, describing the energy shift induced by the strain ε_j. In addition to the symmetries of the strain tensor, by taking into account the symmetries of the crystal structure we limit the amount of independent Ξ_j coefficients. Specifically, for silicon, the energy shift along the conduction band minimum is expressed by only two terms [48, 49].

Moreover, the quantum dots we consider in Paper IV, are formed in a Si/SiGe heterostructure grown along the crystal axis [001]. In such a structure, the degeneracy of the conduction band minimum in silicon[1] is naturally lifted by a lattice mismatch at the interface of the Si/SiGe heterostructure. The six-fold valley degeneracy is reduced to a two-fold band minimum along the growth direction [53]. The remaining two-fold degeneracy can be further lifted by an asymmetric confinement potential [54]. This allows an effective single valley treatment of the Si/SiGe quantum dot, where the energy shift is of the form,

$$\delta E = \Xi_d \mathrm{tr}[\hat{\varepsilon}] + \Xi_u(\boldsymbol{\kappa} \cdot \hat{\varepsilon} \cdot \boldsymbol{\kappa}), \tag{3.17}$$

where $\mathrm{tr}[\hat{\varepsilon}] = \sum_{i=1}^{3} \varepsilon_i$ and $\boldsymbol{\kappa}$ is a unit vector parallel to the crystallographic axis [001], and Ξ_d, Ξ_u are the associated deformation potential coefficients. Using the expression for the lattice displacements in Eq. (3.14) together with the definition of the strain tensor in Eq. (3.12), we obtain the deformation potential electron-

[1] The degeneracy of the conduction band minimum, referred to in literature as the valley degeneracy, is a known obstacle to using silicon-based quantum dots as spin qubits [50, 51, 52].

phonon interaction Hamiltonian,

$$H_{\mathrm{e-ph}}^{\mathrm{def}} = i\sum_{\mathbf{q},\lambda}\sqrt{\frac{\hbar q}{2\rho V c_\lambda}}M_{\mathbf{q}}^{\lambda}[b_{\mathbf{q},\lambda}^{\dagger}e^{i\mathbf{q}\cdot\mathbf{R}} + b_{K,\lambda}^{\dagger}e^{i\mathbf{q}\cdot\mathbf{R}}], \tag{3.18}$$

where

$$M_{\mathbf{q}}^{\lambda} = \Xi_d \mathbf{e}_{\mathbf{q}}^{\lambda}\cdot\mathbf{e}_{\mathbf{q}}^{l} + \Xi_u(\mathbf{e}_{\mathbf{q}}^{\lambda})_z(\mathbf{e}_{\mathbf{q}}^{l})_z, \tag{3.19}$$

is the anisotropic geometric factor of the deformation potential.

3.4.2 Piezoelectric phonons

In crystals without bulk inversion symmetry, an additional electron-phonon coupling emerges. It is a consequence of strain being able to induce a polarization field,

$$\mathbf{P} = \hat{d}\hat{\varepsilon}, \tag{3.20}$$

where $\hat{d}$ is the third-rank piezoelectric tensor, a material property describing how the strain $\hat{\varepsilon}$ induces a polarization $\mathbf{P}$. In the limit of long phonon wavelengths, the transversal component of the resulting electric field is vanishingly small due to $\mathbf{E}_{\perp} \propto (c_\lambda/c)^2$, where c is the speed of light [55]. The phonon induced piezoelectric field is thus given by

$$\mathbf{E}_{\mathrm{pe}} = -\frac{(\hat{d}\hat{\varepsilon})_{||}}{\epsilon} = -\frac{1}{e}\nabla\phi_{\mathrm{pe}}(\mathbf{r}), \tag{3.21}$$

where $(\hat{d}\hat{\varepsilon})_{||}$ denotes the longitudinal component of the combined piezoelectric and strain tensor, and ϵ is the material permittivity. The scalar potential reads,

$$\phi_{\mathrm{pe}}(\mathbf{r}) = -i\frac{e}{q\epsilon}(\hat{d}\hat{\varepsilon})_{||}, \tag{3.22}$$

Inserting the expression for the strain tensor, we obtain the general piezoelectric Hamiltonian

$$H_{\mathrm{pe}} = -i\frac{e}{q^2\epsilon}\sum_{ijk} q_i d_{ijk}\varepsilon_{jk}. \tag{3.23}$$

Taking into account crystal symmetries, some terms vanish identically. Therefore, before continuing with the derivation, we make a remark on the role of crystal symmetries. We may limit which piezoelectric effects are possible by invoking

Table 3.1: Symmetry elements of the point group for the zincblende structure, which describes the lattice structure of GaAs. N denotes the number of operations of a specific type [48].

N	Schönflies notation	Description
1	I	Identity
8	C_3	$\pm\pi$ rotation about axes $[111]$, $[\bar{1}11]$, $[1\bar{1}1]$, $[11\bar{1}]$
3	C_2	π rotation about axes $[100]$, $[010]$, $[001]$
6	S_4	$\pm\pi$ improper rotation about axes $[100]$, $[010]$, $[001]$
6	σ	Reflection about planes (110), $(1\bar{1}0)$, (101), $(10\bar{1})$, (011), $(01\bar{1})$

Neumann's principle; any physical property of a crystal is invariant under the symmetry operations of the crystallographic point group [56].

A point group contains the symmetry operations of the crystal, in which at least one of the points remains fixed. These operations correspond to either proper or improper rotations. As an example, see Table 3.1 for the point group of a zincblende crystal, the crystal structure of GaAs. It follows from the assumption that, since both phonons and electrons are invariant under symmetry operations of the crystal, the electron-phonon coupling should abide the same rules. In the context of this section, the physical property of the crystal is the piezoelectric tensor $\hat{d}$. Under a general symmetry transformation specified by coefficients a_{ij} the transformed piezoelectric tensor is

$$d^*_{i'j'k'} = a_{i'i}a_{j'j}a_{k'k}d_{ijk}. \tag{3.24}$$

If the coefficients describe a symmetry operation of the crystal it must hold that $d^*_{ijk} = d_{ijk}$. For crystals with inversion symmetry, the transformation gives $d^*_{ijk} = -d_{ijk}$ while Neumann's principle states that $d^*_{ijk} = d_{ijk}$. This can only hold if all component of the piezoelectric tensor vanish, which shows why there is no piezoelectric effect in ideal silicon.

For crystal structures which permit a piezoelectric effect, the symmetry elements of its point group specify which components of the piezoelectric tensor vanish. For this thesis, the relevant non-centrosymmetric material is GaAs. Employing symmetry operations of the point group specified in Table. 3.1, yields a piezoelectric tensor which satisfies

$$d_{ijk} = (1 - \delta_{ij})(1 - \delta_{jk})(1 - \delta_{ik})d. \tag{3.25}$$

The piezoelectric coupling between electron and acoustic phonons coupling is then

given by the interaction Hamiltonian,

$$H_{e-ph}^{\mathrm{pe}} = -i\frac{1}{\sqrt{N}}\sum_{\mathbf{q},\lambda}\sqrt{\frac{\hbar}{2\rho V q c_\lambda}}\frac{de}{\epsilon}M_{\mathbf{q}}^{\lambda}(b_{\mathbf{q},\lambda} + b_{-\mathbf{q},\lambda}^{\dagger})e^{i\mathbf{q}\cdot\mathbf{r}}, \tag{3.26}$$

where the anisotropic geometric factor $M_{\mathbf{q}}^{\lambda}$ is

$$M_{\mathbf{q}}^{\lambda} = -2ieh_{14}q^{-3}(q_y q_z, q_z q_x, q_x q_y)\cdot\mathbf{e}_\lambda. \tag{3.27}$$

Here we have introduced the piezoelectric coefficient $eh_{14} = ed/\epsilon$, which is used in Paper IV. We can see from the expression in Eq. (3.26) that for small q, the piezoelectric coupling becomes the dominant electron-phonon coupling.

Chapter 4

Quantum transport

In the previous chapter, we have considered a closed system of a single electron being electrostatically confined in a quantum dot. Here instead we study a current being driven through a nanoscale device comprising a set of tunnel-coupled quantum dots and use the transport statistics as a probe of the nonequilibrium processes taking place.

To describe the dynamics of the electron transport we have to consider an open quantum system, where the surrounding macroscopic environment is integral to the measurement outcomes. However, while the environment is an essential component, in general we cannot fully describe it in terms of a total wavefunction. Instead, we opt for a density matrix approach and study the resulting irreversible dynamics of a smaller quantum system in contact with a macroscopic environment.

In the papers concerning quantum transport, we have limited ourselves to studying devices composed of nearly closed quantum dots, where the conductance is much smaller than the conductance quantum $G \ll 2e^2/h$. Owing to the small conductance, the fluctuation in occupation number is suppressed. We may then avoid the full quantum mechanical treatment by considering the number of electrons of dots a well-defined classical variable. In this scenario, the ideal tool for describing the quantum dynamics of the system is the Markovian quantum master equation [57]. The underlying assumption is that the correlations of the macroscopic environment decay rapidly, and we can therefore treat it as a semi-classical

object.

The environment is assumed to be fully described by a constant known probability distribution, in our case, the Fermi-Dirac distribution. This approach allows us to study the transport in a strong Coulomb blockade regime, where the effects of interactions between electrons within the smaller system becomes essential. In particular, this aspect of the approach is crucial in e.g. Paper II, where we describe how mutual Coulomb interaction between pairs of transport electrons generates entanglement.

Before moving on, we make an important remark on the viability of the master equation approach with an important result of S. A. Gurvitz and Ya. S. Prager. Starting from the many-body Schrödinger equation in Ref. [58] they demonstrate that resonant transport through a nanoscale device can, under certain conditions, be accuratelly modelled using a master equation. As an important example for this thesis, they show that in a high bias regime the dynamics of electrons transported through a double barrier, or dot, structure with significant charging effects, is entirely accessible within the framework of a master equation.

4.1 Lindblad equation

In the important work of Ref. [59] G. Lindblad shows that in general the irreversible dynamics of a reduced density matrix ρ_s, which preserves the trace and positivity of the density matrix, can be represented by a Lindblad-type equation of motion [60],

$$\frac{d\rho}{dt} = -\frac{i}{\hbar}[H_s, \rho] + \sum_{i=1}^{n^2-1}\left[\Gamma_i \gamma_i \rho \gamma_i^\dagger - \frac{1}{2}\{\gamma_i^\dagger \gamma_i, \rho\}\right], \tag{4.1}$$

with $\{,\}$ denoting the anti-commutator, γ_i is a general operator of the reduced system and n denotes the dimension of the reduced density matrix. An equation of motion describing the dynamics of transport electrons should ideally conform to this equation. For our problems on electron transport it is possible to identify the rates Γ_i with the injection or emission rates of electrons in the reduced system, due to tunneling between the reduced system and a semi-classical lead. In addition, owing to the generality of the Lindblad equation, we can incorporate other influences the environment exerts on the reduced system. Specifically, we use the Lindblad equation in Papers I and II to model spin-flip scattering and dephasing.

In this chapter we will briefly show how the Lindblad equation can be obtained for a reduced system of quantum dots. In the remainder of this chapter, we will employ units in which $\hbar = 1$ is satisfied.

4.2 Transport through quantum dots

Here a physical basis for the Markovian equation of motion is sketched using a microscopic model of several quantum dots each comprising a single accessible level (constituting the isolated system) coupled to two leads, corresponding to the macroscopic environment [61]. In our work relating to transport of electrons through quantum dots we consider a local many body basis in second quantisation formalism. The Hamiltonian of the reduced system can then be expressed as

$$H_s = \sum_i \varepsilon_i d_i^\dagger d_i + \sum_{j,i} U_{ij} d_i^\dagger d_j^\dagger d_j d_i + \sum_{j \neq i} \left[\Delta_{ij} d_i^\dagger d_j + \Delta_{ij}^* d_j^\dagger d_i \right] \tag{4.2}$$

where we have introduced the dot i creation (annihilation) operators $d_i^\dagger$ (d_i), satisfying $\{d_i^\dagger, d_j\} = \delta_{ij}$. Here U is the Coulomb interaction strength and Δ_{ij} is the tunneling amplitude between dots i and j. The interaction term connecting these two subsystems is the tunneling Hamiltonian

$$H_T = \sum_{k,\alpha} \left(t_k d_\alpha^\dagger c_{k\alpha} + t_k^* c_{k\alpha}^\dagger d_\alpha \right). \tag{4.3}$$

To obtain the dynamics of the reduced state ρ_s, we start with a Liouville equation in the interaction picture,

$$\frac{d\rho_s^I(t)}{dt} = \frac{d}{dt} \mathrm{tr}_B[\rho^I(t)] = -\mathrm{tr}_B \left[i[H_T^I(t), \rho^I(t)] \right], \tag{4.4}$$

which follows from the interaction picture representation of H_T,

$$H_T^I(t) = e^{i(H_s + H_b)t} H_T(t) e^{-i(H_s + H_b)t}, \tag{4.5}$$

together with an analogous definition for the density matrix $\rho^I(t)$. By integrating both sides and inserting the result back into the Liouville equation, we obtain an integro-differential equation for the reduced density matrix,

$$\frac{d\rho_s^I(t)}{dt} = -i\mathrm{tr}_B \left[H_T^I(t), \rho(0) \right] - \int_0^t ds \mathrm{tr}_B \left[[H_T^I(t), [H_T^I(s), \rho^I(s)]] \right]. \tag{4.6}$$

Instead of repeating this proceedure to obtain higher order corrections, we will turn Eq. (4.6) into a closed set of differential equations. To this end, we employ the assumption that our relevant subsystem is much smaller in comparison to the semi-classical leads and consider a coupling H_T between the two that is small.

Under these conditions the impact of the smaller state on the statistical properties of the reservoir state is insignificant. We express this assumption by approximating the total density matrix as $\rho(t) \approx \rho_s(t) \otimes \rho_B$, the so-called Born approximation. We further specify the constant ρ_B as a state which is in thermal equilibrium,

$$\rho_B = \prod_{k,i} \left[f_i(\varepsilon_k) c_{ki}^\dagger |0\rangle\langle 0| c_{ki} + [1 - f_i(\varepsilon_k)] |0\rangle\langle 0| \right], \quad f_i(\varepsilon) = \frac{1}{1 + e^{\frac{(\varepsilon - \mu_i)}{kT}}} \tag{4.7}$$

defining a temperature T for the system, with the introduction of the Fermi-Dirac distribution function $f_i(\varepsilon)$ of contact i with chemical potential μ_i and k_B is the Boltzmann constant. Additionally, it is assumed that reservoirs and reduced system were intially separated, that is $\rho(0) = \rho_s(0) \otimes \rho_B$. As a consequence, the first term in Eq. (4.6) vanishes, leaving

$$\frac{d\rho_s^I(t)}{dt} = -\int_0^t ds \mathrm{tr}_B \left[[H_T^I(t), [H_T^I(s), \rho_s^I(s) \otimes \rho_B]] \right]. \tag{4.8}$$

Equation (4.8) is, however, still an integro-differential equation, the equation of motion still includes memory effects. To investigate how these effects enter, we focus on the first term of the nested commutator (other terms are analogously obtained).

$$\begin{aligned} &\mathrm{tr}_B \left[H_T^I(t) H_T^I(s) \rho_s(s) \rho_B \right] = \\ &\mathrm{tr}_B \left[\textstyle\sum_{kk'\alpha\alpha' ll'} t_k t_{k'}^* d_\alpha^\dagger(t) c_{\alpha k}(t) c_{\alpha' k'}^\dagger(s) d_{\alpha'}(s) \rho_s(s) \rho_B \right] \\ &+ \mathrm{tr}_B \left[\textstyle\sum_{kk'\alpha\alpha' ll'} t_k^* t_{k'} c_{\alpha' k'}^\dagger(s) d_{\alpha'}(s) d_\alpha^\dagger(t) c_{\alpha k}(t) \rho_s(s) \rho_B \right] \end{aligned} \tag{4.9}$$

From the specified state of the bath in Eq. (4.7) we have e.g. $\mathrm{tr}_B[c_{l'k'}^\dagger c_{lk} \rho_B] = f_l(E_k)\delta(k - k')\delta_{l,l'}$. We may therefore drop the mixed terms in the sum,

$$\begin{aligned} &\mathrm{tr}_B \left[H_T^I(t) H_T^I(s) \rho_s(s) \rho_B \right] = \\ &\sum_{k\alpha\alpha' l} |t_k|^2 d_\alpha^\dagger(t) d_{\alpha'}(s) \rho_s(s) \mathrm{tr}_B \left[\rho_B c_{kl}(t) c_{kl}^\dagger(s) \right] \\ &+ \sum_{k\alpha\alpha' l} |t_k|^2 d_\alpha(s) d_{\alpha'}^\dagger(t) \rho_s(s) \mathrm{tr}_B \left[\rho_B c_{kl}^\dagger(s) c_{kl}(t) \right]. \end{aligned} \tag{4.10}$$

In order to study the time evolution of the operators, we wish express the trace in terms of operators at time $t = 0$. To this end, we insert the identity operator $\hat{1} = \sum_a |a\rangle\langle a|$, where $|a\rangle$ is a complete manybody basis of the reduced system. The reduced system $H_S = \sum_\gamma \varepsilon_\gamma |\gamma\rangle\langle\gamma|$ is diagonal in this basis, and consequently we obtain,

$$\begin{aligned}
&\mathrm{tr}_B\left[H_T^I(t)H_T^I(s)\rho_s(s)\rho_B\right] = \\
&\sum_\zeta |t_k|^2 e^{i\delta\varepsilon_{ab}t}|a\rangle\langle a|d_\alpha^\dagger|b\rangle\langle b|e^{i\delta\varepsilon_{bc}(\tau-t)}|b\rangle\langle b|d_{\alpha'}|c\rangle\langle c|\rho_s(s)\mathrm{tr}_B\left[\rho_B e^{iE_k\tau}c_{kl}c_{kl}^\dagger\right] \\
&+\sum_\zeta |t_k|^2|a\rangle\langle a|e^{i\delta\varepsilon_{ab}(\tau-t)}d_\alpha|b\rangle\langle b|e^{i\delta\varepsilon_{bc}t}d_{\alpha'}^\dagger|c\rangle\langle c|\rho_s(s)\mathrm{tr}_B\left[\rho_B e^{-iE_k\tau}c_{kl}^\dagger c_{kl}\right]
\end{aligned} \tag{4.11}$$

where $\tau = t - s$ and $\delta\varepsilon_{ab} = \varepsilon_a - \varepsilon_b$. The short notation $\{\zeta\} = \{a, b, c, \alpha, l, k\}$ has been introduced, to keep the expressions compact. We want to obtain a Markovian equation of motion, where the dynamics of the reduced system can only depend on the density matrix at the same time. This would correspond to discarding memory effects, which would allow the subtitution $\rho_s(s) \to \rho_s(t)$ in the integral. One scenario which enables this is the high bias limit, to which we have restricted ourselves in our work on electron transport. In this regime two essential properties are fulfilled:

- Constant Fermi function, allowing us to neglect temperature in the equation of motion.
- Memory effects of the reduced system vanish, giving a Markovian equation of motion.

The first point is evident from the Fermi distribution function $f(x) = (1 + e^{(x-eV)/k_BT})^{-1}$, where V is the applied bias. In the relevant energy interval, set by the quantum dot energy levels, the Fermi functions are then roughly constant and we may disregard the energy argument. Accordingly, in our transport problems the reservoirs act exclusively as either 'drain', absorbing electrons from the reduced system, or 'source', injecting electrons.

The second property requires further comments. To elaborate, we consider the factors $\sum_k |t_k|^2 f(E_k) e^{-i(\varepsilon_k - \delta\varepsilon_{\gamma\gamma'})s}$ from Eq. (4.11), which enter all nested commutator terms. Within the flat conduction band approximation, where the density of states $\nu(E)$ is assumed to be constant ($\sum_k \to \int dE\nu(E) = \int dE\nu$), and

with tunneling amplitudes independent of k this factor reads in the continuum limit,

$$\int dE f(E) e^{i(E-\delta\varepsilon_{\gamma\gamma'})\tau} = 2kT \frac{e^{i(eV-\delta\varepsilon_{\gamma\gamma'})\tau}}{\sinh(\pi k_B T\tau)} \tag{4.12}$$

That is, these factors will oscillate with a frequency $(eV - \delta\varepsilon_{\gamma\gamma'})/\hbar$. In contrast, the reduced density matrix ρ_s dynamics occur on a time scale set by H_T. Thus with a large applied bias, ρ_s can be regarded as constant during the correlation time of the bath, making the substitution $\rho(s) \to \rho(t)$ a valid approximation. With these ingredients set, going back to Eq. (4.11), retreating to the original d operators and expressing all operators in the Schrödinger picture gives [1]

$$\begin{aligned}\lim_{t\to\infty} \int_0^t ds \mathrm{tr}_B \left[H_T^I(t) H_T^I(s) \rho_s(t) \rho_B\right] = \quad & \tfrac{1}{2} e^{-iH_s t} d^\dagger d \rho_s(t) \Gamma_i f_i e^{iH_s t} \\ & + \tfrac{1}{2} e^{-iH_s t} d d^\dagger \rho_s(t) \Gamma_i (1 - f_i) e^{iH_s t}.\end{aligned} \tag{4.13}$$

Where we have introduced the rates $\Gamma_i f_i = \pi \sum_k |t_k|^2 f_i \delta(E_k - \varepsilon)$, with the Fermi function f_i being unity for a source reservoir and zero for drain. Here it is used that the lead density of states is constant on the energy scale set by ε, which denotes the possible energy differences of the reduced system. Gathering all the terms of the nested commutator, we obtain an equation of motion of the reduced density operator ρ_s in the Schrödinger picture,

$$\frac{d\rho_s(t)}{dt} = -i[H_s, \rho_s(t)] + \sum_i \left(\Gamma_i f_i \mathcal{D}[d^\dagger, \rho_s] + \Gamma_i (1 - f_i) \mathcal{D}[d, \rho_s] \right), \tag{4.14}$$

where an extra term renormalizing the dot level energies is disregarded. The shorthand notation $\mathcal{D}[d_j^\dagger, \rho_s] = d_j^\dagger \rho_s d_j - \{d_j d_j^\dagger, \rho_s\}/2$, describes the dissipative process of one electron from the source reservoir being injected onto the adjascent dot, and $\mathcal{D}[d_j, \rho_s]$ analogously describes the process of an electron escaping to a drain reservoir. With the result of Eq. (4.14), we have finally obtained the Lindblad-type equation of motion, which is the basis for the transport theory of Papers I and II.

[1] Being interested in the stationary case, we let the upper limit of τ-integrals in Eq. (4.8) go to infinity and obtain $\lim_{t\to\infty} \int_0^t d\tau e^{i(\varepsilon_k - \varepsilon_\gamma + i0^+)\tau} = i\frac{P}{\varepsilon_k - \varepsilon_\gamma} + \pi\delta(\varepsilon_k - \varepsilon_\gamma)$, where δ is the Dirac delta function and P is Cauchy's principal value. The delta function gives the rates, while the principal value will yield an effective correction to H_s, which we neglect.

4.3 Example: double quantum dot

An illustrative example of the Markovian Quantum Master Equation in practice is the electron transport through a double quantum dot structure [58]. We consider two quantum dots, tunnel coupled in series and with a strong on-site Coulomb interaction U which prohibts double occupancy. The Hamiltonian for the reduced system is,

$$H_s = \sum_{i=1,2} \varepsilon_i d_i^\dagger d_i + t d_2^\dagger d_1 + t d_1^\dagger d_2 + \sum_i U d_i^\dagger d_i. \tag{4.15}$$

where for simplicity, we consider a real tunneling amplitude t. The left (right) dot is in contact with a source (drain) reservoir. The equation of motion for the double dot state ρ is

$$\frac{d\rho}{dt} = -i[H_s, \rho] + \Gamma_L \mathcal{D}[d_1^\dagger, \rho] + \Gamma_R \mathcal{D}[d_2, \rho] \tag{4.16}$$

Introducing a matrix notation, where the relevant density matrix elements are placed in a vector $\vec{\rho} = (\rho_0, \rho_{10}, \rho_{01}, \rho_{11}, \Re\rho_{LR}, \Im\rho_{LR})$, with $\Re$ ($\Im$) denoting the real (imaginary) part. Here we define the diagonal matrix elements as $\rho_a = \langle a|\rho|a\rangle$, and off-diagonal (coherences) as $\rho_{LR} = \langle 0|d_1 \rho d_2^\dagger|0\rangle$. The equation of motion can be formulated as the matrix equation,

$$\frac{d}{dt}\vec{\rho} = M\vec{\rho}, \tag{4.17}$$

where M is here referred to as the Lindblad matrix. In the basis described above, the Lindblad matrix reads

$$M = \begin{pmatrix} -\Gamma_L & 0 & \Gamma_R & 0 & 0 & 0 \\ \Gamma_L & 0 & -\Gamma_R & \Gamma_R & 0 & 2t \\ 0 & 0 & -\Gamma & 0 & 0 & -2t \\ 0 & 0 & \Gamma_L & -\Gamma_R & 0 & 0 \\ 0 & 0 & 0 & 0 & -\Gamma/2 & -\delta\varepsilon \\ 0 & -t & t & 0 & \delta\varepsilon & -\Gamma/2 \end{pmatrix}, \tag{4.18}$$

where $\Gamma = \Gamma_L + \Gamma_R$ and $\delta\varepsilon = \varepsilon_2 - \varepsilon_1$ is the difference between the dot energies. We obtain the nonequilibrium steady state $\vec{\rho}_{ss}$ by finding the nullspace of M, that is, finding the eigenvector which satisfies $M\vec{\rho}_{ss} = 0$. Equipped with the normalised $\vec{\rho}_{ss}$ (that is, $\mathrm{tr}[\rho_{ss}] = 1$), the average current transport through the double dot device is directly obtained as transmission rate Γ_R times the occupation probability

of adjascent dot. For compactness considering the case $\Gamma_L = \Gamma_R = \gamma$, the current through the double quantum dot is

$$I = e\Gamma_R(\langle 01|\rho|01\rangle + \langle 11|\rho|11\rangle) = \frac{2e\gamma t^2}{\delta\varepsilon^2 + \gamma^2 + 4t^2}. \tag{4.19}$$

As it stands, the occupation probabilities of a nonequilibrium stationary state provides us with the time averaged measurement. There is however a powerful technique which, by modifying the equation of motion, allows us to access systematically the full statistical distribution of charge transport. The theory of Full Counting Statistics, the subject of next chapter, is the main tool we have employed when studying transport statistics in Papers I and II.

Chapter 5

Electron counting statistics

The aim of this chapter is to introduce the concept of Full Counting Statistics (FCS), which enables us to theoretically investigate not only the average charge current, but the full distribution of charge transfers taking place within a specified time interval. In particular, FCS allows us to theoretically quantify current noise that emerges once a voltage is applied across a quantum dot device. Quantifying the noise of interest since, as will be discussed below, it provides insight into correlations of the transported electrons.

The concept of FCS stems from the field of quantum optics [62, 61], where the statistics of photon counting provides information about the light source. As the name implies, by counting photons over a long time it is possible to infer a probability distribution which fully describes the statistical properties of the detected photons.

With the seminal work of L. Levitov *et al* [63], an electric analogue within the scattering matrix formalism was made available for studying statistics of electron transport in mesoscopic devices. The FCS of electron counting has since been extended to the nonequilibrium Greens functions approach [64, 65] as well as Master equations [57, 66], allowing for transport statistics to be studied in a variety of mesoscopic devices. Moreover, the FCS has also been extended to study the statistics of a general observable [67].

In the quantum master equation approach, used exclusively in this thesis, FCS

is made accessible via a remarkably simple modification to the equation of motion which we introduced in the previous chapter. Before describing how electron counting can be incorporated in the quantum master equation, we briefly review the concept of a cumulant generating function.

5.1 Cumulant generating function

The key quantity when studying the statistics of electron transport is the probability distribution $P_{\Delta t}(N)$, containing the probabilities of the transferring N electrons over a measurement time Δt.

The statistical properties of the electron transport can be expressed in terms of cumulants of the probability distribution. For example, the average current corresponds to the mean value, which is the first cumulant κ_1, the second cumulant κ_2, the width of the distribution, is similarly related to the current fluctuations. Owing to the close relation between cumulants and measurements, it is convenient to work with the cumulants κ_k directly, which collectively characterise the probability distribution. See Fig. 5.1. To this end, we want to use the cumulant generating function (CGF), which is a central component of Papers I and II. As a preliminary, we first introduce the Fourier transform of the probability distribution $P_{\Delta t}(N)$,

$$\Lambda(\chi) = \sum_N P_{\Delta t}(N) e^{iN\chi}, \tag{5.1}$$

which is called the characteristic function of $P_{\Delta t}(N)$. Here we have introduce χ, the conjugate variable of the transferred charges N. The cumulant generating function $F(\chi)$ is then straightforwardly obtained as,

$$F(\chi) = \ln(\Lambda(\chi)). \tag{5.2}$$

The clear benefit of working with $F(\chi)$ is that it generates, as the name implies, every cumulant κ_k by

$$\kappa_k = \left. \frac{\partial^k F(\chi)}{\partial (i\chi)^k} \right|_{\chi \to 0}. \tag{5.3}$$

An additional property of $F(\chi)$, which benefits our analysis, is that independent stochastic events are divided into separate terms. In our work on charge transport, we have targeted transport through weak tunnel junctions, where resulting transport events are rare.

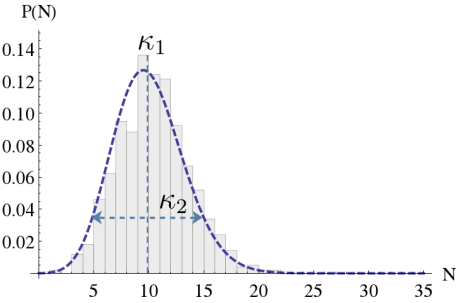

Figure 5.1: A histogram of infrequent charge transfers and fitted Poisson distribution (dashed blue line). The first cumulant κ_1 corresponds to the average value, which for charge transport corresponds to average current. The second cumulant κ_2 corresponds to the variance, which can be related to the auto-correlations. Higher order cumulants describe the non-gaussian features, e.g. κ_3 describing the skewness of the distribution.

To qualitatively describe the typical CGF for such a transport scenario, we consider here a generic example of rare charge transfers onto two sets of spatially separated detectors. During a time interval δt two, rare, independent charge transfers are possible. Either individual electrons are transferred at a rate γ_α and γ_β towards the two sets of detectors α and β, or a pair of electrons are split and transferred with a rate $\Gamma_{\alpha\beta}$. Here rare transport events imply, $\delta t\gamma_\alpha, \delta t\Gamma_{\alpha\beta} \ll 1$. Measuring the currents over a time $\Delta t = N\delta t$, we can sum up the processes of transferring one electron to detector α, $P_\alpha = \delta t\gamma_\alpha$ two onto both α and β, $P_{\alpha\beta} = \delta t\Gamma_{\alpha\beta}$ or none transferred, $P_0 = 1 - \sum_{\alpha\neq\beta}(\delta t\Gamma_{\alpha\beta} + \delta t\gamma_\alpha)$. Using the definition in Eq. (5.2) the CGF is then,

$$F(\chi_\alpha, \chi_\beta) = \ln\left(\left[1 + \sum_{\alpha\neq\beta}\left(\gamma_\alpha\frac{\Delta t}{N}(e^{i\chi_\alpha} - 1) + \Gamma_{\alpha\beta}\frac{\Delta t}{N}(e^{i(\chi_\alpha+\chi_\beta)} - 1)\right)\right]^N\right). \tag{5.4}$$

In limit of $N \to \infty$, we obtain the CGF describing two types of independent Poisson processes,

$$F(\chi_\alpha, \chi_\beta) = \Delta t\sum_{\alpha\neq\beta}\left[\gamma_\alpha\left(e^{i\chi_\alpha} - 1\right) + \Gamma_{\alpha\beta}\left(e^{i(\chi_\alpha+\chi_\beta)} - 1\right)\right]. \tag{5.5}$$

These types of processes are characteristic for the transport statistics we have investigated in our work. In particular, the second term yields the current cross-correlations, a quantity we make extensive use of in Papers I, II and III. The CGF in Eq. (5.5) shows the type of transport statistics that occurs. To quantify the

current cross-correlations, we need to obtain the rates $\Gamma_{\alpha\beta}$, which can depend on structure of the transport system. In the following, we show that the full CGF, with explicit expressions for the transfer rates γ_α and $\Gamma_{\alpha\beta}$, is obtained by studying a modified equation of motion of the reduced system.

5.2 Modified equation of motion

In the following we describe how the transport statistics is obtained by including electron counting in the Lindblad equation. For simplicity, we consider here a single level quantum dot placed between a left (source) and right (drain) contact in the high bias limit.

$$\frac{d\rho}{dt} = -\frac{i}{\hbar}[H_s, \rho] + \Gamma_R \mathcal{D}[d, \rho] + \Gamma_L \mathcal{D}[d^\dagger, \rho], \tag{5.6}$$

where d is the dot annihilation operator of the dot, H_s is the Hamiltonian of the reduced system and $\mathcal{D}[d, \rho] = [d\rho d^\dagger - \{d^\dagger d, \rho\}/2]$ is the Lindblad dissipation operator.

To this end, we consider a microscopic derivation, loosely following the approach detailed in Ref. [68], which is close to the original idea of L. Levitov *et al.* The starting point is to include a measurement device in the Hamiltonian of the problem. Here an auxiliary $1/2$-spin is introduced, which monitors the current flowing through the device. Heuristically, the counting mechanism works as follows; the magnetic field, originating from the electric current, induces a precession angle of the spin which counts the number of transported electrons.

The transport Hamiltonian comprises the reduced system H_s tunnel coupled via H_T with the left and right contacts, described by H_l and H_r, respectively. The $1/2$-spin measurement device is accounted for by the last term in,

$$H_\chi = H_s + H_T + H_l + H_r - \frac{\hbar\chi}{2e}\sigma_z I, \quad I = -\frac{i}{\hbar}[H_\chi, n_r - n_l], \tag{5.7}$$

where σ_z is the Pauli matrix, n_l (n_r) is the number operator of the left (right) contact. Studying the precession angle of the counting spin (see Appendix B for details), averaging over the electronic degrees of freedom, we obtain the quantity

$$\mathrm{tr}_e\left[\exp(-\frac{i}{\hbar}H_\chi t)\rho(0)\exp(\frac{i}{\hbar}H_{-\chi}t)\right] = \langle\exp(i\frac{\chi}{e}It)\rangle_e. \tag{5.8}$$

We find that $\langle \exp(i\chi N)\rangle_e = \sum_N P_t(N) e^{i\chi N} = \Lambda(\chi)$, corresponds to the characteristic function of probability distribution $P_t(N)$ [63]. We further remark that it only depends on the degrees of freedom of the electronic system, and the coupling variable χ is the conjugate variable to the amount of transfered charges N.

The effect of a current probe can be included in the Lindblad equation in Eq. (5.6) by transforming the dissipation operators $\mathcal{D}[d,\rho]$. Specifically, we show in Appendix B, an extra phase factor $e^{i\chi}$ appears in the term which describes a change in occupation number. That is, the transformation to the modified dissipation operator with counting fields χ reads,

$$\mathcal{D}[d,\rho] \to \mathcal{D}^{\chi}[d,\rho] = [d\rho d^{\dagger}\exp(i\chi) - \{d^{\dagger}d,\rho\}/2] \tag{5.9}$$

In the long time limit, the modified Lindblad equation provides us access to the full transport statistics. To see this, we can formulate the equation of motion as the matrix differential equation,

$$\frac{d\vec{\rho}}{dt}(\chi,t) = M(\chi)\vec{\rho}(\chi,t). \tag{5.10}$$

In contrast to the matrix differential equation in the previous chapter, here all quantities now depend on χ, referred to as the counting field. Assuming the typical case of a unique stationary state, we can express the formal solution to the differential equations in terms of the right eigenvectors of $M(\chi)$,

$$\vec{\rho}(\chi,\Delta t) = e^{M(\chi)\Delta t}\vec{\rho}(\chi,0) = e^{\lambda_{ss}(\chi)\Delta t}c_{ss}\vec{\rho}_{ss}(\chi,0) + \sum_i e^{\lambda_i(\chi)\Delta t}c_i\vec{\rho}_i(\chi,0), \tag{5.11}$$

For all non-stationary states the eigenvalues, $\lambda_i \neq \lambda_{ss}$, have a negative real part, ensuring they vanish in the long time limit. Letting the measurement time $\Delta t \to \infty$, we obtain[1]

$$\mathrm{tr}_e[\rho(\chi,\Delta t)] = \langle \exp(iH_{-\lambda}\Delta t)\exp(iH_{\lambda}\Delta t)\rangle_e = e^{\lambda_{ss}(\chi)\Delta t}. \tag{5.12}$$

That is, the measurement time Δt times the eigenvalue of the Lindblad matrix $M(\chi)$ which vanishes for $\chi \to 0$, corresponds to the generating function $F(\chi)$ of the transport problem.

[1]Here we disregard the coefficient c_{ss} (defined by $\vec{\rho}(\chi,0) = \sum_i c_i\vec{\rho}_i(\chi,0)$), which contains information about the initial state. In the long time limit, it has no impact on the CGF.

The discussion above has dealt with a setup where only one drain contact is present, or one terminal system. For transport with n terminals, the transport probability distribution is $P_{\Delta t}(N_1, N_2, ..., N_n)$, with the associated cumulant generating function $F(\chi_1, \chi_2, ...\chi_n)$. The transport statistics in this scenario is made accessible by introducing a phase factor χ_i to each corresponding tunnel-coupling between terminal i and its adjacent quantum dot. We conclude this section by specifying a Lindblad-type equation of motion for quantum dot systems with counting fields in a multiple terminal setup.

$$\frac{d\rho}{dt} = -\frac{i}{\hbar}[H_s, \rho] + \sum_{i\alpha\sigma} \Gamma_i \mathcal{D}^{-\chi_i}[d_{\alpha\sigma}, \rho] + \sum_{j\beta\sigma} \Gamma_j \mathcal{D}^{\chi_j}[d^\dagger_{\beta\sigma}, \rho], \tag{5.13}$$

where σ is the spin index, α (β) corresponds to dots connected to the source (drain) lead and $\mathcal{D}^{\chi_i}[d, \rho] = [d\rho d^\dagger \exp(i\chi_i) - \{d^\dagger d, \rho\}/2]$. The Lindblad operator with counting fields is the principal tool we have used in Papers I and II, to study the current and current noise in transport through quantum dot devices. Before concluding this section we mention an alternative approach of deriving the modified Lindblad equation, which does not need an explicit detector apparatus [66, 69]. Here instead a number resolved master equation is Fourier transformed, where the counting field enters naturally as the conjugate variable of number of transferred charges.

5.3 Current Noise

The transport of electrons through a nanoscopic device is a stochastic process, a fact evident from typical conductance measurements, which fluctuate randomly in time. To obtain a clear signal, we would need to average out these fluctuations. However, in doing so we lose valuable information about the current.

To explain this statement, we need to distinguish different types of current noise. Here we consider two relevant sources [2]. The first source, Thermal or Johnson-Nyquist noise, is ubiquitous for systems with finite temperatures even when no bias is applied. The fluctuations in occupation number that result from finite

[2] 1/f, or flicker noise, is an additional type of unavoidable noise source due to unknown random processes in the background. The name 1/f hints of its importance for low frequencies, where below $\approx 10kHz$ this source becomes important [70, 71]. We disregard this source as in typical quantum transport experiments it is possible to focus on higher frequencies.

temperature will result in a fluctuating conductance because of the fluctuation-dissipation theorem [70]. As such, this noise provides no further information about the system than what is available from conductance measurements.

The second type of electric noise appears once a voltage is applied over an electrical conductor. This non-equilibrium noise, termed shot noise, emerges as a consequence of the discreteness of electron charge, and is the dominant noise source in the so-called shot noise limit, $eV \gg kT$. To understand shot noise, it is instructive to consider the theoretical study which discovered the phenomenon.

The role of shot noise as a diagnostic tool was discovered by W. Schottky in 1918 [72], when he investigated the emission of electrons from the cathode in a vacuum tube. Under the assumption that emission is rare, independent and random, he noted that the fluctuations of the electron counts at the anode should be related to the average value. In the ideal case, where the electron emission is the only stochastic element, a Poisson distribution accurately models the count probability. Owing to the properties of the Poisson distribution, the fluctuations are proportional to the time averaged value of the current,

$$S = 2eI. \tag{5.14}$$

This relation, called the Schottky formula, shows that current noise provides also the electric charge being transferred at each event, information which is not available by only studying the average current. In general when studying charge transport, the Schottky formula does not necessarily hold, interactions inside the system and the statistics of the transported particles affect the noise. Conversely, this implies that the shot noise also provides insight into which transport events are taking place.

Equipped with a complete statistical description of the current, we can quantify shot noise theoretically by studying the current-current correlation functions. In our work, the main interest has been the stationary cross correlations in the shot noise limit. The correlation function of currents measured at contacts α and β at two points in time, here taken as $t = 0$ and $t = \tau$, is,

$$S_{\alpha\beta}(\tau, 0) = \frac{1}{2}\langle\{\delta I_\alpha(\tau), \delta I_\beta(0)\}\rangle, \quad \delta I_i(t) = I_i(t) - \langle I_i(t)\rangle. \tag{5.15}$$

The Fourier tranform of this quantity yields the noise power $S_{\alpha\beta}(\omega)$,

$$S_{\alpha\beta}(\omega) = \int_{-\infty}^{\infty} d\tau e^{j\omega\tau} S_{\alpha\beta}(\tau, 0). \tag{5.16}$$

The transport problem we are studying here can be characterised by the probability distribution, $P_{\Delta t}(N_\alpha, N_\beta)$, describing the transfer of N_α (N_β) electrons to contacts α (β), during a measurement time Δt. The joint cumulant of $P_{\Delta t}(N_\alpha, N_\beta)$ reads after a long measurement time [65],

$$\kappa_2^{\alpha,\beta} = \frac{\Delta t}{2e^2}\int_{-\infty}^{\infty} d\tau \langle\{\delta I_\alpha(\tau), \delta I_\beta(0)\}\rangle. \tag{5.17}$$

By comparing with Eq. (5.16), we note that the zero-frequency current noise in a transport experiment is directly proportional to the joint cumulant $\kappa_2^{\alpha\beta}$ of the distribution $P_{\Delta t}(N_\alpha, N_\beta)$. That is,

$$S_{\alpha\beta}(0) = \frac{2e^2}{\Delta t}\kappa_2^{\alpha\beta}. \tag{5.18}$$

This relation in Eq. (5.18) has been the basis for our investigations in Papers I, II and III. Here we employ the zero frequency shot noise as an experimentally accessible tool for probing correlations of electron pairs in spatially separated currents. In particular, using the equations of motion with counting fields, we relate the joint cumulant to the two particle density matrix of transported electron pairs. Owing to Eq.(5.18), we have been able to use shot noise to formulate a Bell inequality (see Papers I, II), tomographically reconstruct the state of a coherently transported electron pair (see Paper I) and as the building block for an entanglement witness (See Paper III).

5.4 Example: FCS of double quantum dot

To show the workings of Full Counting Statistics with a Lindblad equation, we consider again the transport problem specified in the previous chapter, but with counting fields [69]. In the following we employ units where $\hbar = 1$. After a long time, a steady state electric current traverses two quantum dots which are tunnel-coupled in series. The equation of motion for the reduced dot system state ρ, with counting field χ, then reads,

$$\frac{d\rho}{dt} = -i[H_s, \rho] + \Gamma_L \mathcal{D}[d_L^\dagger, \rho] + \Gamma_R\left[d_R\rho d_R^\dagger e^{i\chi} - \frac{1}{2}\{d_R^\dagger d_R, \rho\}\right]. \tag{5.19}$$

As in the former case, we formulate the equation of motion as a system of linear equations and obtain an eigenvalue problem. In particular for the eigenvector $\vec{\rho}_\chi$, satisfying $\lim_{\chi\to 0}\vec{\rho}_\chi = \vec{\rho}_{ss}$, the eigenvalue problem reads,

$$M_\chi\vec{\rho}_\chi = F(\chi)\vec{\rho}_\chi. \tag{5.20}$$

The Lindblad matrix is nearly identical to that of Eq. (4.18), with the exception of extra phase factor for matrix elements describing the emission of an electron. Explicitly the left-hand side of Eq. (5.20) is,

$$M_\chi\vec{\rho}_\chi = \begin{pmatrix} -\Gamma_L & 0 & \Gamma_R e^{i\chi} & 0 & 0 & 0 \\ \Gamma_L & 0 & -\Gamma_R & \Gamma_R e^{i\chi} & 0 & 2t \\ 0 & 0 & -\Gamma & 0 & 0 & -2t \\ 0 & 0 & \Gamma_L & -\Gamma_R & 0 & 0 \\ 0 & 0 & 0 & 0 & -\Gamma/2 & -\delta\varepsilon \\ 0 & -t & t & 0 & \delta\varepsilon & -\Gamma/2 \end{pmatrix} \begin{pmatrix} \rho_0 \\ \rho_L \\ \rho_R \\ \rho_2 \\ \Re\rho_{LR} \\ \Im\rho_{LR} \end{pmatrix}, \tag{5.21}$$

where the basis and definitions are identical to the example studied in the previous chapter. To obtain compact expressions we consider the case $\Gamma_L = \Gamma_R = \gamma$. Solving this eigenvalue problem, the CGF for this transport system is,

$$F(\chi) = -\gamma + \sqrt{p + \sqrt{q + 16\gamma^2 t^2(e^{i\chi} - 1)}}. \tag{5.22}$$

where $p = (-\delta\varepsilon^2 + \gamma^2 - 4t^2)/2$ and $q = (\delta\varepsilon^2 + \gamma^2 + 4t^2)/4$. From $F(\chi)$ we can straightforwardly recover the current expression from the previous chapter

$$\langle I\rangle = -ie\partial_\chi F|_{\chi\to 0} = \frac{2t^2\gamma e}{\delta\varepsilon^2 + \gamma^2 + 4t^2}. \tag{5.23}$$

However, in contrast to the example of previous chapter, by virtue of FCS, we posses complete information about the transport statistics and can easily obtain the higher order cumulants beyond the average current. For instance, the second cumulant, corresponding to a auto-correlation measurement, reads

$$S = -e^2\partial_\chi^2 F|_{\chi\to 0} = \frac{2e^2 t\gamma}{16q^2}\left[(\delta\varepsilon^2 + \gamma^2)^2 + 2t^2(3\delta\varepsilon^2 - \gamma^2) + 8t^4\right]. \tag{5.24}$$

As a passing remark, we consider the scenario when the tunneling between the dots is weak. The cumulant generating function to leading order in t,

$$F(\chi) = 2\frac{\gamma t^2}{\delta\varepsilon^2 + \gamma^2}(e^{i\chi} - 1), \tag{5.25}$$

corresponds to a typical Poisson process. We infer two interesting points from this expression. First, the coherent evolution is a vital component to the transport statistics. Second, the statistics of a weak tunnel junction allows us to relate the measured current and auto-correlations to electrons entirely localised in the dots adjacent to the contact. We make use of the second point in Paper I, to pinpoint the measured spin correlations to spin properties of transported electron pairs.

Chapter 6

Overview of Paper I

Motivated by experiments on Cooper pairs splitters [73, 74, 75, 76, 77, 78], in Paper I we present an entangler-detector model which can be used to unambiguously test the spin entanglement of the spatially split Cooper pairs. While an efficient splitting of Cooper pairs has been demonstrated using current cross correlations [76], it remains to demonstrate a conclusive signature that the split pairs are entangled.

Ideally the Cooper pair splitter works by emitting a pair of spin entangled electrons, which are then split whilst preserving their coherence. To verify the latter part, it is insufficient to only look at charge current cross-correlations, instead a set

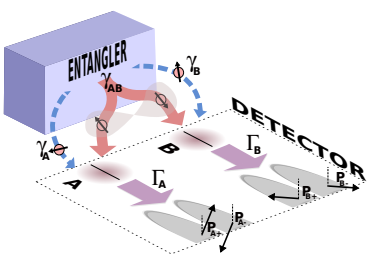

Figure 6.1: (From Paper I) Schematic figure of the setup considered in Paper I. A generic entangler emits independent particles (dashed line) and split pairs of particles (solid line) onto a set of detector dots with spin degenerate energies ε_A, ε_B. The emission is given by a spin dependent rate, described by the matrices $\hat{\gamma}_A$, $\hat{\gamma}_B$ for independent particles and $\hat{\gamma}_{AB}$ for pairs of particles. Detector dots A and B are tunnel coupled with a rate Γ_A and Γ_B to a anti-collinear pair of ferromagnetic contacts

of spin sensitive detectors are required. With this in mind, we use a set of ferromagnetic (FM) contacts with anti-collinear polarisations to probe the spin properties of the transport state [79, 80, 81] without spin polarising the dot density of states. In addition, it is necessary to take into account the possible non-idealities in the system. The setup we consider comprises an unknown entangler, and a detector system consisting of two spatially separated quantum dots tunnel-coupled with two pairs of anti-collinear FM contacts. See Fig. 6.1. In the paper, we specifically address two important questions:

- *How are the spin properties of the pair emitted by the entangler manifested in the cross-correlators of the currents at the FM-leads?*
- *How can system parameters and detector settings be optimized to allow for an unambiguous detection of entanglement of the emitted state?*

To obtain insight into these questions, we study the full transport statistics in the context of transport of entangled electrons [82, 83]. Here we restrict ourselves to the scenario of infrequent charge transport, and employ FCS to provide a clear picture of the contributing transport processes, and effects of perturbation on the detected spin state. In the following, the main results are detailed before briefly describing the model we have used.

6.1 Main results

The main result of Paper I is our expression for the cumulant generating function for the probability distribution $P_{\Delta t}(N_{A+}, N_{A-}, N_{B+}, N_{B-})$, describing the transfer of $N_{\alpha m}$ electrons from detector dot $\alpha = A, B$ onto the FM contact αm of the entangler-detector system, during a long measurement time Δt. Introducing a counting field $\chi_{\alpha m}$ for each FM contact, the cumulant generating function reads

$$\begin{aligned} F(\chi) = \quad & \Delta_t \textstyle\sum_{\alpha m} \mathrm{tr}\left[\hat{Q}^{\zeta}_{\alpha m}\hat{\gamma}_{\alpha}\right](e^{i\chi_{\alpha m}}-1) \\ + \quad & \Delta_t \textstyle\sum_{n,m} \mathrm{tr}\left[(\hat{Q}^{\zeta}_{An}\otimes\hat{Q}^{\zeta}_{Bm})\hat{\gamma}_{AB}\right](e^{i(\chi_{An}+\chi_{Bm})}-1). \end{aligned} \tag{6.1}$$

Here $\hat{\gamma}_{\alpha}$ ($\hat{\gamma}_{AB}$) are Hermitian matrices containing all single (two) particle rates, $\hat{Q}^{\zeta}_{An} = (\hat{1} \pm \zeta_A \mathbf{a}\cdot\boldsymbol{\sigma})$, where ζ_{α} is the overall efficiency of detector α and $\mathbf{a}$ ($\mathbf{b}$)

is the polarisation vector of FM contact $A\pm$ ($B\pm$) . The expression clearly displays the two types of independent Poissonian transport processes that make up the long time transport statistics. The first term describes the unwanted transfer of an independent single charge, emitted by the entangler and detected at the ferromagnetic contact αm. The second term corresponds to the coincident detection of an emitted two-particle state at the FM contacts An and Bm. From Eq. (6.1) we obtain that the current cross-correlations measured at FM contacts $A\pm$ and $B\pm$ are,

$$S_{AB}^{\pm\pm} = e^2\Gamma \mathrm{tr}\left[(\hat{1} \pm \zeta_A \mathbf{a}\cdot\boldsymbol{\sigma}) \otimes (\hat{1} \pm \zeta_B \mathbf{b}\cdot\boldsymbol{\sigma})\rho\right], \quad \Gamma = \mathrm{tr}\left[\gamma_{AB}\right] \tag{6.2}$$

where $\rho = \gamma_{AB}/\Gamma$ is the spin state of an electron pair emitted from the entangler.

The efficiency parameter ζ_α quantifies how well the spin state is resolved when a particle is detected at the FM contacts. For example, an electron spin reaching detector $A\pm$ is projected along the axis defined by $\mathbf{a}$ and with probability ζ_A leaves for either $A+$ or $A-$, while with probability $1-\zeta_A$ the spin is emitted towards both $A+$ and $A-$ with the same rate. An immediate conclusion from Eq. (6.2) is that for an ideal setup, that is $\zeta_A = \zeta_B = 1$, the cross correlators allow for a full tomographic reconstruction of the emitted state from the generic entangler. As has been proposed in earlier works [84, 81]. It follows also from Eq. (6.2) that the spurious current of independent single charges does not contribute to the cross-correlation measurements.

Our results further show how nonidealities of the detector setup, here accounted for by a local spin-flip rate η of electrons in the detector dots and non-ideal polarisation p_α of the FM contacts, enter as an overall reduction of the detector efficiency ζ. In particular for detector α the efficiency is,

$$\zeta_\alpha = p_\alpha(1-\eta_\alpha), \quad \eta_\alpha = \eta/(\Gamma_\alpha + \eta). \tag{6.3}$$

Accounting for nonidealities allows us to address the first question, namely how the detected spin state is related to the spin properties of an emitted electron pair. Specifically, from our result in Eq. (6.2) we note that tomographically reconstructing a state ρ with a set of current cross-correlation measurements yields,

$$e^2\Gamma \mathrm{tr}\left[(\hat{1} \pm \zeta_A \mathbf{a}\cdot\boldsymbol{\sigma}) \otimes (\hat{1} \pm \zeta_B \mathbf{b}\cdot\boldsymbol{\sigma})\rho\right] = e^2\Gamma \mathrm{tr}\left[(\hat{1} \pm \mathbf{a}\cdot\boldsymbol{\sigma}) \otimes (\hat{1} \pm \mathbf{b}\cdot\boldsymbol{\sigma})\varrho\right]. \tag{6.4}$$

That is, tomographic reconstruction of a state ρ with non-ideal detectors is equivalent to reconstructing the state $\varrho = \rho\zeta_A\zeta_B - (1-\zeta_A\zeta_B)\hat{1}/4$ with ideal detectors. In the following, we briefly describe the model used to obtain these results.

6.2 Effective Lindblad equation

A big strength of our model is the ability to study transport statistics with an unknown entangler, which is tunnel-coupled to two detector dots. We achieve this with the main technical detail of Paper I, the effective equation of motion for state of the detector dots ρ,

$$\frac{d\rho}{dt} = \mathcal{L}_H(\rho) + \mathcal{L}_1(\rho) + \mathcal{L}_2(\rho) + \mathcal{L}_\eta(\rho) + \mathcal{L}^\chi_{FM}(\rho). \tag{6.5}$$

Here $\mathcal{L}_H(\rho)$ denotes the free evolution of the dots, $\mathcal{L}_1(\rho)$ ($\mathcal{L}_2(\rho)$) describes the emission of a single particle (two particles) from the entangler onto the detector dots. The remaining two terms describe local spin-flips of electrons residing on the detector dots and emission of the detector dot particles towards the FM contacts. The main result is obtained by solving the eigenvalue equation, described in Chapter 5, using the perturbative scheme outlined in Appendix E. To leading order in γ/Γ, where γ (Γ) denotes the emission rates from the entangler (detector dots), we obtain Eq. (6.1). We now briefly discuss the last four terms.

6.2.1 Effective single- and two particle emission

A principal assumption for our model is that particle emission from the entangler is a rare event. Trapped inside the entangler, the electrons are assumed to evolve into a stationary state, which is unaffected by the subsequent tunneling onto the detector dots. Thus, the function of the entangler is to ideally act as a reservoir which coherently emits entangled two-particle states, with infrequent emission of single uncorrelated particles.

Therefore, to account for these single- and two-particle tunneling processes we introduce two phenomenological Lindblad-type operators $\mathcal{L}_2(\rho)$ and $\mathcal{L}_1(\rho)$, respectively. See Appendix. A for an alternative argument for this model. The two Lindblad-type equations for the detector dot state ρ read,

$$\mathcal{L}_1(\rho) = \sum_{\alpha\sigma\sigma'} \gamma_\alpha^{\sigma\sigma'} \left[d^\dagger_{\alpha\sigma}\rho d_{\alpha\sigma'} - \frac{1}{2}\{d_{\alpha\sigma' d^\dagger_{\alpha\sigma}}, \rho\} \right], \tag{6.6}$$

$$\mathcal{L}_2(\rho) = \sum_{\tau\sigma\tau'\sigma'} \gamma_{AB}^{\tau\sigma\tau'\sigma'} \left[d^\dagger_{A\sigma} d^\dagger_{B\tau} \rho d_{B\tau'} d_{A\sigma'} - \frac{1}{2}\{d_{B\tau'} d_{A\sigma'} d^\dagger_{A\sigma} d^\dagger_{B\tau}, \rho\} \right]. \tag{6.7}$$

We enforce that these equations preserve the positivity and trace of the density matrices, the hallmark of a Lindblad equation. The effective single particle (pair) emission rates from the entangler are then restricted to being the matrix elements $\gamma_i^{\sigma\sigma'}$ ($\gamma_{AB}^{\sigma\tau\sigma'\tau'}$) of a Hermitian matrix $\hat{\gamma}_i$ ($\hat{\gamma}_{AB}$).

6.2.2 Non-idealities

We incorporate two non-idealities in the proposed entangler-detector system, which in conjunction contribute to an overall reduction of the detection efficiencies ζ_A, ζ_B. The first perturbation is the process of local spin-flips at the detector dots, due to e.g. fluctuating nuclear spins. We include this perturbing source by adding a Lindblad-type operator

$$\mathcal{L}_\eta(\rho) = \eta \sum_{\alpha\sigma} \left[d_{\alpha\sigma}\rho d_{\alpha\sigma}^\dagger - \frac{1}{2}\{d_{\alpha\sigma}^\dagger d_{\alpha\sigma}, \rho\} \right] \tag{6.8}$$

where η is the spin-flip rate, assumed to be the same in both detector dots. Detector dot dynamics due to the FM contacts is accounted for by,

$$\mathcal{L}_{FM}^\chi(\rho) = \sum_{\alpha m\sigma\sigma'} \Gamma_\alpha \left[d_{\alpha\sigma}\rho d_{\alpha\sigma'}^\dagger Q_{\alpha m}^{\sigma'\sigma} e^{i\chi_{\alpha m}} - \frac{1}{2}\{d_{\alpha\sigma}^\dagger d_{\alpha\sigma}, \rho\} \right]. \tag{6.9}$$

The effect of non-ideal polarisations is contained in the matrix elements $Q_{\alpha m}^{\sigma'\sigma}$, of the 2-by-2 matrix $Q_{\alpha m} = (\hat{1} + \mathbf{p}_\alpha \cdot \boldsymbol{\sigma})$. Here $|\mathbf{p}_\alpha| = p_\alpha \leq 1$ is introduced to account for nonideal polarisations of FM contacts $\alpha\pm$. A fully polarised FM contact α corresponds to $|\mathbf{p}_\alpha| = 1$, accepting only spins along the quantization axis of $\mathbf{p}_\alpha$, while $|\mathbf{p}_\alpha| = 0$ describes a normal contact which absorbs electrons irrespective of spin.

6.3 Remarks on operating regime

It is presumed that the generic entangler has been engineered such that the two-particle emission from the entangler is the dominant contribution to the current, such that $\gamma_\alpha^{\sigma\sigma',\tau\tau'} \gg \gamma_\alpha^{\sigma\sigma'}$ is satisfied. The operating regime is instead focused on ensuring that the setup works as an entanglement detection device. That is, we need to ensure that measured cross-correlations at the ferromagnetic contacts

are directly related to the two-particle state which has been emitted. We therefore want to minimise any back-action from the detector dots to the entangler.

To this end, we consider $\gamma_\alpha^{\sigma\sigma'}/\Gamma_\alpha \ll 1$ and $\gamma_\alpha^{\sigma\sigma',\tau\tau'}/\Gamma_\alpha \ll 1$ and choose anti-collinear pairs of FM contacts. The first condition ensures that charge pair being transferred to the detector dots cannot tunnel back, as they are rapidly absorbed by the detector leads. The effect of the latter condition can be seen explicitly in the term $\mathcal{L}_{FM}(\rho)$. We note that, if both FM contacts are equally coupled to the adjacent detector dot, without the counting fields χ_{An} and χ_{Bm}, the spin-sensitive matrix vanishes as $\sum_m Q_{\alpha m} = \hat{1}$. The anti-collinear FM contacts act therefore as an effective normal contact, which ensures that the spin state of the electron residing in the detector dots is not affected by the readout.

6.4 Applying the effective model

In practice, to apply our effective model, it is necessary to find an expression for the matrix rates. For this purpose, a T-matrix approach to time-dependent perturbation theory [85] is viable. Focusing on the key quantity for our setup, the two-particle rate matrix is,

$$\hat{\gamma}_{AB} = \hat{T}\frac{\Gamma_A + \Gamma_B}{(\varepsilon_A + \varepsilon_B - E_e)^2 + (\Gamma_A + \Gamma_B)^2/4}. \tag{6.10}$$

Here it is assumed that the energy of the entangler E_e is well defined. The matrix $\hat{T}$ is identified as the two-particle matrix golden rule rate, where its matrix elements are

$$(\hat{T})_{\sigma\sigma',\tau\tau'} = \mathrm{Tr}\{\rho_e H_T^{(2)}|\sigma_A\tau_B\rangle\langle\tau'_B\sigma'_A|H_T^{(2)}\}, \tag{6.11}$$

with ρ_e being the reduced density matrix of the isolated entangler. Using this approach, we have tested our effective model by comparing our current and current cross-correlation expressions to known results. Specifically we have considered the Andreev entangler of Ref. [86] and triple dot entangler [87]. See Fig. 6.2. The effective two-particle tunnelling Hamiltonians are,

$$\begin{aligned} H^{(2)}_{Andreev} &= J\left(b_0[d^\dagger_{A\uparrow}d^\dagger_{B\downarrow} - d^\dagger_{A\downarrow}d^\dagger_{B\uparrow}]\right) + h.c. \\ H^{(2)}_{3dot} &= \tfrac{2t^2}{U}\left(d_{e\uparrow}d_{e\downarrow}[d^\dagger_{A\uparrow}d^\dagger_{B\downarrow} - d^\dagger_{A\downarrow}d^\dagger_{B\uparrow}]\right) + h.c, \end{aligned} \tag{6.12}$$

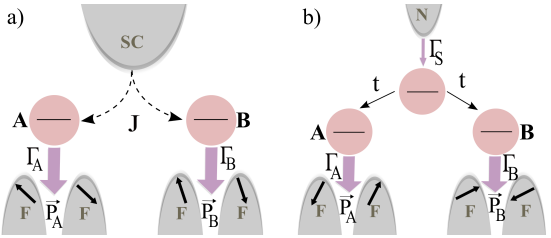

Figure 6.2: Schematics of a) the Andreev entangler and b) triple dot entangler in a transport setup. a) Cooper pairs escape the superconducting (SC) contact via tunneling amplitude J to two spatially separated detector dots, before being absorbed by the ferromagnetic (F) leads at rates Γ_A, Γ_B. b) The entangler dot is populated by a normal contact (N) with the tunneling rate Γ_S. Due to single particle energies being off resonant, the dominant transport is due to a two-particle tunneling events

Here, using the notation to our entangler-detector model, $d_{\alpha\sigma}$ denotes the annihilation operator of an electron in detector dot $\alpha = A, B$ (entangler dot $\alpha = e$) with spin σ. The effective two-particle tunneling amplitude J describes the tunneling of a Cooper pair between the superconductor and spatially separated dot pair and t is the tunneling amplitude between the entangler and detector dots and U onsite Coulomb interaction of the entangler dot. The operator b_0 is annihilates a cooper-pair in the superconductor, where the expectation value $\langle b_0 \rangle = 1$, for the superconducting ground state. We find in our operating regime that the resulting two-particle rate matrices,

$$\begin{aligned} \hat{\gamma}_{AB}^{Andreev} &= \frac{2J^2(\Gamma_A+\Gamma_B)}{(\varepsilon_A+\varepsilon_B)^2+(\Gamma_A+\Gamma_B)^2/4} |\Psi_S\rangle\langle\Psi_S| \\ \hat{\gamma}_{AB}^{3dot} &= \frac{8t^4}{U^2} \frac{(\Gamma_A+\Gamma_B)}{\delta\varepsilon^2+(\Gamma_A+\Gamma_B)^2/4} |\Psi_S\rangle\langle\Psi_S|, \end{aligned} \tag{6.13}$$

reproduce the known expressions for the current and cross-correlations. Here $|\Psi_S\rangle$ denotes the spin singlet state.

Chapter 7

Overview of Paper II

The downside of spin entanglement detection is that it requires a versatile spin sensitive detector. Such a detector, as proposed in Paper I, constitutes a big experimental challenge. An alternative scheme based on the orbital degree of freedom, such as the charge state in a quantum dot system, is in this regard more suitable. However, the orbital degree of freedom for electrons in a solid state device is plagued by a rapid decoherence rate, presenting a challenge to realise orbital-based quantum information processing.

However, despite the high susceptibility to charge noise, recent experiments [88, 89, 90] have demonstrated control of quantum dot charge qubit on a time scale orders of magnitude shorter than the decoherence time. These findings present an opportunity to investigating a scheme for detecting and generating pairs of orbitally entangled transport electrons. An interesting question is thus,

- *Is there an entanglement scheme which enables the generation and detection on a sub decoherence time scale?*

In this work, we propose such a scheme which, in the same nanoscale device, generates and detects orbitally entangled states with the usage of a co-tunneling process. The attractive properties of resonant co-tunneling are, i) it is a demonstrably coherent process [91, 92], and ii) it occurs on a time scale of picoseconds. In contrast, the decoherence time is reported to be on the order of nanoseconds [13, 14]. Specifically, we have proposed an entangler-detector device in Paper II, illustrated

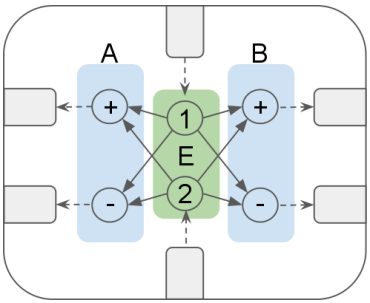

Figure 7.1: Schematic figure of the entangler-detector setup proposed in Paper II. The structure can be divided into an entangler (E) part, with quantum dots 1 and 2, and two spatially separated detectors (A) and (B) comprising dots $A+$, $A-$ and $B+$, $B-$. The solid lines show the participating tunnel couplings between entangler- and detector dots. The dashed lines indicate the role of leads, as either source or drain.

schematically in Fig. 7.1, consisting of six weakly tunnel-coupled quantum dots. Due to strong on-site Coulomb repulsion, none of the dots permits double occupation. By detuning the energy level of the individual quantum dots, we can obtain an ideal operation, where single particle tunnelling events are suppressed, leaving a dominating contribution from the transport of electron pairs. Similar to our work in Paper I, we explore the ramification of these cotunneling processes on the current cross-correlation measurements by studying the transport statistics.

7.1 Main results

The key result of Paper II is the cumulant generating function for the charge transport through the entangler-detector system

$$F(\chi) = \sum_{\alpha\beta} (e^{i(\chi_\alpha + \chi_\beta - \chi_1 - \chi_2)} - 1) P_{\alpha\beta}. \tag{7.1}$$

The long time transport statistics are clearly displayed, with four separate contributing Poisson processes. The contributions correspond to electrons emitted from leads 1 and 2 (counted by fields χ_1 and χ_2) populate entangler dots 1, 2, which are subsequently transferred in pairs to detector leads $\alpha = A\pm$ and $\beta = B\pm$ (counted by fields χ_α and χ_β) with transfer rate,

$$P_{\alpha\beta} = \frac{|t_{\alpha\beta 21}|^2(\Gamma_\alpha + \Gamma_\beta + \Gamma_\phi)}{\frac{\hbar^2}{4}(\Gamma_\alpha + \Gamma_\beta + \Gamma_\phi)^2 + \varepsilon_{12\alpha\beta}^2}, \tag{7.2}$$

where Γ_α is the tunnelling rate from detector dot α to the neighbouring lead, Γ_ϕ is the dephasing rate, $t_{\alpha\beta 21}$ is an effective two-particle tunnelling amplitude, and $\varepsilon_{12\alpha\beta}$ denotes the energy away from the two-particle resonance. Equipped with Eq. (7.2), we formulate a Bell inequality in terms of current cross-correlations, to detect orbitally entangled states. Identifying the probability for an electron pair initially populating the entangler dots 1 and 2, to be detected at leads α and β as $E_{\alpha,\beta} = P_{\alpha,\beta}(\sum_{\eta,\zeta} P_{\eta,\zeta})^{-1}$, we express the CHSH function [29, 35] in terms of cross correlation measurements

$$\mathcal{S} = |E_{AB} - E_{A'B} - E_{AB'} - E_{A'B'}|. \tag{7.3}$$

Here the correlation functions for the different settings A, B, A', B' are defined as,

$$E_{AB} = E_{A+,B+} - E_{A+,B-} - E_{A-,B+} + E_{A-,B-}. \tag{7.4}$$

As discussed in Chapter 2 for classical correlations there is an upper bound for the CHSH function, $\mathcal{S} \leq 2$. Under ideal operation, two resonant co-tunneling events are possible. Namely, an electron initially residing in entangler dot 1 can leave for detector dots in A, while the electron in dot 2 leaves for a detector dot in B, and the reverse. The resulting orbitally entangled state due to two-particle interference then reads,

$$|\psi\rangle_{\text{ent}} = \sin(\theta/2)|1\rangle_A|2\rangle_B - \cos(\theta/2)|2\rangle_A|1\rangle_B, \tag{7.5}$$

where $|1\rangle_A$ describes an electron being emitted from entangler dot 1 to detector subsystem A with analogous definition for e.g. $|2\rangle_B$. In Ref. [93] it was shown that choosing optimal detector settings A, A', B, B', the CHSH operator will yield $\mathcal{S} = 2\sqrt{1+\sin^2\theta}$. That is, in an ideal setup all pure entangled states can be detected.

In addition to using the long time statistics, it is possible to formulate a Bell inequality in terms of short-time properties of the charge current. To this end, we have obtained an expression for the electronic analogue of Glauber's second degree of coherence [94],

$$g^{(2)}_{\alpha\beta}(\tau) \approx P_{\alpha\beta}\frac{\Gamma_\alpha\Gamma_\beta}{\Gamma_\alpha+\Gamma_\beta}\frac{e^2}{I_\alpha I_\beta}(e^{-\Gamma_\alpha\tau} + e^{-\Gamma_\beta\tau}), \tag{7.6}$$

where terms on the order of unity have been neglected. The function $g^{(2)}_{\alpha\beta}(\tau)$ describes the conditional probability that an electron is emitted towards the lead α or

β at time τ, given that an electron was detected at lead β or α at time t=0, respectively. This opens up the possiblity for detecting entanglement by monitoring the detector dot population in real time, by e.g. placing quantum point contacts in close proximity to the detector dots. To clarify how we obtain the primary results, below we will discuss our model.

7.2 Model

7.2.1 Effective Hamiltonian

The entangler-detector system is described by the Hamiltonian

$$H = H_0 + V = \sum_{\gamma=1,2,\alpha\beta} \varepsilon_\gamma d_\gamma^\dagger d_\gamma + \sum_{\gamma\neq\gamma'} t_{\gamma\gamma'} d_\gamma^\dagger d_{\gamma'} + h.c., \tag{7.7}$$

where H_0 describes the single particle dot energies and V describes the tunnel coupling between different quantum dots. Here we use the notation from the paper, where indices $\alpha = A+, A-$ and $\beta = B+, B-$ label the four detector dots, while entangler dots are labelled 1 and 2.

Due to growing size of the Lindblad matrix, discussed in Chapter 4, accounting for all possible contributing processes in a transport setup is a computationally demanding task. Instead, we will restrict our analysis to a parameter regime where sequential tunnelling between the dots is very slow, and study an effective Hamiltonian which only reproduces co-tunneling correctly. The effective picture becomes a valid approximation by tuning the single dot energy levels to satisfy

$$\varepsilon_\alpha + \varepsilon_\beta + U_{\alpha\beta} \approx \varepsilon_1 + \varepsilon_2 + U_{12}, \tag{7.8}$$

whilst keeping all intermediate steps, describing a single particle tunnelling, off resonant. Under these conditions, we can from the outset recognise that sequential tunnelling is suppressed and employ a Schrieffer-Wolff transformation [95]. The resulting effective Hamiltonian,

$$H_{\text{eff}} = UHU^\dagger \approx H_0 + V^{\text{eff}}, \tag{7.9}$$

where we have discarded the slow single particle tunnelling part, which significantly reduces the complexity of the problem. For details about the transformation

see Paper II and Appendix C. The transformed Hamiltonian includes an effective two-particle tunneling part,

$$V^{\text{eff}} = H_T^{(2)} = \sum_{\alpha\beta} \left(t_{\beta\alpha 21} d_\beta^\dagger d_\alpha^\dagger d_2 d_1 + h.c. \right), \quad t_{\alpha\beta 21} = \frac{t_{\beta 1} t_{\alpha 2}}{\Delta E_{\beta\alpha}} - \frac{t_{\alpha 1} t_{\beta 2}}{\Delta E_{\alpha\beta}}. \tag{7.10}$$

The dependence of the effective two-particle tunneling on the dot energies enters via $\Delta E_{\alpha\beta}$,

$$\Delta E_{\alpha\beta} = \sum_{v,i} \frac{1}{\varepsilon_r - \varepsilon_i}, \tag{7.11}$$

where r runs over the resonant states of both entangler dots being populated, and both electrons residing detector dots α and β. The energies ε_i in the sum correspond to the energies of intermediate states when an electron from dot 1 leaves for dots α, and an electron from dot 2 to dots β. We obtain the definition of $\Delta E_{\beta\alpha}$ by exchanging α and β. As a passing remark, it is interesting to note that the effective two-particle tunnelling amplitude $t_{\alpha\beta 21}$ describes the coherent superposition of two individual paths taken by the electron pair.

7.2.2 Transport statistics

The transport measurements we consider, are conducted in a high-bias regime. The dynamics of the dot system are then described well by the Lindblad equation,

$$\frac{d\rho}{dt} = \mathcal{L}_0 \rho + \sum_{\gamma=\alpha,\beta} \mathcal{D}^\gamma_{-\chi_\gamma}[d_\gamma^\dagger, \rho] + \sum_{\gamma=1,2} \mathcal{D}^\gamma_{\chi_\gamma}[d_\gamma, \rho] + \sum_\gamma \mathcal{D}^\phi_0[d_\gamma^\dagger d_\gamma, \rho] \tag{7.12}$$

where $\mathcal{D}^\gamma_\chi[d,\rho] = \Gamma_\gamma \left[\exp(i\chi) d\rho d^\dagger - \{d^\dagger d, \rho\}/2 \right]$, and $\mathcal{L}_0\rho = -\frac{i}{\hbar}[V^{\text{eff}}, \rho]$ describes the free evolution of the system without leads. The second and third term describe the absorption of electrons residing in the detector dots and injection onto the entangler dots respectively. We further include a source of dephasing of the orbital state, which corresponds to the last term.

Similar to the operating regime studied in Paper I, we consider the limit $\Gamma_\alpha, \Gamma_\beta \gg \Gamma_1, \Gamma_2 \gg t_{\beta\alpha 21}/\hbar$ to eliminate unwanted back-tunneling from detector dots onto the entangler dots, and the ensure that only one pair at a time is contributing to the cross-correlation measurement. In this regime, once the detector dots have been populated, the electrons immediately leave for the neighbouring leads one

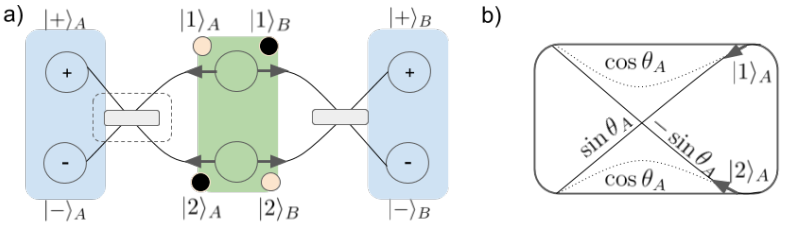

Figure 7.2: a) A schematic of the effective beamsplitter, with the resulting orbitally entangled state leaving dot 1 (2) for a detector dot in A and B (B and A). b) The effective beamsplitter for an electron moving towards A. The electron path is uninterrupted (solid line) for $\theta_A = \pi/2$, whereas they are entirely reflected (dotted line) for $\theta_A = 0$.

after another before the entangler dots are repopulated. Further, it is assumed that $\hbar\Gamma_\alpha \gg t_{A+A-}, \hbar\Gamma_\beta \gg t_{B+B-}$ and we accordingly neglect any tunnelling between the detector dots.

To find the cumulant generating function specified in the main results section, we solve the eigenvalue equation to leading order in the tunnelling amplitude $t_{\beta\alpha 21}$.

7.2.3 Effective beam splitter

As a consequence of the high bias regime, and suppressed back-tunneling from detector dots to entangler dots, the charge transport is unidirectional. We can then interpret the ideal transport scenario as an orbitally entangled pair of electrons passing through effective beam splitters, specified by the tunnelling amplitudes, before finally arriving at the detector dots.

Specifically, by tuning the dot energies to ensure two-particle resonance, then for a parameter regime where $\Delta E_{\alpha\beta} = \Delta E_{AB}$ and $\Delta E_{\beta\alpha} = \Delta E_{BA}$, we can parametrise the tunnelling amplitudes as, for example, $\tan\theta_A = t_{A-1}/t_{A+1}$. See Fig. 7.2. Operating with the co-tunneling Hamiltonian on the intially populated entangler dots yields the unnormalised state,

$$|\Psi\rangle_{\text{dot}} = -\sum_{\alpha\beta} \frac{t_{\beta 2} t_{\alpha 1}}{\Delta E_{AB}} |\alpha\rangle|\beta\rangle + \sum_{\alpha\beta} \frac{t_{\beta 1} t_{\alpha 2}}{\Delta E_{BA}} |\alpha\rangle|\beta\rangle. \tag{7.13}$$

These two terms can be identified as the orbitally entangled state,

$$|\Psi\rangle_{\text{ent}} = c_{21}|2\rangle_A|1\rangle_B - c_{12}|1\rangle_A|2\rangle_B, \tag{7.14}$$

where $|i\rangle_\alpha$ denotes the emission of an electron from entangler dot i towards detector dot α, with a scattering matrix. The coefficients c_{21} and c_{12} correspond to $t_{B1}t_{A2}/\Delta_{AB}$ and $t_{B2}t_{A1}/\Delta_{AB}$ respectively. See Appendix D for details. In this picture the resulting state is described by

$$|\Psi\rangle_{\rm dot} = (S_A \otimes S_B)|\Psi\rangle_{\rm ent}, \quad S_i = \begin{pmatrix} \sin\theta_i & \cos\theta_i \\ \cos\theta_i & -\sin\theta_i \end{pmatrix}. \tag{7.15}$$

The transport process is thus, an entangled pair of electrons, emitted towards the detector, locally rotated in orbital space by the effective beam splitter S_i before arriving at the detector dots in i. The angle characterising the beam-splitter, e.g. $\tan\theta_A = t_{A-1}/t_{A+1}$, can in principle be varied by adjusting the tunneling barriers, from $\theta_i = \pi/2$ for a transparent beam splitter and $\theta_i = 0$, where the electrons are completely reflected. If these are adjusted optimally, we obtain an expectation value of the CHSH function $\mathcal{S} = S_{max} = 2\sqrt{1+\sin^2(2\phi)}$, with $\phi = \arctan(c_{12}/c_{21})$[93].

7.3 Short time properties

In addition to the long time statistics, in Paper II we also investigate a short-time property of charge transport. Specifically, we study an electronic analogue of the second order correlation function $g^{(2)}(\tau)$ of Quantum Optics [94]. In our system, $g^{(2)}(\tau)$ corresponds to the conditional probability that an electron is emitted towards a drain contact at a particular time $t+\tau$, given that an electron was transferred at time t.

In particular, aiming to provide a real-time entanglement test, we are interested in the correlated transport of electrons emitted towards leads $\alpha = A\pm$ and $\beta = B\pm$. Within the framework of a Markovian quantum master equation, this function is obtained as [96]

$$g^{(2)}_{\alpha\beta}(\tau) = \frac{\langle\langle \mathcal{J}_\alpha e^{\mathcal{L}\tau}\mathcal{J}_\beta\rangle\rangle + \langle\langle \mathcal{J}_\beta e^{\mathcal{L}\tau}\mathcal{J}_\alpha\rangle\rangle}{2\langle\langle \mathcal{J}_\alpha\rangle\rangle\langle\langle \mathcal{J}_\beta\rangle\rangle}. \tag{7.16}$$

where, using the vector notation introduced in Chapter 5, we have

$$\begin{aligned} \langle\langle J_\alpha\rangle\rangle &= \vec{tr}\tfrac{\partial M}{\partial\chi_\alpha}\vec{\rho}_{ss}\big|_{\chi_\alpha,\chi_\beta\to 0}, \\ \langle\langle \mathcal{J}_\alpha e^{\mathcal{L}\tau}\mathcal{J}_\beta\rangle\rangle &= \vec{tr}\tfrac{\partial M}{\partial\chi_\alpha}e^{M\tau}\tfrac{\partial M}{\partial\chi_\beta}\vec{\rho}_{ss}\big|_{\chi_\alpha,\chi_\beta\to 0}, \end{aligned} \tag{7.17}$$

where $\vec{tr}$, is defined to satisfy $\vec{tr}\vec{\rho} = \mathrm{tr}[\rho] = 1$. To obtain the result specified in the main results section, we evaluate Eq. (7.16) to leading order in the tunneling amplitudes $t_{\beta\alpha 21}$. In this limit, the factor $e^{M\tau} = e^{M\tau}|_{t_{\beta\alpha 21}\to 0}$ and we obtain,

$$g^{(2)}_{\alpha\beta}(\tau) = P_{\alpha\beta}\frac{\Gamma_\alpha\Gamma_\beta}{\Gamma_\alpha+\Gamma_\beta}\frac{e^2}{2I_\alpha I_\beta}(\exp(-\Gamma_\alpha\tau)+\exp(-\Gamma_\beta\tau)), \tag{7.18}$$

where an additional term on the order of unity is disregarded. Here the electron pair transport taking place can be described as, once an electron has left for detector α, the second electron, unable to tunnel to any of the other dots, leaves subsequently for detector β, leaving room for the next pair. This is reflected by the exponential decay of cross correlations attributed to the transport of pairs.

The $g^{(2)}_{\alpha\beta}(\tau)$ expression provides insights into how a short time Bell test would work. Importantly, Eq. (7.18) displays a principal limitation of using real-time joint detection probabilities to detect entanglement. In contrast to the long time correlation measurements, where all the electrons will be contributing to the current cross-correlation, the short-time correlations have a decay time set by the rates $\Gamma_\alpha, \Gamma_\beta$, resulting in non-ideal detection efficiencies. To accurately detect correlated pair transport real-time monitoring would need to resolve dot occupations on a time $t \ll \Gamma_\alpha, \Gamma_\beta$. In practice, the measurement resolution is set by a finite bandwidth $\Delta\omega$ of the detector, that is, for e.g. detecting dot populations in dot α the non-ideal efficiency is $\eta_\alpha = e^{-\Gamma_\alpha/\Delta\omega}$.

Chapter 8

Overview of Paper III

A significant obstacle to realising an entanglement detection scheme in a nanoscale solid state device is the necessity for a highly versatile detector which allows for a set of distinct cross-correlation measurements. A prime example of this is a conventional Bell test, as the CHSH function outlined in Paper II. To experimentally verify a violation of a Bell inequality using the CHSH function, it is necessary to perform sixteen distinct cross-correlation measurements.

With the work of Papers I and II as a basis, where we formulate Bell inequalities using current cross-correlations, in Paper III we seek to facilitate the entanglement detection with a more measurement conservative detection scheme. To this end, we use the concept of entanglement witnesses (See Chapter 2). In contrast to a Bell inequality, the entanglement witness approach targets specifically to distinguish separable states from the non-separable. This is however not a serious drawback, since we cannot rule out any LHV theories in a nanoscale transport setup. We are only interested in detecting entangled, or non-separable, states. The main question we have aimed to address is

- *Employed with only current cross-correlation measurements, what is the most efficient scheme to detect the presence of non-separable states faithfully?*

To answer this question, we consider a general entanglement detection scheme, consisting of an entangler emitting pairs of electrons with a rate Γ. These pairs pass through two beamsplitters with splitting efficiencies ζ_A and ζ_B prior to being

detected at the detector leads. From Paper I, we know that the current cross-correlation measurement at detectors $A\pm$ and $B\pm$ is of the form

$$S_{AB}^{\pm\pm} = e^2\Gamma \mathrm{tr}\left[(\hat{1} \pm \zeta_A \mathbf{a}\cdot\boldsymbol{\sigma}) \otimes (\hat{1} \pm \zeta_B \mathbf{b}\cdot\boldsymbol{\sigma})\rho\right]. \tag{8.1}$$

We identify $(\hat{1}+\zeta_A\mathbf{a}\cdot\boldsymbol{\sigma})\otimes(\hat{1}+\zeta_B\mathbf{b}\cdot\boldsymbol{\sigma})$, which has been the basic building block in our entanglement detection schemes, as the current cross-correlation operator. With this starting point, in Paper III we formulate an entanglement witness as a sum of different cross correlation measurements. That is, an N-measurement entanglement witness is,

$$W^{(N)} = \sum_{i=1}^{N} (\hat{1} + \zeta_A \mathbf{a}_i \cdot \boldsymbol{\sigma}) \otimes (\hat{1} + \zeta_B \mathbf{b}_i \cdot \boldsymbol{\sigma}). \tag{8.2}$$

Equipped with $W^{(N)}$, we can reformulate the main question as the following fundamental questions:

- *What is the minimum amount of current cross-correlation measurements necessary for $W^{(N)}$ to constitute an entanglement witness? That is,*

$$\mathrm{tr}\{W^{(N)}\rho\} > \max_{\rho_s} \mathrm{tr}\{W^{(N)}\rho_s\} \quad \text{or} \quad \mathrm{tr}\{W^{(N)}\rho\} < \min_{\rho_s} \mathrm{tr}\{W^{(N)}\rho_s\}. \tag{8.3}$$

Additionally, since a specific entanglement witness only specifies that there exists a state which satisfies the above stated conditions, a natural follow up question is:

- *Which entangled states can be detected by such a witness?*

Answers to these two questions, discussed below, are the main results of this paper.

8.1 Main results

Our most important result answers the first question. We find it is sufficient to carry out two distinct cross-correlation measurements to detect entangled states. That is, $W^{(2)}$ is an entanglement witness, that can detect entangled states which violate both the upper and lower bound,

$$\mathrm{tr}\{W^{(2)}\rho\} > \max_{\rho_s} \mathrm{tr}\{W^{(2)}\rho_s\} \quad \text{and} \quad \mathrm{tr}\{W^{(2)}\rho\} < \min_{\rho_s} \mathrm{tr}\{W^{(2)}\rho_s\}. \tag{8.4}$$

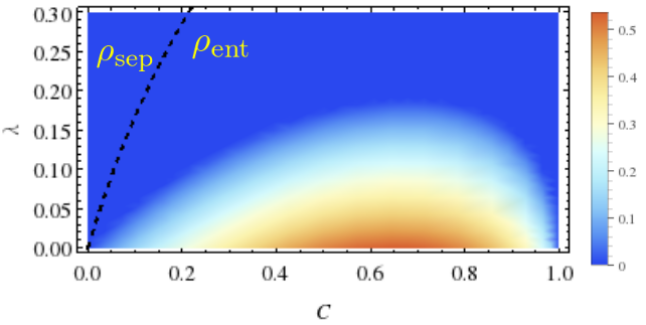

Figure 8.1: Optimal detection margin Δ_{σ}^{W+} for states $\sigma = \lambda\hat{1}/4 + (1-\lambda)\rho_C$ as a function of concurrance $\mathcal{C}$ and λ. The separation between σ being separable and entangled is indicated by the dashed line

To answer the second question, which entangled states can be detected, we consider first the case of pure states. We find the interesting result that the detection range of our minimal witness $W^{(2)}$ consists of all entangled states, except the maximally entangled Bell states. Extending our analysis to the more general mixed states, we find a significant reduction in detection range. In Fig. 8.1 this effect is demonstrated by considering the mixed state

$$\sigma = \lambda\hat{1}/4 + (1-\lambda)\rho_C, \tag{8.5}$$

where $\hat{1}/4$ is a completely mixed separable state and ρ_C is an entangled state with concurrence C. The state σ is within the detection range for $\lambda < (1 + \Delta_{\rho}^{W\pm}/|\Delta_{\hat{1}}^{W\pm}|)^{-1}$, whereas it is entangled for $\lambda < (1 + (2C)^{-1})^{-1}$. Here Δ_{ρ}^{W+} (Δ_{ρ}^{W-}) denotes the maximal distance between upper (lower) bound for separable states ρ_s and the full spectrum of $W^{(2)}$,

$$\begin{aligned} \Delta_{\rho}^{W+} &= \text{tr}\left[W^{(2)}\rho\right] - \max_{\rho_s} \text{tr}\left[W^{(2)}\rho_s\right] \\ \Delta_{\rho}^{W-} &= -\text{tr}\left[W^{(2)}\rho\right] + \min_{\rho_s} \text{tr}\left[W^{(2)}\rho_s\right]. \end{aligned} \tag{8.6}$$

We note from Figure 4 that the detection range is more strict, from which it follows that not all entangled mixed states are detected.

Owing to the importance of Bell states, for example when studying the Cooper Pair Splitters discussed in Paper I, we have further investigated how many measurements are required to also resolve maximally entangled states. We find, following the same approach, it is enough to introduce a third measurement in the same plane to obtain a witness operator $W^{(3)}$ whose detection range contains also the maximally entangled states.

In addition to this, with $W^{(3)}$ we reproduce the lowest efficiency $\zeta = 1/\sqrt{3}$ required to detect the Bell states, found in Paper I and e.g., Ref. [97]. In the following, we briefly describe how we have reached the conclusions stated above.

8.2 Showing that $W^{(N)}$ is a witness

To show the first result, we focus here on the lower boundary. For $W^{(2)}$ to be a witness, the smallest eigenvalue λ_1 must be smaller than $\min_{\rho_s} \mathrm{tr}[W^{(2)}\rho_s]$. This, in turn, is possible only if λ_1 is a non-degenerate eigenvalue, and the corresponding eigenvector describes an entangled state[98]

To show that $W^{(2)}$ is an entanglement witness it is sufficient to consider the case of symmetric settings, that is $\zeta_A = \zeta_B = \zeta$ and $\theta_A = \theta_B = \theta$, where the angles are defined as $\cos\theta_A = \mathbf{a}_1 \cdot \mathbf{a}_2$ and $\cos\theta_B = \mathbf{b}_1 \cdot \mathbf{b}_2$. We first minimise the expectation value for separable states $\min_{\rho_s} \mathrm{tr}[W^{(2)}\rho_s] = \min_{\chi_a,\chi_b} \langle\chi_a|\langle\chi_b|W^{(2)}|\chi_a\rangle|\chi_b\rangle$. This minimisation can be carried out by e.g., parametrising the spinor as $|\chi_i\rangle = (\cos\phi_i, \exp(i\varphi_i)\sin\phi_i)$. Solving this minimisation problem gives two solutions, valid in different parameter regimes,

$$\min_{\rho_s} \mathrm{tr}[W^{(2)}\rho_s] = \begin{cases} 2(1-\zeta\cos\left(\frac{\theta}{2}\right))^2 \\ 2(1-\zeta^2)\sin^2\left(\frac{\theta}{2}\right) \end{cases}, \tag{8.7}$$

where switching between the two solutions occurs as they intersect. Second, we study the minimal eigenvalues of $W^{(2)}$. One particularly convenient representation is

$$W^{(2)} = 2\left[\pm s_A s_B \sigma_x \otimes \sigma_x + (\hat{1} \pm c_A\sigma_z) \otimes (\hat{1} \pm c_A\sigma_z)\right], \tag{8.8}$$

which gives the minimal eigenvalue $\lambda_1 = 2(1 + c_A c_B - \sqrt{(c_A + c_B)^2 + s_A^2 s_B^2})$, where $c_\alpha = \zeta_\alpha \cos(\theta_\alpha/2)$ and $s_\alpha = \zeta_\alpha \sin(\theta_\alpha/2)$. This eigenvalue is unique for all angles θ, except for $\theta = \pi$, where it becomes equal to the second smallest eigenvalue. The associated eigenstate is also a nonseparable state for all parameters, except $\theta = 0$ and $\zeta = 0$. Comparing the minimised values shows that operators of the form $W^{(2)}$ satisfy the criteria of an entanglement witness.

To show that three measurements are sufficient to detect Bell states, we consider the symmetric detector settings $\mathbf{a}_1 \cdot \mathbf{a}_2 = 0$ and $\mathbf{a}_1 \cdot \mathbf{a}_3 = -1$, and similarly for detector B. Using the same approach as for $W^{(2)}$, the minimum expectation of

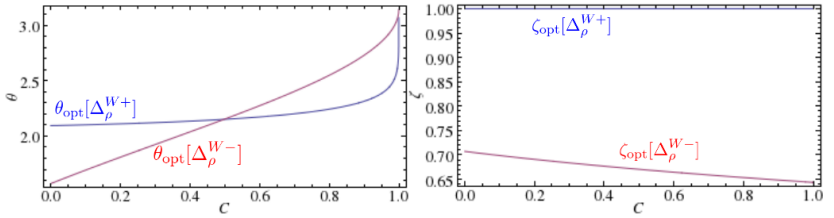

Figure 8.2: Optimal splitting efficiency ζ_{opt} and polarisation orientation θ_{opt} of the detector which maximise Δ_ρ^{W+} and Δ_ρ^{W-}, as a function of concurrence C.

$W^{(3)}$ for separable states reads

$$\min_{\rho_s} \mathrm{tr}\left[W^{(3)}\rho_s\right] = \begin{cases} 8/3 - 2\zeta^2 & 1/3 \le \zeta \le 1 \\ 2 + (1-\zeta)^2 & 0 \le \zeta \le 1/3 \end{cases}, \tag{8.9}$$

where again the two minimal solutions switch as they intersect. The minimal eigenvalue of $W^{(3)}$ similarly

$$\min_{\rho} \mathrm{tr}\left[W^{(3)}\rho\right] = \begin{cases} 3(1-\zeta^2) & 1/\sqrt{3} \le \zeta \le 1 \\ 3 + \zeta^2 - 2\zeta\sqrt{1+\zeta^2} & 0 \le \zeta \le 1/\sqrt{3}, \end{cases} \tag{8.10}$$

switches between two eigenstates. Crucially, for $\zeta \ge 1/\sqrt{3}$, the eigenstate corresponding to the smallest eigenvalue is a maximally entangled singlet state. That is, $W^{(3)}$ resolves the maximally entangled states. Interesting to note, this is the same lower bound on the efficiency as found in Paper I.

8.3 Optimal witness

For our claims regarding which states can be detected, we must find $W^{(2)}$ which also optimises the detection margin Δ_ρ^{W-}. To this end, we have investigated which parameters optimise our entanglement witness and how these parameters vary for different states. Using that a general pure two qubit state can be uniquely characterised by its concurrence [99], we investigate the expectation value of the entanglement witness for a state of concurrence C,

$$\mathrm{tr}\left[W^{(2)}\rho_C\right] = \mathrm{tr}\left[\bar{W}^{(2)}\bar{\rho}_C\right], \tag{8.11}$$

where $\bar{\rho}_C$ denotes the two qubit state where the local basis of A and B, has been rotated to bring the state, which gives the smallest eigenvalue, into a Schmidt form

$|\bar{\psi}_1\rangle = \sum_{\sigma=\uparrow,\downarrow} c_{\sigma\sigma}|\sigma\sigma\rangle$. Numerically it is found that maximising the detector margin, is possible with $\bar{W}^{(2)}$ of the form described in Eq. (8.8) with symmetric settings $\zeta_A = \zeta_B = \zeta$ and $\theta_A = \theta_B = \theta$. The optimal parameters are then obtained as the parameters which maximise the detection margin $\Delta_\rho^{W^-} = -\mathrm{tr}\left[W^{(2)}\rho\right] + \min_{\rho_s} \mathrm{tr}[W^{(2)}\rho_s]$. This condition translates into the set of equations

$$\begin{aligned} \partial_\zeta \Delta_\rho^{W^-} &= 4\cos\tfrac{\theta}{2}\cos 2x - 2\zeta\,(2 + \cos\theta\sin 2x + \cos 2x) = 0, \\ \partial_\theta \Delta_\rho^{W^-} &= -2\zeta\cos 2x \sin\tfrac{\theta}{2} + \sin\theta + \zeta^2 \sin\theta\sin 2x = 0, \end{aligned} \tag{8.12}$$

where we have used the notation of the paper $\sin 2x = C$. Solving these equations, we obtain the optimal parameters displayed in Fig. 8.2. To obtain the optimal parameters for a violation of the upper bound, which instead maximise ΔW_ρ^+, one proceeds in a similar fashion.

In Figure 8.2, it is also seen how the optimal witness fails to resolve states which are maximally entangled, that is, states for which $C = 1$. For maximally entangled states, the optimal setting $\theta = \pi$ results in the minimal (maximal) eigenvalue to be degenerate and $W^{(2)}$ stops being an entanglement witness. Before concluding, we point out another interesting detail seen in Fig. 8.2, namely for an optimal witness which violates the lower bound, a non-optimal efficiency ζ is required to detect entangled states. Moreover, with an ideal detector efficiency ζ the optimal detection margin is zero.

Chapter 9

Overview of Paper IV

Quantum dot based spin qubits in semiconductor heterostructures are a promising candidate for storing and processing quantum information. In particular for this purpose spins in lateral GaAs [100, 101, 19, 102, 103, 104] and Si/SiGe [105, 106, 107, 108, 109, 110] quantum dots have seen promising results. Owing to the presence of spin-orbit interactions in these materials, by applying a magnetic field it is possible to coherently manipulate a localised spin via EDSR, as has already been experimentally demonstrated[41]. However, the spin-orbit mediated coupling of spin and electric field also enables a notable spin relaxation due to acoustic phonons [111, 112, 113, 114, 115, 116, 117].

A recent experiment on EDSR with a GaAs quantum dot [101] verified the the-

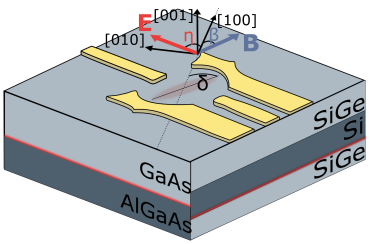

Figure 9.1: (From Paper IV) Schematic figure of the EDSR setup considered in Paper IV. An electron from the 2DEG at the interface is trapped in a biharmonic trap potential. The orientation of the dot is specified by the angle δ between the major axis, and crystallograpic axis [100]. An inplane magnetic field $\mathbf{B} = (\cos\beta, \sin\beta, 0)$ is applied.

oretical predictions that, due to the anisotropy of the spin-orbit interactions, the phonons induce a spin relaxation which depends on the orientation of the magnetic field and the direction of the dot. This prompted us to, with the work of Paper IV, investigate optimising EDSR control of a spin, by varying the controllable parameters of the setup. See Fig. 9.1.

We define the optimal EDSR scheme as allowing for the maximum amount of single qubit operations, quantified by the induced Rabi frequency Ω, under the constraint of a finite spin lifetime T. To this end we introduce a figure of merit for the spin qubit device, $\zeta = T\Omega$, and examine how the geometry of the dot and orientation of the applied magnetic field can be used to optimise this quantity. Before addressing the main results of the paper, we briefly introduce our model.

9.1 Model

The lateral quantum dots we study are defined by a bi-harmonic oscillator potential in a quasi-two dimensional system, owing to the strong confinement along the growth direction. We apply a magnetic field $\mathbf{B} = \mathbf{b}B$ in-plane to avoid any orbital effects, and consider the Zeeman split lowest spin pair $|\Psi_\uparrow\rangle, |\Psi_\uparrow\rangle$ as the spin qubit states. To ensure that only these states are populated, we consider temperatures which are well below the energy separation of orbital states $T \ll \hbar^2/2m^*l^2$. Here the confinement length l of the dot is on the order of 10nm, and m^* is the effective electron mass. We account for non-circular dots by introducing an ellipticity ϵ parameter which relates the confinement length along the major $l_{x'} = l$ and minor axis $l_{y'} = l(1-\epsilon)^{1/4}$.

As discussed in Chapter 3, in the quasi-two dimensional picture the spin-orbit Hamiltonian is approximated by the two dimensional linear Rashba and Dresselhaus spin-orbit interactions. The main consequence of this interaction, present in both GaAs and Si/SiGe dots, is the emergence of a finite dipole moment $\mathbf{d}$, which couples the spin qubit states

$$\mathbf{d} = \langle\Psi_\uparrow|\mathbf{r}|\Psi_\downarrow\rangle = \frac{g^*\mu_b m^* l'^4}{4\hbar^2 l_{so}}\mathbf{v}, \quad \mathbf{v} = \sum_{i=x',y'} \frac{l_i'^4}{l'^4}(\mathbf{n}_{so}^i \times \mathbf{b})_z \mathbf{e}_i \tag{9.1}$$

where g^* is the electron g-factor, μ_B is the Bohr magneton and $l_{so} = (l_d^2 + l_r^2)^{1/2}$, with $l_r(l_d)$ being the spin-orbit length of the Rashba-type (Dresselhaus-type) spin-

orbit interaction. The vectors $\mathbf{n}_{so}^{i}$ are defined by expressing $\mathbf{n}_{so} = (x\sin\nu + y\cos\nu, -x\cos\nu - y\sin\nu)$ in the dot coordinates (x', y'), that is, $\mathbf{n}_{so} = x'\mathbf{n}_{so}^{x'} + y'\mathbf{n}_{so}^{y'}$. Here we have introduced the spin-orbit mixing angle $\nu = \arctan(l_r/l_d)$, which is $\nu = 0$ for dominant Rashba term and $\nu = \pi/2$ for dominant Dresselhaus. We note that the dimensionless vector $\mathbf{v}$ gives rise to an anisotropic dipole moment, defined by spin-orbit interactions and dot geometry.

With the finite dipole moment $\mathbf{d}$ in place, we achieve electric control of the spin by applying an oscillating electric field $\mathbf{E} = \mathbf{E}_0\cos\omega t$. To leading order in the spin-orbit coupling, the electric field, tuned to be on resonance, induces Rabi oscillations with a Rabi frequency

$$\Omega = \frac{eE_0}{\hbar}|\mathbf{d}|. \tag{9.2}$$

To evaluate the spin relaxation rate due to acoustic phonons we use Fermi's golden rule with zero temperature. For instance, in the case of piezoelectric acoustic phonons, the spin relaxation rate reads,

$$\Gamma_{\rm ph} = \frac{\pi}{\rho V}\sum_{\mathbf{K}\lambda}\frac{K|M_{\mathbf{K}}^{\lambda}|^2}{c_\lambda}|\langle\Psi_\downarrow|e^{i\mathbf{K}\cdot\mathbf{R}}|\Psi_\uparrow\rangle\delta(\hbar\omega_K^{\lambda} - \varepsilon_z). \tag{9.3}$$

The experiment we model, consists of a quantum dot whose confinement length is much smaller than the wavelength of phonons corresponding to the Zeeman splitting energy ε_z. We accordingly limit our analysis to the dipole limit, where $e^{i\mathbf{K}\cdot\mathbf{R}} \approx 1 + i(\mathbf{K}\cdot\mathbf{R})$. The factor $|M_{\mathbf{K}}^{\lambda}|^2$ in Eq. (9.3) is the anisotropic geometric factor introduced in Chapter 3.

9.2 Measure of spin qubit quality

To quantify the efficiency of a controllable spin qubit via EDSR we consider a figure of merit ζ

$$\zeta = \Omega T = \frac{\Omega}{\Gamma_{\rm ph} + \Gamma_o}, \tag{9.4}$$

where $\Gamma_{\rm ph}$ is the dipolar charge noise contribution to T, Γ_o is introduced to account for additional decay channels, and Ω is the Rabi frequency

$$\Omega \propto |\mathbf{E}\cdot\mathbf{v}|. \tag{9.5}$$

We find that the expression for the figure of merit can be simplified. Despite a generally anisotropic electron-phonon interaction in GaAs and Si/SiGe, in the dipole limit, the phonon induced relaxation rate can be approximated as

$$\Gamma_{\mathrm{ph}} \approx \gamma |\mathbf{v}|^2. \tag{9.6}$$

This proportionality is a consequence of the crystal symmetries of GaAs and Si/SiGe, and is argued for in detail in the appendices B and C of Paper IV. It is further shown to be a good approximation for magnetic fields up to order of Tesla. In addition, we consider an applied electric field in the direction $\mathbf{E} \parallel \mathbf{d}$, since a misalignment only yields an overall reduction to the Rabi frequency. The key quantity of Paper IV, the EDSR figure of merit, then reads

$$\zeta = \zeta_0 \frac{|\mathbf{v}|}{|\mathbf{v}|^2 + \Gamma_0/\gamma}. \tag{9.7}$$

From this expression we note that the anisotropy of the figure of merit is entirely contained within the dimensionless vector $\mathbf{v}$, defined in Equation (9.1).

9.3 Main results

With the model and definitions formulated, we pose the core questions of Paper IV as follows:

- *Is it possible to improve the figure of merit by varying the magnetic field orientation?*
- *For elliptical quantum dots, is there a preferred major axis?*
- *Are there designs with elliptical quantum dots for which ζ can be maximized by only orienting the magnetic field?*

To answer these questions we maximize the figure of merit with respect to the controllable parameters, that is, the orientation of the magnetic field and major dot axis, relative to the crystallographic axes. We find then that optimal magnetic field- and dot orientation, β_{opt} and δ_{opt} are the angles for which the dimensionless

vector is given by,

$$|\mathbf{v}| = \begin{cases} \sqrt{1+|\sin 2\nu|}, & \text{if } \frac{\Gamma_0}{\gamma} > 1+|\sin 2\nu| \\ \sqrt{1+|\sin 2\nu|}(1-\epsilon), & \text{if } \frac{\Gamma_0}{\gamma} < (1-|\sin 2\nu|)(1-\epsilon)^2 \\ \sqrt{\frac{\Gamma_0}{\gamma}}, & \text{otherwise,} \end{cases} , \quad (9.8)$$

With this expression, together with the magnitude of the spin-orbit vector in the dot coordinate system,

$$|\mathbf{v}|^2 = |\mathbf{n}_{so}^{x'} \times \mathbf{b}|^2 + (1-\epsilon)^2 |\mathbf{n}_{so}^{y'} \times \mathbf{b}|^2, \quad (9.9)$$

we draw a series of conclusions, which can be seen qualitatively in Fig. 9.2 for elliptical dots. To answer the first question, we find that the figure of merit ζ can be improved by properly orienting the magnetic field, with the exception of circular dots if either Rashba- or Dresselhaus spin-orbit interaction is absent. When the spin relaxation is due to piezoelectric and deformation potential acoustic phonons is dominant, that is $\gamma \gg \Gamma_0$, the figure of merit is maximised by the magnetic field orientation $\beta_{opt} = \text{sgn}(l_r l_d)\pi/4$. This corresponds to applying a magnetic field along the $[110]$ axis when the Rashba and Dresselhaus spin-orbit terms share the same sign, $[1\bar{1}0]$ otherwise.

When the rates γ, Γ_0 are comparable, for elliptical dots we find that the orientation of the major axis becomes important. Importantly, as an answer to the second question, we note for a major axis direction $\delta = \text{sgn}(l_d l_r)\pi/4$, we are able to obtain the global maximum of ζ by varying only the magnetic field orientation. This ideal dot geometry would correspond to aligning the major axis along the crystallographic axes $[110]$ or $[1\bar{1}0]$ depending on the relative sign of $l_r l_d$.

To address the last question we study quantum dot devices for different spin-orbit strengths. We find the answer to be yes, there are devices where it is sufficient to reorient the magnetic field. We notice that for elliptical quantum dots, when either Rashba- or Dresselhaus-type spin-orbit interaction is dominant, the figure of merit only depends on the relative angle between magnetic field- and dot orientation, that is $\zeta(\delta, \beta) = \zeta(\beta - \delta)$. This effect starts to emerge in the left and right column of Fig. 9.2b.

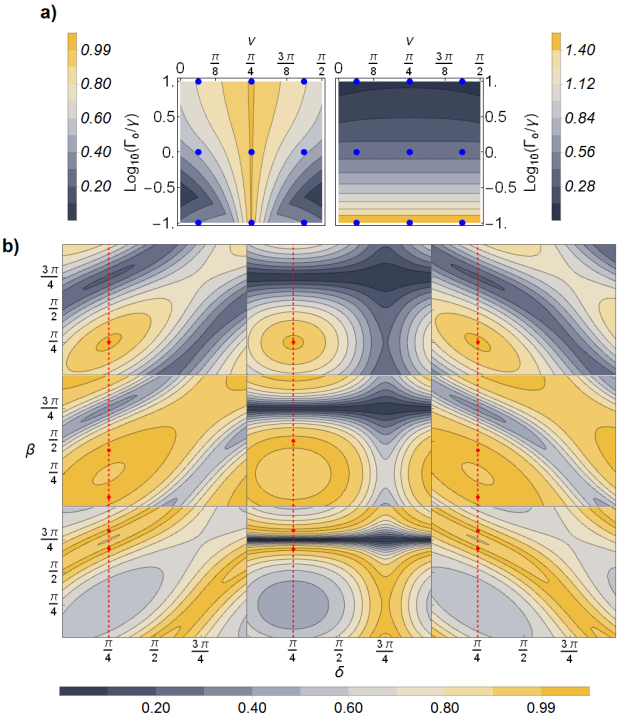

Figure 9.2: (From Paper IV) (a) Left (right) figure shows the tunability $\mathcal{T} = 1 - \min_{\beta,\delta} \zeta / \max_{\beta,\delta} \zeta$ (maximal quality $\mathcal{Q} = \max_{\beta,\delta} \zeta/\zeta_0$) of the figure of merit. Each blue point, specifying a spin-orbit mixing angle ν and ratio Γ_0/γ, gives the parameters of the corresponding figure in (b). (b) Normalized ζ as a function of magnetic field and dot orientation. In all figures an elliptic dot with $\epsilon = 0.75$ is considered, and $l_d l_r > 0$. The vertical dashed line is the optimal dot orientation and the red points correspond to the optimal device configuration.

Chapter 10

Summary and outlook

In this thesis we have presented our work on two closely related topics. The first topic concerns the coherent control of a quantum dot based spin qubit, using EDSR. Specifically, we have studied how dot geometry and orientation of the magnetic field affect the efficiency of an EDSR setup. In Paper IV our results show the emergence of a robust, unique, dot orientation, despite a generally anisotropic electron-phonon coupling. With the setup considered in Paper IV being in line with current experiments, we predict our results relevant for future experiments on EDSR control of spin qubits.

The second topic concerns the presence of entanglement in the constituent electrons of an electric current, with an emphasis on facilitating entanglement detection in non-ideal devices. To this end, we have in Paper I proposed a generic entangler-dot model, in a hybrid nanoscale device consisting of quantum dots coupled to ferromagnetic contacts. In addition to this, in Paper II we have proposed a scheme for generating and detecting orbitally entangled states using a cotunneling processes to circumvent the well-known difficulty of short decoherence time for orbital coherences.

To obtain a physically clear picture, we have employed the tools of Full Counting Statistics to identify the contributing transport events as the collection of Poissonian stochastic processes, a distinctive sign of independent discrete transfers of charge. Finally, following this route we have used our primary quantity, the current cross-correlator, to go beyond the conventional means of detecting entangle-

ment in pursuit of a more efficient scheme. In doing so, we have come across a minimal detection scheme consisting of only two current cross-correlation measurements.

During our work we have encountered new questions, in part due to our schemes not yet being within reach of current experiments, and in part because of interesting results which are not fully understood. Based on these questions, in the following we present possible extensions to our work.

In Paper I, our entangler-detector model provides a physically transparent picture, which relates the measured current correlations to the spin properties of entangled electron pairs being transported. However, the required versatility, the ability to actively manipulate the spin density of states of the ferromagnetic contact, puts the model outside what is currently feasible. This motivates a further study into alternative methods of realising a non-invasive spin sensitive measurement.

We avoid the difficulty of realising devices with adjustable spin-sensitive contacts, by focusing on the orbitally entangled states in Paper II. However, to ensure that the co-tunneling process which generates the entangled state is dominant, the scheme requires an array of six well-defined and tunable quantum dots. An interesting extension is to study the possibility of simplifying the structure. The proposed device can be considered a proof of principle, to be used as a basis to investigate a minimal scheme which can employ cotunneling events to generate and detect orbitally entangled states.

During our work with entanglement witnesses in Paper III, we found an interesting detail, namely the inability of resolve the maximally entangled states using two correlation measurements, while all other pure entangled states were within the detection range. This thought-provoking result invites a further investigation to understand the underlying reason. In addition, we may consider non-linear witness operators [118, 119] as a means of expanding the detectable range of entangled states. In particular this extension would be of interest when studying the entanglement of mixed states, where detection range of linear witness operators is limited. While there is room for improvement, with the recent advances of fabricating multiple controllable quantum dots devices [18, 16, 17], we believe the future prospects for experimentally realising our proposed schemes are promising.

In conclusion, while many obstacles remain to achieving the ambitious goal of quantum information processing in solid-state devices, it is a personal hope of the

thesis' author that our work presents a step in the right direction. In particular, by advancing future work on coherent control of quantum dot spin qubits, and by providing a solid platform for unambiguous entanglement detection in future solid-state devices.

References

[1] R.P. Feynman. Simulating physics with computers. International journal of theoretical physics **21**(6), 467 (1982)

[2] M.A. Nielsen, I.L. Chuang, *Quantum computation and quantum information* (Cambridge university press, 2010)

[3] P.W. Shor. Polynomial-Time Algorithms for Prime Factorization and Discrete Logarithms on a Quantum Computer. SIAM Journal on Computing **26**(5), 1484 (1997)

[4] A. Montanaro. Quantum algorithms: an overview. npj Quantum Information **2**, 15023 (2016)

[5] T.D. Ladd, F. Jelezko, R. Laflamme, Y. Nakamura, C. Monroe, J.L. O'Brien. Quantum computers. Nature **464**(7285), 45 (2010)

[6] Y. Nakamura, Y.A. Pashkin, J. Tsai. Coherent control of macroscopic quantum states in a single-Cooper-pair box. Nature **398**(6730), 786 (1999)

[7] C.F. Roos, M. Riebe, H. Häffner, W. Hänsel, J. Benhelm, G.P. Lancaster, C. Becher, F. Schmidt-Kaler, R. Blatt. Control and measurement of three-qubit entangled states. science **304**(5676), 1478 (2004)

[8] J.I. Cirac, P. Zoller. Quantum Computations with Cold Trapped Ions. Phys. Rev. Lett. **74**, 4091 (1995)

[9] F. Koppens, C. Buizert, K.J. Tielrooij, I. Vink, K. Nowack, T. Meunier, L. Kouwenhoven, L. Vandersypen. Driven coherent oscillations of a single electron spin in a quantum dot. Nature **442**(7104), 766 (2006)

[10] E. Kawakami, P. Scarlino, D. Ward, F. Braakman, D. Savage, M. Lagally, M. Friesen, S. Coppersmith, M. Eriksson, L. Vandersypen. Electrical control of a long-lived spin qubit in a Si/SiGe quantum dot. Nature nanotechnology **9**(9), 666 (2014)

[11] D. Loss, D.P. DiVincenzo. Quantum computation with quantum dots. Phys. Rev. A **57**, 120 (1998)

[12] C. Kloeffel, D. Loss. Prospects for Spin-Based Quantum Computing. Annu. Rev. Cond. Mat. Phys. **4**, 51 (2013)

[13] T. Hayashi, T. Fujisawa, H.D. Cheong, Y.H. Jeong, Y. Hirayama. Coherent Manipulation of Electronic States in a Double Quantum Dot. Phys. Rev. Lett. **91**, 226804 (2003)

[14] K.D. Petersson, J.R. Petta, H. Lu, A.C. Gossard. Quantum Coherence in a One-Electron Semiconductor Charge Qubit. Phys. Rev. Lett. **105**, 246804 (2010)

[15] R. Hanson, L.P. Kouwenhoven, J.R. Petta, S. Tarucha, L.M.K. Vandersypen. Spins in few-electron quantum dots. Rev. Mod. Phys. **79**, 1217 (2007)

[16] T. Otsuka, T. Nakajima, M.R. Delbecq, S. Amaha, J. Yoneda, K. Takeda, G. Allison, T. Ito, R. Sugawara, A. Noiri, et al. Single-electron Spin Resonance in a Quadruple Quantum Dot. arXiv preprint arXiv:1510.02547 (2015)

[17] A. Noiri, J. Yoneda, T. Nakajima, T. Otsuka, M.R. Delbecq, K. Takeda, S. Amaha, G. Allison, A. Ludwig, A.D. Wieck, et al. Coherent electron-spin-resonance manipulation of three individual spins in a triple quantum dot. Applied Physics Letters **108**(15), 153101 (2016)

[18] T. Ito, T. Otsuka, S. Amaha, M.R. Delbecq, et al. Detection and control of charge states in a quintuple quantum dot. arXiv preprint arXiv:1604.04426 (2016)

[19] J. Yoneda, T. Otsuka, T. Nakajima, T. Takakura, T. Obata, M. Pioro-Ladrière, H. Lu, C.J. Palmstrøm, A.C. Gossard, S. Tarucha. Fast Electrical Control of Single Electron Spins in Quantum Dots with Vanishing Influence from Nuclear Spins. Phys. Rev. Lett. **113**, 267601 (2014)

[20] K. Takeda, J. Kamioka, T. Otsuka, J. Yoneda, T. Nakajima, M.R. Delbecq, S. Amaha, G. Allison, T. Kodera, S. Oda, S. Tarucha. A fault-tolerant addressable spin qubit in a natural silicon quantum dot. Science Advances **2**(8) (2016)

[21] E. Schrödinger. Naturwissenschaften **23**(823), 152 (1935)

[22] A. Einstein, B. Podolsky, N. Rosen. Can Quantum-Mechanical Description of Physical Reality Be Considered Complete? Phys. Rev. **47**, 777 (1935)

[23] D. Bohm, Y. Aharonov. Discussion of Experimental Proof for the Paradox of Einstein, Rosen, and Podolsky. Phys. Rev. **108**, 1070 (1957)

[24] J.S. Bell. On the Einstein Podolsky Rosen Paradox. Physics **1**, 195 (1964)

[25] B. Hensen, H. Bernien, A. Dréau, A. Reiserer, N. Kalb, M. Blok, et al. Loophole-free Bell inequality violation using electron spins separated by 1.3 kilometres. Nature **526**(7575), 682 (2015)

[26] L.K. Shalm, E. Meyer-Scott, B.G. Christensen, P. Bierhorst, et al. Strong Loophole-Free Test of Local Realism*. Phys. Rev. Lett. **115**, 250402 (2015)

[27] M. Giustina, M.A.M. Versteegh, S. Wengerowsky, J. Handsteiner, et al. Significant-Loophole-Free Test of Bell's Theorem with Entangled Photons. Phys. Rev. Lett. **115**, 250401 (2015)

[28] R.F. Werner. Quantum states with Einstein-Podolsky-Rosen correlations admitting a hidden-variable model. Phys. Rev. A **40**, 4277 (1989)

[29] R. Horodecki, P. Horodecki, M. Horodecki, K. Horodecki. Quantum entanglement. Rev. Mod. Phys. **81**, 865 (2009)

[30] A. Aspect, P. Grangier, G. Roger. Experimental Realization of Einstein-Podolsky-Rosen-Bohm *Gedankenexperiment* : A New Violation of Bell's Inequalities. Phys. Rev. Lett. **49**, 91 (1982)

[31] J.F. Clauser, M.A. Horne, A. Shimony, R.A. Holt. Proposed Experiment to Test Local Hidden-Variable Theories. Phys. Rev. Lett. **23**, 880 (1969)

[32] B.S. Cirel'son. Quantum generalizations of Bell's inequality. Letters in Mathematical Physics **4**(2), 93 (1980)

[33] U. Fano. Description of states in quantum mechanics by density matrix and operator techniques. Reviews of Modern Physics **29**(1), 74 (1957)

[34] A. Peres. Separability Criterion for Density Matrices. Phys. Rev. Lett. 77, 1413 (1996)

[35] O. Gühne, G. Tóth. Entanglement detection. Physics Reports **474**(1), 1 (2009)

[36] W.K. Wootters. Entanglement of formation of an arbitrary state of two qubits. Physical Review Letters **80**(10), 2245 (1998)

[37] M. Horodecki, P. Horodecki, R. Horodecki. Separability of mixed states: necessary and sufficient conditions. Physics Letters A **223**(1), 1 (1996)

[38] C. Kloeffel, D. Loss. Prospects for Spin-Based Quantum Computing in Quantum Dots. Annual Review of Condensed Matter Physics **4**, 51 (2013)

[39] M. Ciorga, A.S. Sachrajda, P. Hawrylak, C. Gould, P. Zawadzki, S. Jullian, Y. Feng, Z. Wasilewski. Addition spectrum of a lateral dot from Coulomb and spin-blockade spectroscopy. Phys. Rev. B **61**, R16315 (2000)

[40] S. Gustavsson, R. Leturcq, B. Simovič, R. Schleser, P. Studerus, T. Ihn, K. Ensslin, D.C. Driscoll, A.C. Gossard. Counting statistics and super-Poissonian noise in a quantum dot: Time-resolved measurements of electron transport. Phys. Rev. B **74**, 195305 (2006)

[41] K. Nowack, F. Koppens, Y.V. Nazarov, L. Vandersypen. Coherent control of a single electron spin with electric fields. Science **318**(5855), 1430 (2007)

[42] G. Dresselhaus. Spin-orbit coupling effects in zinc blende structures. Physical Review **100**(2), 580 (1955)

[43] Y.A. Bychkov, E.I. Rashba. Oscillatory effects and the magnetic susceptibility of carriers in inversion layers. Journal of physics C: Solid state physics **17**(33), 6039 (1984)

[44] M. Pioro-Ladriere, T. Obata, Y. Tokura, Y.S. Shin, T. Kubo, K. Yoshida, T. Taniyama, S. Tarucha. Electrically driven single-electron spin resonance in a slanting Zeeman field. Nature Physics **4**(10), 776 (2008)

[45] M. Dyakonov, V. Perel. Spin relaxation of conduction electrons in noncentrosymmetric semiconductors. Soviet Physics Solid State, Ussr **13**(12), 3023 (1972)

[46] L.E. Golub, E.L. Ivchenko. Spin splitting in symmetrical SiGe quantum wells. Phys. Rev. B **69**, 115333 (2004)

[47] J.H. Van Vleck. Paramagnetic Relaxation Times for Titanium and Chrome Alum. Phys. Rev. **57**, 426 (1940)

[48] P. YU, M. Cardona, *Fundamentals of Semiconductors: Physics and Materials Properties*. Graduate Texts in Physics (Springer, 2010)

[49] C. Herring, E. Vogt. Transport and Deformation-Potential Theory for Many-Valley Semiconductors with Anisotropic Scattering. Phys. Rev. **101**, 944 (1956)

[50] Q. Li, L. Cywiński, D. Culcer, X. Hu, S. Das Sarma. Exchange coupling in silicon quantum dots: Theoretical considerations for quantum computation. Phys. Rev. B **81**, 085313 (2010)

[51] M. Prada, R.H. Blick, R. Joynt. Singlet-triplet relaxation in two-electron silicon quantum dots. Phys. Rev. B 77, 115438 (2008)

[52] D. Culcer, L. Cywiński, Q. Li, X. Hu, S. Das Sarma. Realizing singlet-triplet qubits in multivalley Si quantum dots. Phys. Rev. B **80**, 205302 (2009)

[53] F. Schäffler. High-mobility Si and Ge structures. Semiconductor Science and Technology **12**(12), 1515 (1997)

[54] M. Raith, P. Stano, J. Fabian. Theory of single electron spin relaxation in Si/SiGe lateral coupled quantum dots. Physical Review B **83**(19), 195318 (2011)

[55] A. Grodecka, L. Jacak, P. Machnikowski, K. Roszak. Phonon impact on the coherent control of quantum states in semiconductor quantum dots. arXiv preprint cond-mat/0404364 (2004)

[56] R.E. Newnham, *Properties of materials: anisotropy, symmetry, structure* (Oxford University Press on Demand, 2005)

[57] D.A. Bagrets, Y.V. Nazarov. Full counting statistics of charge transfer in Coulomb blockade systems. Phys. Rev. B **67**, 085316 (2003)

[58] S. Gurvitz, Y.S. Prager. Microscopic derivation of rate equations for quantum transport. Physical Review B **53**(23), 15932 (1996)

[59] G. Lindblad. On the generators of quantum dynamical semigroups. Communications in Mathematical Physics **48**(2), 119 (1976)

[60] H.P. Breuer, F. Petruccione, *The theory of open quantum systems* (Oxford University Press on Demand, 2002)

[61] C. Gardiner, P. Zoller, *Quantum noise: a handbook of Markovian and non-Markovian quantum stochastic methods with applications to quantum optics*, vol. 56 (Springer Science & Business Media, 2004)

[62] R.J. Glauber, *Optical Coherence and Photon Statistics* (Wiley-VCH Verlag, 2007), pp. 23–182

[63] L.S. Levitov, H. Lee, G.B. Lesovik. Electron counting statistics and coherent states of electric current. Journal of Mathematical Physics **37**(10), 4845 (1996)

[64] W. Belzig, Y.V. Nazarov. Full Counting Statistics of Electron Transfer between Superconductors. Phys. Rev. Lett. **87**, 197006 (2001)

[65] W. Belzig, in *Quantum Noise in Mesoscopic Physics* (Springer, 2003), pp. 463–496

[66] C. Flindt, T. Novotny, A.P. Jauho. Full counting statistics of nano-electromechanical systems. EPL (Europhysics Letters) **69**(3), 475 (2005)

[67] Y.V. Nazarov, M. Kindermann. Full counting statistics of a general quantum mechanical variable. The European Physical Journal B - Condensed Matter and Complex Systems **35**(3), 413 (2003)

[68] T. Monnai. Derivation of quantum master equation with counting fields by monitoring a probe. Phys. Rev. E **82**, 051113 (2010)

[69] G. Kießlich, P. Samuelsson, A. Wacker, E. Schöll. Counting statistics and decoherence in coupled quantum dots. Physical Review B **73**(3), 033312 (2006)

[70] Y.M. Blanter, M. Büttiker. Shot noise in mesoscopic conductors. Physics reports **336**(1), 1 (2000)

[71] C. Beenakker, C. Schönenberger, et al. Quantum shot noise. Physics Today **56**(5), 37 (2003)

[72] W. Schottky. Regarding spontaneous current fluctuation in different electricity conductors. Ann. der Physik **57**(23), 541 (1918)

[73] L. Hofstetter, S. Csonka, J. Nygård, C. Schönenberger. Cooper pair splitter realized in a two-quantum-dot Y-junction. Nature **461**(7266), 960 (2009)

[74] L.G. Herrmann, F. Portier, P. Roche, A.L. Yeyati, T. Kontos, C. Strunk. Carbon Nanotubes as Cooper-Pair Beam Splitters. Phys. Rev. Lett. **104**, 026801 (2010)

[75] L. Hofstetter, S. Csonka, A. Baumgartner, G. Fülöp, S. d'Hollosy, J. Nygård, C. Schönenberger. Finite-Bias Cooper Pair Splitting. Phys. Rev. Lett. **107**, 136801 (2011)

[76] A. Das, Y. Ronen, M. Heiblum, D. Mahalu, A.V. Kretinin, H. Shtrikman. High-efficiency Cooper pair splitting demonstrated by two-particle conductance resonance and positive noise cross-correlation. Nature communications **3**, 1165 (2012)

[77] J. Schindele, A. Baumgartner, C. Schönenberger. Near-Unity Cooper Pair Splitting Efficiency. Phys. Rev. Lett. **109**, 157002 (2012)

[78] L. Herrmann, P. Burset, W. Herrera, F. Portier, P. Roche, C. Strunk, A.L. Yeyati, T. Kontos. Spectroscopy of non-local superconducting correlations in a double quantum dot. arXiv preprint arXiv:1205.1972 (2012)

[79] S. Kawabata. Test of Bell's inequality using the spin filter effect in ferromagnetic semiconductor microstructures. Journal of the Physical Society of Japan **70**(5), 1210 (2001)

[80] N.M. Chtchelkatchev, G. Blatter, G.B. Lesovik, T. Martin. Bell inequalities and entanglement in solid-state devices. Physical Review B **66**(16), 161320 (2002)

[81] A. Di Lorenzo, Y.V. Nazarov. Full counting statistics with spin-sensitive detectors reveals spin singlets. Physical review letters **94**(21), 210601 (2005)

[82] A. Bednorz, W. Belzig. Proposal for a cumulant-based Bell test for mesoscopic junctions. Phys. Rev. B **83**, 125304 (2011)

[83] J.P. Morten, D. Huertas-Hernando, W. Belzig, A. Brataas. Elementary charge transfer processes in a superconductor-ferromagnet entangler. EPL (Europhysics Letters) **81**(4), 40002 (2008)

[84] P. Samuelsson, M. Büttiker. Quantum state tomography with quantum shot noise. Phys. Rev. B **73**, 041305 (2006)

[85] H. Bruus, K. Flensberg, *Many-body quantum theory in condensed matter physics: an introduction* (Oxford University Press, 2004)

[86] P. Recher, E.V. Sukhorukov, D. Loss. Andreev tunneling, Coulomb blockade, and resonant transport of nonlocal spin-entangled electrons. Physical Review B **63**(16), 165314 (2001)

[87] D.S. Saraga, D. Loss. Spin-entangled currents created by a triple quantum dot. Physical review letters **90**(16), 166803 (2003)

[88] Y. Dovzhenko, J. Stehlik, K. Petersson, J. Petta, H. Lu, A. Gossard. Nonadiabatic quantum control of a semiconductor charge qubit. Physical Review B **84**(16), 161302 (2011)

[89] M. Yamamoto, S. Takada, C. Bäuerle, K. Watanabe, A.D. Wieck, S. Tarucha. Electrical control of a solid-state flying qubit. Nature nanotechnology 7(4), 247 (2012)

[90] G. Cao, H.O. Li, T. Tu, L. Wang, C. Zhou, M. Xiao, G.C. Guo, H.W. Jiang, G.P. Guo. Ultrafast universal quantum control of a quantum-dot charge qubit using Landau–Zener–Stückelberg interference. Nature communications **4**, 1401 (2013)

[91] M. Sigrist, T. Ihn, K. Ensslin, D. Loss, M. Reinwald, W. Wegscheider. Phase coherence in the inelastic cotunneling regime. Physical review letters **96**(3), 036804 (2006)

[92] S. Gustavsson, R. Leturcq, M. Studer, T. Ihn, K. Ensslin, D. Driscoll, A. Gossard. Time-resolved detection of single-electron interference. Nano letters **8**(8), 2547 (2008)

[93] P. Samuelsson, E.V. Sukhorukov, M. Büttiker. Orbital Entanglement and Violation of Bell Inequalities in Mesoscopic Conductors. Phys. Rev. Lett. **91**, 157002 (2003)

[94] R.J. Glauber. The quantum theory of optical coherence. Physical Review **130**(6), 2529 (1963)

[95] J.R. Schrieffer, P.A. Wolff. Relation between the Anderson and Kondo Hamiltonians. Phys. Rev. **149**, 491 (1966)

[96] C. Emary, C. Pöltl, A. Carmele, J. Kabuss, A. Knorr, T. Brandes. Bunching and antibunching in electronic transport. Physical Review B **85**(16), 165417 (2012)

[97] W. Kłobus, A. Grudka, A. Baumgartner, D. Tomaszewski, C. Schönenberger, J. Martinek. Entanglement witnessing and quantum cryptography with nonideal ferromagnetic detectors. Physical Review B **89**(12), 125404 (2014)

[98] N.R. Wallach. An unentangled Gleason's theorem. Contemporary Mathematics **305**, 291 (2002)

[99] N. Linden, S. Popescu. On Multi-Particle Entanglement. Fortschritte der Physik **46**(4-5), 567 (1998)

[100] M. Delbecq, T. Nakajima, T. Otsuka, S. Amaha, J. Watson, M.J. Manfra, S. Tarucha. Full control of quadruple quantum dot circuit charge states in the single electron regime. Applied Physics Letters **104**(18), 183111 (2014)

[101] P. Scarlino, E. Kawakami, P. Stano, M. Shafiei, C. Reichl, W. Wegscheider, L.M.K. Vandersypen. Spin-Relaxation Anisotropy in a GaAs Quantum Dot. Phys. Rev. Lett. **113**, 256802 (2014)

[102] M.D. Shulman, O.E. Dial, S.P. Harvey, H. Bluhm, V. Umansky, A. Yacoby. Demonstration of Entanglement of Electrostatically Coupled Singlet-Triplet Qubits. Science **336**(6078), 202 (2012)

[103] M. Busl, G. Granger, L. Gaudreau, R. Sánchez, A. Kam, M. Pioro-Ladriere, S. Studenikin, P. Zawadzki, Z. Wasilewski, A. Sachrajda, et al. Bipolar spin blockade and coherent state superpositions in a triple quantum dot. Nature nanotechnology **8**(4), 261 (2013)

[104] A.P. Higginbotham, F. Kuemmeth, M.P. Hanson, A.C. Gossard, C.M. Marcus. Coherent Operations and Screening in Multielectron Spin Qubits. Phys. Rev. Lett. **112**, 026801 (2014)

[105] B. Maune, M. Borselli, B. Huang, T. Ladd, P. Deelman, K. Holabird, A. Kiselev, I. Alvarado-Rodriguez, R. Ross, A. Schmitz, et al. Coherent singlet-triplet oscillations in a silicon-based double quantum dot. Nature **481**(7381), 344 (2012)

[106] E. Kawakami, P. Scarlino, D. Ward, F. Braakman, D. Savage, M. Lagally, M. Friesen, S. Coppersmith, M. Eriksson, L. Vandersypen. Electrical control of a long-lived spin qubit in a Si/SiGe quantum dot. Nature nanotechnology **9**(9), 666 (2014)

[107] K. Takeda, T. Obata, Y. Fukuoka, W. Akhtar, J. Kamioka, T. Kodera, S. Oda, S. Tarucha. Characterization and suppression of low-frequency noise in Si/SiGe quantum point contacts and quantum dots. Applied Physics Letters **102**(12), 123113 (2013)

[108] Z. Shi, C. Simmons, D.R. Ward, J. Prance, X. Wu, T.S. Koh, J.K. Gamble, D. Savage, M. Lagally, M. Friesen, et al. Fast coherent manipulation of three-electron states in a double quantum dot. Nature communications **5** (2014)

[109] X. Hao, R. Ruskov, M. Xiao, C. Tahan, H. Jiang. Electron spin resonance and spin–valley physics in a silicon double quantum dot. Nature communications **5** (2014)

[110] M. Veldhorst, C. Yang, J. Hwang, W. Huang, J. Dehollain, J. Muhonen, S. Simmons, A. Laucht, F. Hudson, K.M. Itoh, et al. A two-qubit logic gate in silicon. Nature (2015)

[111] E.I. Rashba, A.L. Efros. Orbital Mechanisms of Electron-Spin Manipulation by an Electric Field. Phys. Rev. Lett. **91**, 126405 (2003)

[112] D.V. Bulaev, D. Loss. Spin relaxation and anticrossing in quantum dots: Rashba versus Dresselhaus spin orbit coupling. Phys. Rev. B **71**, 205324 (2005)

[113] V.I. Fal'ko, B.L. Altshuler, O. Tsyplyatyev. Anisotropy of Spin Splitting and Spin Relaxation in Lateral Quantum Dots. Phys. Rev. Lett. **95**, 076603 (2005)

[114] P. Stano, J. Fabian. Theory of Phonon-Induced Spin Relaxation in Laterally Coupled Quantum Dots. Phys. Rev. Lett. **96**, 186602 (2006)

[115] P. Stano, J. Fabian. Orbital and spin relaxation in single and coupled quantum dots. Phys. Rev. B **74**, 045320 (2006)

[116] O. Olendski, T.V. Shahbazyan. Theory of anisotropic spin relaxation in quantum dots. Phys. Rev. B **75**, 041306(R) (2007)

[117] V.N. Golovach, A. Khaetskii, D. Loss. Spin relaxation at the singlet-triplet crossing in a quantum dot. Phys. Rev. B 77, 045328 (2008)

[118] O. Gühne, N. Lütkenhaus. Nonlinear Entanglement Witnesses. Phys. Rev. Lett. **96**, 170502 (2006)

[119] J.M. Arrazola, O. Gittsovich, N. Lütkenhaus. Accessible nonlinear entanglement witnesses. Phys. Rev. A **85**, 062327 (2012)

[120] E.M. Kessler. Generalized Schrieffer-Wolff formalism for dissipative systems. Phys. Rev. A **86**, 012126 (2012)

[121] S. Bravyi, D.P. DiVincenzo, D. Loss. Schrieffer–Wolff transformation for quantum many-body systems. Annals of physics **326**(10), 2793 (2011)

[122] I. Shavitt, L.T. Redmon. Quasidegenerate perturbation theories. A canonical van Vleck formalism and its relationship to other approaches. The Journal of Chemical Physics **73**(11), 5711 (1980)

Appendices

Appendix A: Derivation of effective equation of motion of Paper I.

Using the notation of Paper I, the proposed effective equation of motion reads,

$$\frac{d\rho}{dt} = -\frac{i}{\hbar}[H_d, \rho] + \mathcal{L}_1(\rho) + \mathcal{L}_2(\rho) + \mathcal{L}_\eta(\rho) + \mathcal{L}^\chi_{FM}(\rho). \tag{A.1}$$

The second and third terms have been heurestically argued for as effective Lindblad-type operators, describing the emission of independent single and two particles, respectively. Here we show that these terms can be obtained by using a generalized Schrieffer-Wolff transformation [120]. Because the main quantity is the cross correlator, where the single particle emission is missing, the following derivation is going to focus on the effective two-particle rate.

The system comprises two sub-systems - one entangler (E) and one detector (D) part. For simplicity, the explicit system will be the triple dot entangler considered in Paper I but the approach allows for a more general setup. The essential criteria for our effective treatment are

- The entangler state is independent of the electron transport.
- The single particle energies are highly off-resonance, resulting in a dominant co-tunneling contribution to the overall charge transport.

The proceedure of obtaining an effective equation of motion for the detector dots is as follows,

- Partition the full Hilbert space into a high and low energy set of states. Obtain an effective two particle tunneling Hamiltonian.
- Partition the equation of motion into an equation of motion leaving the entangler state constant and its complement. Obtain an effective equation of motion.
- Trace out the entangler degrees of freedom.

Our starting point is the initial Lindblad-type equation of motion for the states in both entangler and detector dots. In units which satisfy $\hbar = 1$, the equation of

motion reads,

$$\frac{d\rho}{dt} = -i[H_D + H_E + H_{ED}, \rho] + \mathcal{D}_E(\rho) + \mathcal{D}_D^{\chi}(\rho) = -i[H_{ED}, \rho] + \mathcal{L}_0(\rho). \quad \text{(A.2)}$$

where dissipation operators are

$$\begin{aligned} \mathcal{D}_E(\rho) &= \Gamma_e \sum_\sigma \left[-\{e_\sigma^\dagger e_\sigma, \rho\} + 2 e_\sigma \rho e_\sigma^\dagger \right], \\ \mathcal{D}_D(\rho) &= \Gamma_d \sum_\sigma \left[-\{d_\sigma d_\sigma^\dagger, \rho\} + 2 d_\sigma^\dagger \rho d_\sigma e^{i\chi} \right]. \end{aligned} \quad \text{(A.3)}$$

Here H_D, H_E are the Hamiltonians of the isolated dot and entangler part respectively, $\mathcal{D}_E(\rho)$ describes the process of injecting additional electrons into the entangler to ensure that it can return to its initial state. The dissipation term $\mathcal{D}_D(\rho)$ is a measurement event as the particles tunnel from the detector dots onto the leads. The entangler-dot tunnelling Hamiltonian is given by

$$H_{ED} = \sum_\sigma \left(\Delta d_\sigma^\dagger e_\sigma + \Delta^* e_\sigma^\dagger d_\sigma \right). \quad \text{(A.4)}$$

We may decompose the Hilbert space into a set of low energy states $\mathbf{P}$, with an 'intial' P^i and one 'final' state projection P^f, and its complement $\mathbf{Q}$. This decomposition can be understood as $\mathbf{P}$ being the low energy sector, the complement $\mathbf{Q}$ constituting the high energy sector. The extra energy required to populate the virtual states in $\mathbf{Q}$, here labelled U, corresponds to the separation between these two spaces.

$$\mathbf{P} = \{|2\rangle_E \otimes |00\rangle_D, |0\rangle_E \otimes |11\rangle_D\} \quad \text{(A.5)}$$

Using the projection approach outlined in Ref. [121], a two-particle tunneling Hamiltonian can then be deduced

$$v = \frac{1}{2}(P^i + P^f) H_{ED} \left[\frac{1}{\varepsilon_i - H_0} H_{ED} P^i + \frac{1}{\varepsilon_f - H_0} H_{ED} P^f \right] \quad \text{(A.6)}$$

This results in four separate terms

$$\begin{aligned} v &= \tfrac{1}{2} P^i \textstyle\sum_\sigma |\Delta|^2 e_\sigma^\dagger d_\sigma \frac{1}{\varepsilon_i - H_0} d_\sigma^\dagger e_\sigma P^i \\ &\quad + \tfrac{1}{2} P^f \textstyle\sum_{\sigma\tau} \Delta^2 d_\sigma^\dagger e_\sigma \frac{1}{\varepsilon_i - H_0} d_\tau^\dagger e_\tau P^i \\ &\quad + \tfrac{1}{2} P^i \textstyle\sum_{\sigma\tau} (\Delta^*)^2 e_\sigma^\dagger d_\sigma \frac{1}{\varepsilon_f - H_0} e_\tau^\dagger d_\tau P^f \\ &\quad + \tfrac{1}{2} P^f \textstyle\sum_\sigma |\Delta|^2 d_\sigma^\dagger e_\sigma \frac{1}{\varepsilon_f - H_0} e_\sigma^\dagger d_\sigma P^f \\ &= h^{ii} + h^{fi} + h^{if} + h^{ff}, \end{aligned} \quad \text{(A.7)}$$

where h^{fi} and h^{if} describe a two-particle tunneling. Here a compact notation has been introduced, where h^{ii} and h^{if} denote the terms which are diagonal and off-diagonal in the low energy states, respectively.

Additionally, we introduce a shorthand notation for commutators. Here $\hat{H}_{ED}\rho = -i[H_{ED}, \rho]$ where a dimensionless small parameter, $\epsilon \ll 1$, is introduced, $\hat{H}_{ED} = \epsilon\hat{V}$[1]. We separate the density matrices into two sets, $\mathcal{P}\rho$ and the complement $\mathcal{Q}\rho$. We remark here that two types of projection operators have been introduced. In the state space, the projection operators are denoted P and Q, while projections in the Liouville space are specified as $\mathcal{P}$ and $\mathcal{Q}$.

Similar to the starting point of deriving the Markovian master equation with projection operators, the projection $\mathcal{P}$ to the 'relevant' density matrices is defined by

$$\mathcal{P}\rho = \gamma \otimes tr_E[\rho] \equiv \bar{\rho}, \quad \mathcal{Q}\rho = (\hat{1} - \mathcal{P})\rho \tag{A.8}$$

where γ is a two-electron density matrix of the entangler. This incorporates the aforementioned criterion for our entangler-model

- The entangler state is unchanged on the transport time scale.

Since, despite including counting fields, by operating with $\mathcal{P}$ on the unperturbed equation of motion, it must be satisfied that [2]

$$\mathcal{P}\mathcal{L}_0 = \mathcal{L}_0\mathcal{P} = 0 \tag{A.9}$$

The effective superoperator is [120]

$$\mathcal{W} = \epsilon^2\mathcal{P}\hat{V}\mathcal{Q}\mathcal{L}_0^{-1}\mathcal{Q}\hat{V}\mathcal{P}. \tag{A.10}$$

In our case, v will have no diagonal terms, that is, $\mathcal{P}v\mathcal{P} = \mathcal{Q}v\mathcal{Q} = 0$. The complement projection in $\mathcal{W}$ accordingly be set to identity and the effective equation of motion reads,

$$\mathcal{W}\rho = \epsilon^2\mathcal{P}\hat{V}\mathcal{L}_0^{-1}\hat{V}\bar{\rho}. \tag{A.11}$$

[1] In the considered setup, we may identify the parameter as $\epsilon = \Delta/U$. The single particle energies being off-resonance is the principal blockage of the transport scheme.

[2] Note that this means we must look at the stationary solution when solving this effective eq. of motion

Evaluating now factor by factor, in the following order of h and ρ is important.

$$i\frac{1}{\mathcal{L}_0}\hat{V}\bar{\rho} = i\frac{1}{\mathcal{L}_0}[v,\bar{\rho}] = \frac{1}{2}\left(\frac{1}{\mathcal{L}_0^{fi}}h^{fi}\bar{\rho} - \frac{1}{\mathcal{L}_0^{if}}\bar{\rho}h^{if}\right) \tag{A.12}$$

Next step,

$$\hat{V}\tfrac{1}{\mathcal{L}_0}\hat{V}[\bar{\rho}] = \hat{V}\left(\tfrac{1}{2}\left(\tfrac{1}{\mathcal{L}_0^{fi}}h^{fi}\bar{\rho} - \tfrac{1}{\mathcal{L}_0^{if}}\bar{\rho}h^{if}\right)\right) \tag{A.13}$$

The first term and second term are respectivley

$$\tfrac{1}{2}\tfrac{1}{\mathcal{L}_0^{fi}}\left((h^{if}+h^{ff})h^{fi}\bar{\rho} - h^{fi}\bar{\rho}(h^{if}+h^{ii})\right) \tag{A.14}$$

$$\tfrac{1}{2}\tfrac{1}{\mathcal{L}_0^{if}}\left((h^{fi}+h^{ii})\bar{\rho}h^{if} - \bar{\rho}h^{if}(h^{ff}+h^{fi})\right) \tag{A.15}$$

We may throw away terms which are of the form h^{ifff} because of the last $\mathcal{P}$-projection. This follows from

$$\mathcal{P}[h^{ifff}\bar{\rho}] \sim \mathcal{P}[P^i\cdots P^f\bar{\rho}] = \gamma\otimes \mathrm{tr}_E[P^i\cdots P^f\bar{\rho}] = 0. \tag{A.16}$$

Going back,

$$\begin{aligned}\hat{V}\tfrac{1}{\mathcal{L}_0}\hat{V}[\bar{\rho}] = \tfrac{1}{2}\tfrac{1}{\mathcal{L}_0^{fi}}\left(h^{if}h^{fi}\bar{\rho} - h^{fi}\bar{\rho}h^{if}\right) - \tfrac{1}{2}\tfrac{1}{\mathcal{L}_0^{if}}\left(h^{fi}\bar{\rho}h^{if} - \bar{\rho}h^{if}h^{fi}\right) = \\ -\tfrac{1}{2}\left(\tfrac{1}{\mathcal{L}_0^{fi}}+\tfrac{1}{\mathcal{L}_0^{if}}\right)h^{fi}\bar{\rho}h^{if} + \tfrac{1}{2}\left[\tfrac{1}{\mathcal{L}_0^{fi}}h^{if}h^{fi}\bar{\rho} + \tfrac{1}{\mathcal{L}_0^{if}}\bar{\rho}h^{if}h^{fi}\right].\end{aligned} \tag{A.17}$$

The unperturbed Lindblad operator $\mathcal{L}_0$ is diagonal in the $\mathcal{Q}$-space. In particular we have that

$$\begin{aligned}\mathcal{L}_0^{fi} = \mathcal{L}_0[|0\rangle_E|11\rangle_D\langle 2|_E\langle 00|_D] = \left(-i\delta - \tfrac{\Gamma_1^d}{2} - \tfrac{\Gamma_2^d}{2}\right)|0\rangle_E|11\rangle_D\langle 2|_E\langle 00|_D, \\ \mathcal{L}_0^{if} = \mathcal{L}_0[|2\rangle_E|00\rangle_D\langle 0|_E\langle 11|_D] = \left(i\delta - \tfrac{\Gamma_1^d}{2} - \tfrac{\Gamma_2^d}{2}\right)|2\rangle_E|00\rangle_D\langle 0|_E\langle 11|_D.\end{aligned} \tag{A.18}$$

where $\delta = \varepsilon_{200} - \varepsilon_{011}$, is the off-resonance energy of the two low energy states. Here $\varepsilon_{n_e,n_l,n_r}$ denotes the energy of the dot system with n_e (n_l and n_r) particles in the entangler dot (left and right dots, respectively). As such,

$$\frac{1}{\mathcal{L}_0^{fi}} \sim \frac{1}{\left(-i\delta - \frac{\Gamma_1^d}{2} - \frac{\Gamma_2^d}{2}\right)} = \frac{(\frac{\Gamma_1^d}{2}+\frac{\Gamma_2^d}{2})}{\left(\delta^2 + (\frac{\Gamma_1^d}{2}+\frac{\Gamma_2^d}{2})^2\right)} + \frac{i\delta}{\left(\delta^2 + (\frac{\Gamma_1^d}{2}+\frac{\Gamma_2^d}{2})^2\right)} \tag{A.19}$$

Equipped with these expressions, we obtain an effective equation motion of the form,

$$\begin{aligned}\mathcal{P}\hat{V}\tfrac{1}{\mathcal{L}_0}\hat{V}[\bar{\rho}] &= \Re[\tfrac{1}{\mathcal{L}_0^{fi}}]\mathcal{P}\left(h^{fi}\bar{\rho}h^{if} - \tfrac{1}{2}\{h^{if}h^{fi},\bar{\rho}\}\right)\\ &\quad + i\Im[\tfrac{1}{\mathcal{L}_0^{fi}}]\mathcal{P}[h^{if}h^{fi},\bar{\rho}].\end{aligned} \tag{A.20}$$

Using the projection operator definitions and expressions for the h terms, we can obtain an explicit form of our effective equation of motion. Starting with the first term,

$$\begin{aligned}&\mathcal{P}\left(h^{fi}\bar{\rho}h^{if}\right)\\ &= \gamma\otimes \mathrm{tr}_E\{h^{fi}\bar{\rho}h^{if}\}\\ &= \tfrac{|\Delta|^4}{U^2}\sum_{\sigma\tau\sigma'\tau'}\gamma\otimes \mathrm{tr}_E\{\left(d^\dagger_\sigma e_\sigma d^\dagger_\tau e_\tau\right)\gamma\otimes\rho_D\left(e^\dagger_{\sigma'}d_{\sigma'}e^\dagger_{\tau'}d_{\tau'}\right)\}\\ &= \tfrac{|\Delta|^4}{U^2}\sum_{\sigma\tau\sigma'\tau'}\gamma\otimes \mathrm{tr}_E\{e_\sigma e_\tau\gamma e^\dagger_{\sigma'}e^\dagger_{\tau'}\}d^\dagger_\sigma d^\dagger_\tau\rho_D d_{\sigma'}d_{\tau'}\\ &= \tfrac{|\Delta|^4}{U^2}\sum_{\sigma\tau\sigma'\tau'}\gamma\otimes\gamma^{\sigma\tau}_{\sigma'\tau'}d^\dagger_\sigma d^\dagger_\tau\rho_D d_{\sigma'}d_{\tau'},\end{aligned} \tag{A.21}$$

where it has been used that all intermediate steps (occupying the virtual states) cost U energy, $\gamma^{\sigma\tau}_{\sigma'\tau'}$ is the matrix element $\mathrm{tr}_E[e_\sigma e_\tau\gamma e^\dagger_{\sigma'}e^\dagger_{\tau'}]$ and $\mathrm{tr}_E[\rho]=\rho_D$ denotes the dot state. Analogously for the second term

$$\begin{aligned}&\mathcal{P}\left(\{h^{if}h^{fi},\bar{\rho}\}\right)\\ &= \tfrac{|\Delta|^4}{U^2}\mathcal{P}\left(\{\sum_{\sigma\tau\sigma'\tau'}e^\dagger_{\sigma'}d_{\sigma'}e^\dagger_{\tau'}d_{\tau'}d^\dagger_\sigma e_\sigma d^\dagger_\tau e_\tau,\bar{\rho}\}\right)\\ &= \tfrac{|\Delta|^4}{U^2}\gamma\otimes\mathrm{tr}_E\left[\{\sum_{\sigma\tau\sigma'\tau'}e^\dagger_{\sigma'}d_{\sigma'}e^\dagger_{\tau'}d_{\tau'}d^\dagger_\sigma e_\sigma d^\dagger_\tau e_\tau,\bar{\rho}\}\right]\\ &= \sum_{\sigma\tau\sigma'\tau'}\tfrac{|\Delta|^4}{U^2}\gamma\otimes\mathrm{tr}_E\left[e^\dagger_{\sigma'}d_{\sigma'}e^\dagger_{\tau'}d_{\tau'}d^\dagger_\sigma e_\sigma d^\dagger_\tau e_\tau\bar{\rho}+\bar{\rho}e^\dagger_{\sigma'}d_{\sigma'}e^\dagger_{\tau'}d_{\tau'}d^\dagger_\sigma e_\sigma d^\dagger_\tau e_\tau\right]\\ &= \sum_{\sigma\tau\sigma'\tau'}\tfrac{|\Delta|^4}{U^2}\gamma\otimes\left(\mathrm{tr}_E\left[e_\sigma e_\tau\gamma e^\dagger_{\sigma'}e^\dagger_{\tau'}\right]\{d_{\sigma'}d_{\tau'}d^\dagger_\sigma d^\dagger_\tau,\rho_D\}\right)\\ &= \sum_{\sigma\tau\sigma'\tau'}\tfrac{|\Delta|^4}{U^2}\gamma\otimes\gamma^{\sigma\tau}_{\sigma'\tau'}\left\{d_{\sigma'}d_{\tau'}d^\dagger_\sigma d^\dagger_\tau,\rho_D\right\}.\end{aligned} \tag{A.22}$$

The last term can be obtained analogously by following the steps of the anti-commutator term,

$$\mathcal{P}[h^{if}h^{fi},\bar{\rho}] = \sum_{\sigma\tau\sigma'\tau'}\frac{|\Delta|^4}{U^2}\gamma\otimes\gamma^{\sigma\tau}_{\sigma'\tau'}\left[d_{\sigma'}d_{\tau'}d^\dagger_\sigma d^\dagger_\tau,\rho_D\right]. \tag{A.23}$$

The effective equation of motion for the detector density matrix is then, using the normalization condition $\mathrm{tr}_E[\gamma] = 1$, given by

$$\begin{aligned}
\tfrac{d\rho_D}{dt} &= \mathrm{tr}_E[\mathcal{L}_0(\rho) + \mathcal{W}(\rho)] \\
&= \mathrm{tr}_E[-i[H_D + H_E, \rho] + \mathcal{D}_E(\rho) + \mathcal{D}_D^{\chi}(\rho) + \mathcal{W}(\rho)] \\
&= -i[H_D, \rho_D] + \mathcal{D}_D^{\chi}(\rho_D) + \mathrm{tr}_E[\mathcal{W}(\rho)] \\
&= -i[H_D, \rho_D] + \mathcal{D}_D^{\chi}(\rho_D) \\
&+ \tfrac{|\Delta|^4}{U^2} \Re[\tfrac{1}{\mathcal{L}_0^{fi}}] \left(\sum_{\sigma\tau\sigma'\tau'} \gamma^{\sigma\tau}_{\sigma'\tau'} d_\sigma^\dagger d_\tau^\dagger \rho_D d_{\sigma'} d_{\tau'} - \tfrac{1}{2} \left\{ d_{\sigma'} d_{\tau'} d_\sigma^\dagger d_\tau^\dagger, \rho_D \right\} \right) \\
&+ \tfrac{|\Delta|^4}{U^2} \Im[\tfrac{1}{\mathcal{L}_0^{fi}}] \sum_{\sigma\tau\sigma'\tau'} \gamma^{\sigma\tau}_{\sigma'\tau'} \left[d_{\sigma'} d_{\tau'} d_\sigma^\dagger d_\tau^\dagger, \rho_D \right].
\end{aligned} \tag{A.24}$$

To compare the above expression with the effective equation of motion in Paper I, we redefine the matrix elements of γ as

$$\frac{|\Delta|^4}{U^2} \frac{(\Gamma_1^d/2 + \Gamma_2^d/2)}{\left(\delta^2 + (\Gamma_1^d/2 + \Gamma_2^d/2)^2\right)} \gamma^{\sigma\tau}_{\sigma'\tau'} \to \gamma^{\sigma\tau}_{\sigma'\tau'} \tag{A.25}$$

and exclude energy renormalization term $\propto \delta$. Finally, the effective equation of motion with only two particle emission is

$$\begin{aligned}
\tfrac{d\rho_D}{dt} = \; & -i[H_D, \rho_D] + \mathcal{D}_D^{\chi}(\rho_D) \\
& + \sum_{\sigma\tau\sigma'\tau'} \gamma^{\sigma\tau}_{\sigma'\tau'} \left(d_\sigma^\dagger d_\tau^\dagger \rho_D d_{\sigma'} d_{\tau'} - \tfrac{1}{2} \left\{ d_{\sigma'} d_{\tau'} d_\sigma^\dagger d_\tau^\dagger, \rho_D \right\} \right)
\end{aligned} \tag{A.26}$$

Appendix B: Lindblad equation with counting fields

Here we show how the counting field enter the Lindblad equation by considering a minimally coupled current-sensor attached to the transport system consisting of quantum dots tunnel-coupled to drain and source contacts. We consider the minimal coupling, $\chi \ll 1$, which makes the spin precess as an electron leaves the dot for the drain contact. The Hamiltonian for such a system is

$$\mathcal{H} = H_d + H_r + H_T - \frac{\chi\hbar}{2e} I = H_d + H_r + H_T + \frac{i\sigma_z\chi}{2}[\mathcal{H}, N] \tag{B.1}$$

where $N = N_r - N_l$ and N_α is the number of electrons in contact α. Here H_T is the tunneling Hamiltonian, describing tunneling between the quantum dot α and lead l,

$$H_T = \sum_{\alpha kl} \left[t_l d_\alpha^\dagger c_{lk} + t_l^* c_{lk}^\dagger d_\alpha \right], \tag{B.2}$$

where we have assumed that the tunneling amplitude is independent of k and α. We may identify the current probe term as the result of a unitary transformation,

$$H_T + \frac{i}{2}\sigma_z\chi[\mathcal{H}, N] = UWU^\dagger = e^S W e^{-S} = W + [S, W] + \mathcal{O}(\chi^2). \tag{B.3}$$

Noting that all terms except H_T commute with the number operator N, that is $[\mathcal{H}, N] = [H_d + H_r + H_T, N] = [H_T, N]$ we are able to identify

$$S = -\frac{i\chi}{2}\sigma_z N, \quad W = H_T. \tag{B.4}$$

Keeping in mind that U commutes with all other terms, we obtain that

$$H = U\mathcal{H}U^\dagger = H_d + H_r + e^{-\frac{i\chi}{2}\sigma_z N} H_T e^{\frac{i\chi}{2}\sigma_z N} = H_d + H_r + H_T(\chi). \tag{B.5}$$

That is, the current probe enters as an additional phase factor in the tunneling Hamiltonian.

Spin precession angle

The total density matrix of the reduced electronic system and the probing spin degree of freedom is denoted by σ. Assuming the spin state ϱ and electronic

system ρ were decoupled before measurement started at $t = 0$, at which point the spin was in a superposition state. We can express the total density matrix in the interaction picture, after a measurement time t,

$$\sigma(t) = \begin{pmatrix} \sigma_{\uparrow\uparrow}(0) & e^{-\frac{i}{\hbar}H_T^{\chi}t}\sigma_{\uparrow\downarrow}(0)e^{\frac{i}{\hbar}H_T^{-\chi}t} \\ e^{-\frac{i}{\hbar}H_T^{-\chi}t}\sigma_{\downarrow\uparrow}(0)e^{\frac{i}{\hbar}H_T^{\chi}t} & \sigma_{\downarrow\downarrow}(0) \end{pmatrix}, \tag{B.6}$$

where we have introduced $H_T^{\chi} = \langle\uparrow |H_T(\chi)| \uparrow\rangle$ and $H_T^{-\chi} = \langle\downarrow |H_T(\chi)| \downarrow\rangle$. We note that that the off-diagonal matrix elements when averaged over all electronic states, yield the function,

$$\Lambda(\chi) = \mathrm{tr}_e \left[e^{-\frac{i}{\hbar}H_T^{\chi}t}\rho(0)e^{\frac{i}{\hbar}H_T^{-\chi}t} \right] \tag{B.7}$$

which is the characteristic function of the probability distribution $P_{\Delta t}(N)$, discussed in Chapter 5. Note that the constant $\varrho_{\uparrow\downarrow}(0)$ is dropped to normalise $P_{\Delta t}(N)$. In order show how the counting fields appear in the Quantum Master Equation, we need to take care of two points.

- Obtain explicit expression for $e^{-\frac{i}{\hbar}H_T^{\chi}t}\rho(0)e^{\frac{i}{\hbar}H_T^{-\chi}t}$.
- Derive an equation of motion for the density matrix with the probe.

To address the first point, we use the Baker-Campbell-Hausdorff identity to leading order in χ,

$$\begin{aligned} H_T^{\chi} &= e^{-\frac{i\chi}{2}N}H_T e^{\frac{i\chi}{2}N} = H_T + \tfrac{i\chi}{2}[N, H_T] + \mathcal{O}(\chi^2) \\ H_T^{-\chi} &= e^{\frac{i\chi}{2}N}H_T e^{\frac{-i\chi}{2}N} = H_T - \tfrac{i\chi}{2}[N, H_T] + \mathcal{O}(\chi^2) \end{aligned} . \tag{B.8}$$

Carrying out the commutator

$$[N, H_T(\chi)] = \sum_{\alpha k} \left[t d_\alpha^\dagger c_{lk} - t^* c_{lk}^\dagger d_\alpha \right]. \tag{B.9}$$

For a minimally coupled probe, that is by discarding higher order χ-terms, we obtain $1 \pm i\chi = e^{\pm i\chi}$. The new tunneling Hamiltonian then reads,

$$H_T^{\pm\chi} = \sum_{\alpha k} \left[t_l e^{\mp i\chi/2} d_\alpha^\dagger c_k + t^* e^{\pm i\chi/2} c_k^\dagger d_\alpha \right]. \tag{B.10}$$

Equation of motion

For the second point, we start by introducing an operator ρ_χ, which satisfies the condition $\mathrm{tr}[\rho_\chi] = \Lambda(\chi)$. Studying the equation of motion in the interaction picture,

$$\frac{d\rho_\chi}{dt} = \frac{d}{dt} e^{-\frac{i}{\hbar}H_T(\chi)t} \rho e^{\frac{i}{\hbar}H_T(-\chi)t} = \frac{-i}{\hbar}\left(H_T(\chi)\rho - \rho H_T(-\chi)\right) = \frac{-i}{\hbar}[H_T, \rho]_\chi, \tag{B.11}$$

where the last equality serves as the definition for a modified Liouville equation. Identifying Λ as modified density matrix with counting fields, we can use Eq. (B.11) as the starting point for the derivation of the Lindblad equation in Chapter 4. We obtain then nested commutators of the form,

$$\left[H_T, [H_T, \rho_S \rho_B]_\chi\right]_\chi . \tag{B.12}$$

We then note that only terms $H_T(\chi)\rho_S H_T(-\chi)$ have a χ-dependence. These correspond to the terms in the Lindblad equation which change the occupation number of the reduced system by ± 1.

Following the derivation of the Lindblad equation in Chapter 4, with the modified Liouville equation, we obtain the Lindblad equation with counting fields. As an example, a Lindblad equation for transport via one single level quantum dot, reads

$$\frac{d\rho}{dt} = -\frac{i}{\hbar}[H_s, \rho] + \Gamma_R \left[d\rho d^\dagger e^{i\chi t} - \frac{1}{2}\{d^\dagger d, \rho\}\right] + \Gamma_L \left[d^\dagger \rho d e^{-i\chi t} - \frac{1}{2}\{d d^\dagger, \rho\}\right] \tag{B.13}$$

Appendix C: Schrieffer-Wolff transformation

The Schrieffer-Wolff (SW) transformation is a unitary transformation which makes it possible to obtain an effective low-energy Hamiltonian. In particular for our work in Paper II, we have been interested in obtaining an effective two-particle tunneling Hamiltonian. Here we sketch how the approach of SW transformation is used in Paper II. Given a Hamiltonian H,

$$H = H_0 + H_T, \tag{C.1}$$

where H_T describes a single particle tunneling Hamiltonian. By introducing a unitary transformation $U = e^S H e^{-S}$, by virtue of the Baker-Hausdorff identity, the transformed Hamiltonian can be expressed as,

$$UHU^\dagger = H_0 + H_T + [S, H_0] + [S, H_T] + \frac{1}{2}[S, [S, H_0]] + \frac{1}{2}[S, [S, H_T]] + \ldots \tag{C.2}$$

We note then, if $[S, H_0] = -H_T$ we obtain that the transformed Hamiltonian $UHU^\dagger = H_{\text{eff}}$

$$H_{\text{eff}} = H_0 + \frac{1}{2}[S, H_T] + \frac{1}{2}[S, [S, H_T]] + \ldots \tag{C.3}$$

Since $[S, H_0] = -H_T$, it must hold that S is proportional to the tunneling parameter. From this, we identify the second term as containing the two-particle tunneling Hamiltonian, and discard higher order terms in S. The remaining task is then, find an operator S, which satisfies $[S, H_0] = -H_T$, and identify the term in $[S, H_T]$ which corresponds to a two-particle tunneling contribution.

Derivation of effective two-particle tunneling Hamiltonian

In the supplementary material of Paper II, the effective tunneling Hamiltonian is obtained by finding a suitable operator S, which satisfies the commutator relation as stated above.

Here we provide an alternative derivation of the effective Hamiltonian using a projection operator approach [122, 121]. Starting with the Hamiltonian

$$H = \sum_{\gamma=1,2,\alpha,\beta} \varepsilon_\gamma d_\gamma^\dagger d_\gamma + \sum_{\gamma,\gamma'} U_{\gamma,\gamma'} d_\gamma^\dagger d_{\gamma'}^\dagger d_{\gamma'} d_\gamma + \sum_{\gamma \neq \gamma'} \left(t_{\gamma\gamma'} d_\gamma^\dagger d_{\gamma'} + t_{\gamma\gamma'}^* d_{\gamma'}^\dagger d_\gamma \right), \tag{C.4}$$

we restrict ourselves to a regime which ensures that the spectrum of H can be separated into two groups of states. A low energy sector consiting of the set of states $\{|1100\rangle, |00\alpha\beta\rangle\}$, where we denote both entangler dots occupied as $|1100\rangle = |E\rangle$, detector dots α and β populated $|00\alpha\beta\rangle = |D\rangle$. We introduce the projection operator $P = |e\rangle\langle e| + |d\rangle\langle d|$, for the relevant low energy space and its complement $Q = \hat{1} - P$, where $\hat{1}$ is the identity operator.

We represent the unitary transformation $U = \exp(S)$, where S is an anti-hermitian operator taken to be off-diagonal. That is, $PSP = QPQ = 0$. Expressing the transformed Hamiltonian in the low energy states we obtain,

$$H_{\text{eff}} = Pe^{S}He^{-S}P = H_0P_O + \epsilon PVP + \epsilon^2 P[S_1, QVP + PVQ]P. \tag{C.5}$$

Here the second term vanishes identically since V is the tunneling portion of Hamiltonian H, which is by definition off-diagonal. To obtain an expression for the third term, we need to find an expression for $\hat{S}_1(V) = [S_1, V]$. To this end, we introduce the operator R which satisfies

$$R(X) = \sum_{i,j} \frac{\langle i|X|j\rangle}{E_i - E_j} |i\rangle\langle j|. \tag{C.6}$$

Here $H_0|j\rangle = E_j|j\rangle$ and X is an off diagonal operator, Equipped with R we obtain the effective Hamiltonian,

$$H_{\text{eff}} = H_0P + \epsilon^2 P[R(V), V]P. \tag{C.7}$$

The second term corresponds to the higher-order tunneling Hamiltonian $H_T^{(2)}$

$$H_T^{(2)} = |e\rangle\langle d|\langle e|[R(V), V]|d\rangle + |d\rangle\langle e|\langle d|[R(V), V]|e\rangle \tag{C.8}$$

plus a renormalization of the single particle energies δH

$$\delta H = |e\rangle\langle e|\langle e|[R(V), V]|e\rangle + |d\rangle\langle d|\langle d|[R(V), V]|d\rangle. \tag{C.9}$$

Here we will disregard the renormalization terms and instead focus only on $H_T^{(2)}$. Each term of the tunneling Hamiltonian depends on factors

$$\langle e|[R(V), V]|d\rangle = \sum_v \langle e|H_T|v\rangle\langle v|H_T|d\rangle \left\{ \frac{1}{E_E - E_v} - \frac{1}{E_v - E_D} \right\}, \tag{C.10}$$

where $E_E = \varepsilon_1 + \varepsilon_2 + U_{12}$, $E_D = \varepsilon_\alpha + \varepsilon_\beta + U_{\alpha\beta}$ and v runs over all states in Q. The only nonvanishing terms are when $v = |10\rangle|\alpha 0\rangle, |10\rangle|0\beta\rangle, |01\rangle|\alpha 0\rangle, |01\rangle|0\beta\rangle$. Carrying out the calculations term by term,

$$\begin{aligned}\langle e|[R(V),V]|d\rangle = \quad & -t_{2\alpha}t_{1\beta}\left(\tfrac{1}{E_E-E_{10\alpha 0}} - \tfrac{1}{E_{10\alpha 0}-E_D}\right) \\ & +t_{2\beta}t_{1\alpha}\left(\tfrac{1}{E_E-E_{100\beta}} - \tfrac{1}{E_{100\beta}-E_D}\right) \\ & +t_{1\alpha}t_{2\beta}\left(\tfrac{1}{E_E-E_{01\alpha 0}} - \tfrac{1}{E_{01\alpha 0}-E_D}\right) \\ & -t_{1\beta}t_{2\alpha}\left(\tfrac{1}{E_E-E_{010\beta}} - \tfrac{1}{E_{010\beta}-E_D}\right).\end{aligned} \tag{C.11}$$

With this result, going back to Eq. (C.8) we obtain the expression

$$H_T^{(2)} = |e\rangle\langle d|t_{\alpha\beta 21} + |d\rangle\langle e|t^*_{\alpha\beta 21}, \tag{C.12}$$

where $t_{\alpha\beta 21}$ denotes an effective two-particle tunneling amplitude,

$$\begin{aligned}t_{\alpha\beta 21} = \quad & t_{1\alpha}t_{2\beta}\left\{\tfrac{1}{E_E-E_{100\beta}} + \tfrac{1}{E_D-E_{100\beta}} + \tfrac{1}{E_E-E_{01\alpha 0}} + \tfrac{1}{E_E-E_{01\alpha 0}}\right\} \\ & -t_{1\beta}t_{2\alpha}\left\{\tfrac{1}{E_E-E_{10\alpha 0}} + \tfrac{1}{E_D-E_{10\alpha 0}} + \tfrac{1}{E_E-E_{010\beta}} + \tfrac{1}{E_E-E_{010\beta}}\right\}.\end{aligned} \tag{C.13}$$

As a final step, we can express everything in terms of creation and annihilation operators, e.g. $|e\rangle\langle d| = d_1^\dagger d_2^\dagger d_\alpha d_\beta$. With this we reproduce the tunneling Hamiltonian from the supplementary material,

$$H_T^{(2)} = \sum_{\alpha\beta}\left(t_{\alpha\beta 21}d_1^\dagger d_2^\dagger d_\alpha d_\beta + t^*_{\alpha\beta 21}d_\beta^\dagger d_\alpha^\dagger d_1 d_2\right). \tag{C.14}$$

Appendix D: Effective beam splitter

Here we discuss how the detector dot state after operating with the cotunneling Hamiltonian, can be expressed in terms of an entangled orbital state. Using the notation from Paper II, we parametrise the tunneling amplitudes as

$$t_{i+1} = t_{i1}\cos\theta_i, \quad t_{i-1} = t_{i1}\sin\theta_i, \quad t_{i+2} = -t_{i2}\sin\theta_i, \quad t_{i-2} = t_{i2}\cos\theta_i \tag{D.1}$$

where $|t_{A1}|^2 = |t_{A+1}|^2 + |t_{A-1}|^2$. Starting from the initial state where both entangler dots are occupied, operating with the co-tunneling Hamiltonian we obtain

$$|\psi\rangle_{\rm dot} \propto -\sum_{\alpha\beta}\frac{t_{\beta 2}t_{\alpha 1}}{\Delta_{AB}}|\alpha\rangle|\beta\rangle + \sum_{\alpha\beta}\frac{t_{\beta 1}t_{\alpha 2}}{\Delta_{BA}}|\alpha\rangle|\beta\rangle = |\psi\rangle^1_{\rm dot} + |\psi\rangle^2_{\rm dot} \tag{D.2}$$

Using the parametrisation defined above, the first and second terms become

$$\begin{aligned}|\psi\rangle^1_{\rm dot} = -\tfrac{t_{B2}t_{A1}}{\Delta E_{AB}}[\quad & -\sin\theta_B\cos\theta_A|+\rangle_A|+\rangle_B - \sin\theta_B\sin\theta_A|-\rangle_A|+\rangle_B \\ & \cos\theta_B\cos\theta_A|+\rangle_A|-\rangle_B + \cos\theta_B\sin\theta_A|-\rangle_A|-\rangle_B]\end{aligned} \tag{D.3}$$

$$\begin{aligned}|\psi\rangle^2_{\rm dot} = \tfrac{t_{B1}t_{A2}}{\Delta E_{BA}}[\quad & \cos\theta_B(-\sin\theta_A)|+\rangle_A|+\rangle_B + \cos\theta_B\cos\theta_A|-\rangle_A|+\rangle_B \\ & \sin\theta_B(-\sin\theta_A)|+\rangle_A|-\rangle_B + \sin\theta_B\cos\theta_A|-\rangle_A|-\rangle_B]\end{aligned} \tag{D.4}$$

These relations can be expressed in terms a scattering matrix of subsystem i, relating the detector dot states $|i\pm\rangle$ to the orbital states $|1\rangle_i, |2\rangle_i$, describing an electron from dot 1 or 2 being emitted towards detector i. Using the basis of Paper II,

$$\begin{pmatrix} |-\rangle_i \\ |+\rangle_i \end{pmatrix} = \begin{pmatrix} \sin\theta_i & \cos\theta_i \\ \cos\theta_i & -\sin\theta_i \end{pmatrix}\begin{pmatrix} |1\rangle_i \\ |2\rangle_i \end{pmatrix} \tag{D.5}$$

We note then that by expressing the resulting detector states $|\psi_{dot}\rangle$ in terms of the orbital states we obtain

$$|\psi\rangle_{\rm dot} = -\frac{t_{B2}t_{A1}}{\Delta E_{AB}}|1\rangle_A|2\rangle_B + \frac{t_{B1}t_{A2}}{\Delta E_{BA}}|2\rangle_A|1\rangle_B \tag{D.6}$$

From this expression we can identiy the coefficients of the entangled orbital state in Paper II as $c_{12} = t_{B2}t_{A1}/\Delta E_{AB}$ and $c_{21} = t_{B1}t_{A2}/\Delta E_{BA}$

Appendix E: Perturbative schemes

Solving the full eigenvalue problem analytically becomes cumbersome quickly as the dimensions of matrix M grow. In some cases it is possible to make the problem tractable by, instead of the full CGF $F(\chi) = F$, obtain only the cumulants using a perturbation expansion [66]. By expanding the steady state eigenvalue equation on both sides in terms of the counting field $i\chi$,

$$M\rho + i\chi\left(\frac{\partial M_\chi}{\partial i\chi}\rho_\chi + M_\chi\frac{\partial \rho_\chi}{\partial i\chi}\right) + \ldots = i\chi\frac{\partial F}{\partial i\chi}\rho_\chi + i\chi F\frac{\partial \rho_\chi}{\partial i\chi} - \frac{\chi^2}{2}\frac{\partial^2 F}{\partial (i\chi)^2}\rho_\chi + \ldots \tag{E.1}$$

Letting $\chi \to 0$, identifying terms order by order and introducing the vector $\vec{tr}$, satisfying $\vec{tr}\vec{\rho} = \sum_d \langle d|\rho|d\rangle = 1$, where d runs over all states, we can obtain expressions for the different cumulants. As an example, expressions for the current and current correlations at contacts k and l read,

$$\begin{aligned} I_k &= e\,\vec{tr}\frac{\partial M}{\partial i\chi_k}\vec{\rho}\Big|_{\chi\to 0} \\ S_{kl} &= e^2\,\vec{tr}\left(\frac{1}{2}\frac{\partial^2 M_\chi}{\partial i\chi_k \partial i\chi_l} + \frac{\partial M_\chi}{\partial i\chi_k} Q M^{-1} Q\left(\frac{\partial M}{\partial i\chi_l} - I_l\right) + [k \leftrightarrow l]\right)\vec{\rho}\Big|_{\chi\to 0}, \end{aligned} \tag{E.2}$$

where $Q = \hat{1} - P$ with $P = \rho_\chi \vec{tr}$, a projection operator taking a general state in vector form $\vec{\rho}$ to the stationary state. As an example, applying this to the case of a double quantum dot (see Chapter 5 for details) we find

$$\begin{aligned} \vec{tr} &= (1,1,1,1,0,0) \\ \vec{\rho} &= \tfrac{1}{\delta\varepsilon^2+\gamma^2+4t^2}\left(t^2, \delta\varepsilon^2+\gamma^2+t^2, t^2, t^2, \delta\varepsilon t, -\gamma t\right) \end{aligned} \tag{E.3}$$

which reproduces the expressions of current I in Eq. (5.23) and auto-correlation S in Eq. (5.24),

$$\begin{aligned} I &= \tfrac{2t^2\gamma e}{\delta\varepsilon+\gamma^2+4t^2}, \\ S &= \tfrac{2e^2 t\gamma}{16q^2}\left[(\delta\varepsilon^2+\gamma^2)^2 + 2t^2(3\delta\varepsilon^2-\gamma^2) + 8t^4\right]. \end{aligned} \tag{E.4}$$

Cumulant generating function with small emission rate

For cases where the source emission rate γ is small compared to a drain absorption rate Γ, we can obtain an expression for the cumulant generating function F to

leading order in γ/Γ. The starting point is the eigenvalue equation

$$\dot{\rho}^{\chi} = M^{\chi}\rho^{\chi} = F\rho^{\chi}, \tag{E.5}$$

In Papers I and II we consider charge transport where at most two particles are present in the reduced system. Moreover, we decompose the system into an A and B part, for example the two detector dots in our generic entangler-detector model of Paper I. For a stationary current, the eigenvalue equation can then be expressed in the block form,

$$\begin{pmatrix} M_{o,o} & M^{\chi}_{o,a} & M^{\chi}_{o,b} & M^{\chi}_{o,ab} \\ M_{a,o} & M_{a,a} & M^{\chi}_{a,b} & M^{\chi}_{a,ab} \\ M_{b,o} & M_{b,a} & M_{b,b} & M^{\chi}_{b,ab} \\ M_{ab,o} & M_{ab,a} & M_{ab,b} & M_{ab,ab} \end{pmatrix} \begin{pmatrix} \vec{\rho}_0 \\ \vec{\rho}_a \\ \vec{\rho}_b \\ \vec{\rho}_{ab} \end{pmatrix} = F \begin{pmatrix} \vec{\rho}_0 \\ \vec{\rho}_a \\ \vec{\rho}_b \\ \vec{\rho}_{ab} \end{pmatrix} \tag{E.6}$$

Here the different block matrices $M_{i,j}$ denote the matrix elements relating $\partial_t\vec{\rho}_i$ to $\vec{\rho}_j$, where the superscript χ denotes which matrix elements contain a counting field. The vector $\vec{\rho}_a$ ($\vec{\rho}_b$) denotes the vector of density matrices describing part A (B) being populated, and $\vec{\rho}_{ab}$ ($\vec{\rho}_o$) denoting both (none) being occupied. The general structure of the Lindblad matrix is

$$\begin{pmatrix} M_{o,o} & A^{\chi} \\ B & C^{\chi} \end{pmatrix}, \tag{E.7}$$

Instead of directly solving the eigenvalue equation, we can consider the block matrix determinant identity,

$$\det(M - I\cdot F) = \det(C^{\chi} - I\cdot F)\det(M_{o,o} - F - A^{\chi}(C^{\chi} - I\cdot F)^{-1}B) = 0 \tag{E.8}$$

Now we employ the condition of a small emission rate γ. We note that the factors F, B and $M_{o,o} \sim \gamma$. As such, the second factor becomes $\det(M_{o,o} - F - A^{\chi}(C^{\chi})^{-1}B) = 0$. We find then the cumulant generating function,

$$F = M_{o,o} - A^{\chi}(C^{\chi})^{-1}B. \tag{E.9}$$

Following this approach, we find that to leading order in the small emission rate γ, the cumulant generating function in terms of the block matrices $M_{i,j}$ from Eq. (E.6) is given by,

$$F = M_{o,o} - \sum_{\alpha=a,b} M^{\chi}_{o,a}M^{-1}_{\alpha,\alpha}\left[M_{\alpha,o} - M^{\chi}_{\alpha,ab}M^{-1}_{ab,ab}M_{ab,o}\right]. \tag{E.10}$$

Using this method, we have obtained the cumulant generating function describing the long time transport statistics in the Papers I and II. By combining the approaches of this appendix, we could in Paper I relate the emitted state from the entangler and detector dot state.

Printed by Media-Tryck, Lund University 2017 | Nordic Ecolabel 3041 0903

Faculty of Science
Department of Physics
ISBN 978-91-7753-132-6